

A NEW APPROACH TO ESTIMATE SETTLEMENTS  
UNDER FOOTINGS  
ON RAMMED AGGREGATE PIER GROUPS

A THESIS SUBMITTED TO  
THE GRADUATE SCHOOL OF NATURAL AND APPLIED SCIENCES  
OF  
MIDDLE EAST TECHNICAL UNIVERSITY

BY

ÖZGÜR KURUOĞLU

IN PARTIAL FULFILLMENT OF THE REQUIREMENTS  
FOR  
THE DEGREE OF DOCTOR OF PHILOSOPHY  
IN  
CIVIL ENGINEERING

JULY 2008

**I hereby declare that all information in this document has been obtained and presented in accordance with academic rules and ethical conduct. I also declare that, as required by these rules and conduct, I have fully cited and referenced all material and results that are not original to this work.**

Name, Last Name : Özgür Kuruoğlu

Signature

: 

Approval of the thesis:

**A NEW APPROACH TO ESTIMATE SETTLEMENTS UNDER FOOTINGS  
ON RAMMED AGGREGATE PIER GROUPS**

submitted by **ÖZGÜR KURUOĞLU** in partial fulfillment of the requirements for  
the degree of **Doctor of Philosophy in Civil Engineering Department, Middle  
East Technical University** by,

Prof. Dr. Canan Özgen  
Dean, Graduate School of **Natural and Applied Sciences**

Prof. Dr. Güney Özcebe  
Head of Department, **Civil Engineering**

Prof. Dr. Orhan Erol  
Supervisor, **Civil Engineering Dept., METU**

**Examining Committee Members:**

Prof. Dr. Ufuk Ergun  
Civil Engineering Dept., METU

Prof. Dr. Orhan Erol  
Civil Engineering Dept., METU

Prof. Dr. Tamer Topal  
Geological Engineering Dept., METU

Prof. Dr. Gökhan Baykal  
Civil Engineering Dept., Boğaziçi University

Assoc. Prof. Dr. K.Önder Çetin  
Civil Engineering Dept., METU

**Date:**

16.07.2008

## **ABSTRACT**

### **A NEW APPROACH TO ESTIMATE SETTLEMENTS UNDER FOOTINGS ON RAMMED AGGREGATE PIER GROUPS**

Kuruoğlu, Özgür

Ph.D., Department of Civil Engineering

Supervisor: Prof. Dr. Orhan Erol

July 2008, 145 pages

This study uses a 3D finite element program, calibrated with the results of a full scale instrumented load test on a limited size footing, to estimate the settlement improvement factor for footings resting on rammed aggregate pier groups. A simplified 3D finite element model (Composite Soil Model) was developed, which takes into account the increase of stiffness around the piers during the ramming process.

Design charts for settlement improvement factors of square footings of different sizes ( $B = 2.4\text{m}$  to  $4.8\text{m}$ ) resting on aggregate pier groups of different area ratios ( $AR = 0.087$  to  $0.349$ ), pier moduli ( $E_{\text{column}} = 36\text{MPa}$  to  $72\text{MPa}$ ), and with various compressible clay layer strengths ( $c_u = 20\text{kPa}$  to  $60\text{kPa}$ ) and thicknesses ( $L = 5\text{m}$  to  $15\text{m}$ ) were prepared using this calibrated 3D finite element model.

It was found that, the settlement improvement factor increases as the area ratio, pier modulus and footing pressure increase. On the other hand, the settlement improvement factor is observed to decrease as the undrained shear strength and thickness of compressible clay and footing size increase.

After using the model to study the behaviour of floating piers, it was concluded that, the advantage of using end bearing piers instead of floating piers for reducing settlements increases as the area ratio of piers increases, the elasticity modulus value of the piers increases, the thickness of the compressible clay layer decreases and the undrained shear strength of the compressible clay decreases.

Key Words: Ground Improvement, Stone Column, Rammed Aggregate Pier, Settlement Improvement Factor, Floating Piers.

## ÖZ

### TOKMAKLANMIŞ TAŞ KOLON GRUPLARINA OTURAN TEMELLERDEKİ OTURMALARIN TAHMİNİ İÇİN YENİ BİR YAKLAŞIM

Kuruoğlu, Özgür

Doktora, İnşaat Mühendisliği Bölümü

Tez Yöneticisi: Prof. Dr. Orhan Erol

Temmuz 2008, 145 sayfa

Bu çalışmada, enstrümente edilmiş temeller üzerinde gerçekleştirilen arazi grup yükleme deneylerinin sonuçları kullanılarak kalibre edilmiş, üç boyutlu bir sonlu elemanlar programı tokmaklanmış taş kolon gruplarına oturan temellerde oturma iyileştirme faktörünün tahmin edilmesinde kullanılmıştır. Bu amaçla, kolonlar etrafında tokmaklama sırasında meydana gelen sıkışmayı dikkate alan basitleştirilmiş bir üç boyutlu sonlu elemanlar modeli (Kompozit Zemin Modeli) geliştirilmiştir.

Bu kalibre edilmiş üç boyutlu sonlu elemanlar modeli kullanılarak, değişik alan oranlarına ( $AR = 0.087 - 0.349$ ) ve kolon modüllerine ( $E_{column} = 36\text{MPa} - 72\text{MPa}$ ) sahip tokmaklanmış taş kolon grupları üzerine oturan değişik boyutlardaki ( $B = 2.4\text{m} - 4.8\text{m}$ ) kare temellerin farklı mukavemet özelliklerinde ( $c_u = 20\text{kPa} - 60\text{kPa}$ ) ve kalınlıklardaki ( $L = 5\text{m} - 15\text{m}$ ) sıkışabilir kil tabakalarındaki oturma iyileştirme faktörleri için tasarım abakları üretilmiştir.

Analizler sonucunda oturma iyileştirme faktörünün alan oranı, kolon modülü ve temel basıncının artması ile arttığı sonucuna varılmıştır. Öte yandan, oturma iyileştirme faktörünün sıkışabilir kil tabakasının mukavemetinin ve kalınlığının ve temel boyutlarının artması ile azaldığı gözlenmiştir.

Aynı model yüzen taş kolon gruplarının davranışlarının araştırılması için de kullanılmıştır. Analizler sonucunda, alan oranı, kolon modülü arttıkça, sıkışabilir kil tabakası kalınlığı azaldıkça ve sıkışabilir kil tabakasının mukavemeti azaldıkça, oturmayı azaltmak için yüzen kolonlar yerine uç kolonları kullanmanın avantajının arttığı sonucuna varılmıştır.

Anahtar Kelimeler: Zemin İyileştirmesi, Taş Kolon, Tokmaklanmış Taş Kolon, Oturma İyileştirme Faktörü, Yüzen Taş Kolon.

*To Aelya and Arda*

## **ACKNOWLEDGMENTS**

I express my grateful appreciation to Prof.Dr. Orhan Erol for his guidance and moral support throughout this long study. Special thanks goes to Mr. Atilla Horoz and Yüksel Proje for their support and understanding. Finally, I offer my sincere acknowledgments to my family for their encouragement and unshakable faith in me.

## TABLE OF CONTENTS

ABSTRACT .....	iv
ÖZ .....	vi
ACKNOWLEDGMENTS.....	ix
TABLE OF CONTENTS .....	x
LIST OF TABLES .....	xiii
LIST OF FIGURES.....	xiv
CHAPTER	
1. INTRODUCTION.....	1
1.1 General .....	1
1.2 Aim of the Study .....	3
2. LITERATURE REVIEW ON SETTLEMENT OF STONE COLUMNS.....	5
2.1 Introduction .....	5
2.2 Equilibrium Method .....	5
2.3 Priebe Method .....	13
2.4 Greenwood Method.....	18
2.5 Incremental Method .....	20
2.6 Granular Wall Method.....	21
2.7 Finite Element Method.....	25
2.8 Subgrade Modulus Approach.....	42
3. CALIBRATION OF THE FINITE ELEMENT MODEL.....	45
3.1 Introduction .....	45
3.2 Details of the Full-Scale Load Tests .....	45
3.3 Details of the Finite Element Model .....	51
3.4 Modeling of Field Tests on Rammed Aggregate Pier Groups.....	55

4.	RESULTS OF THE PARAMETRIC STUDY .....	75
4.1	Introduction .....	75
4.2	Details of the Parametric Study.....	75
4.3	Presentation of the Results of the Parametric Study .....	78
4.4	Design Example .....	80
5.	DISCUSSION OF THE ANALYSIS RESULTS .....	84
5.1	Introduction .....	84
5.2	Effect of Area Ratio on Settlement Improvement Factor ....	84
5.3	Effect of Undrained Shear Strength of Compressible Clay Layer on Settlement Improvement Factor .....	85
5.4	Effect of Elasticity Modulus of Rammed Aggregate Pier on Settlement Improvement Factor .....	85
5.5	Effect of Footing Pressure on Settlement Improvement Factor .....	85
5.6	Effect of Compressible Layer Thickness on Settlement Improvement Factor .....	85
5.7	Effect of Footing Size on Settlement Improvement Factor..	90
5.8	Comparison of Calculated Settlement Improvement Factors with Conventional Methods .....	90
5.9	Effect of Floating Columns on Settlement Improvement Factor .....	91
6.	CONCLUSIONS AND RECOMMENDATIONS .....	97
6.1	Summary .....	97
6.2	Effect of Area Ratio on Settlement Improvement Factor ....	98
6.3	Effect of Undrained Shear Strength of Compressible Clay Layer on Settlement Improvement Factor .....	99
6.4	Effect of Elasticity Modulus of Rammed Aggregate Pier on Settlement Improvement Factor .....	99
6.5	Effect of Footing Pressure on Settlement Improvement Factor .....	99

6.6 Effect of Compressible Layer Thickness on Settlement Improvement Factor .....	99
6.7 Effect of Footing Size on Settlement Improvement Factor .	100
6.8 Comparison of Calculated Settlement Improvement Factors with Conventional Methods .....	100
6.9 Effect of Floating Columns on Settlement Improvement Factor .....	101
6.10 Further Research.....	101
REFERENCES .....	103
APPENDICES .....	108
A. SITE INVESTIGATION DATA .....	108
B. DESIGN CHARTS.....	127
CURRICULUM VITAE .....	145

## LIST OF TABLES

### TABLES

Table 4.1 Strength and deformation properties of the compressible clay layer used at the study .....	76
--	----

## LIST OF FIGURES

### FIGURES

Figure 2.1 A typical layout of stone columns a) triangular arrangement b) square arrangement (Balaam and Booker, 1981).....	7
Figure 2.2 Unit cell idealizations (Barksdale and Bachus, 1983).....	8
Figure 2.3 Maximum reductions in settlement that can be obtained using stone columns- equilibrium method of analysis (Barksdale and Bachus, 1983).....	13
Figure 2.4 Settlement reduction due to stone column- Priebe and Equilibrium Methods (Barksdale and Bachus, 1983).....	15
Figure 2.5 Consideration of column compressibility (Priebe, 1995).....	16
Figure 2.6 Determination of the depth factor (Priebe, 1995).....	16
Figure 2.7 Limit value of the depth factor (Priebe, 1995) .....	17
Figure 2.8 Settlement of small foundations a) for single footings b) for strip footings (Priebe, 1995).....	18
Figure 2.9 Comparison of Greenwood and Equilibrium Methods for predicting settlement of stone column reinforced soil (Barksdale and Bachus, 1989).....	19
Figure 2.10 Definitions for Granular Wall Method (Van Impe and De Beer, 1983) .....	23
Figure 2.11 Stress distribution of stone columns (Van Impe and De Beer, 1983) .....	24
Figure 2.12 Improvement on the settlement behavior of the soft layer reinforced with the stone columns (Van Impe and De Beer, 1983) .....	24
Figure 2.13 Effect of stone column penetration length on elastic settlement (Balaam et.al., 1977) .....	26

Figure 2.14 Notations used in unit cell linear elastic solutions and linear elastic settlement influence factors for area ratios, $a_s = 0.10, 0.15, 0.25$ (Barksdale and Bachus, 1983) .....	28
Figure 2.15 Variation of stress concentration factor with modular ratio- Linear elastic analysis (Barksdale and Bachus, 1983).....	29
Figure 2.16 Notation used in unit cell nonlinear solutions given in Figure 2.17 .....	31
Figure 2.17 Nonlinear Finite Element unit cell settlement curves (Barksdale and Bachus, 1983) .....	32
Figure 2.18 Variation of stress concentration with modular ratio- nonlinear analysis (Barksdale and Bachus, 1983).....	36
Figure 2.19 Effect of $c_u$ on stiffness improvement factor (Ambily and Gandhi, 2007) .....	38
Figure 2.20 Effect of $s/d$ and $\phi$ on stiffness improvement factor (Ambily and Gandhi, 2007) .....	38
Figure 2.21 Comparison of stiffness improvement factor with existing theories (Ambily and Gandhi, 2007).....	39
Figure 2.22 Comparison of Priebe 1993 and FLAC IF (improvement factor) Versus ARR (area ratio) for the 1x1 configuration (Clemente et.al., 2005) .....	40
Figure 2.23 Comparison of Priebe 1993 and FLAC IF (improvement factor) Versus ARR (area ratio) for the 2x2 configuration (Clemente et.al., 2005) .....	40
Figure 2.24 Comparison of Priebe 1993 and FLAC IF (improvement factor) Versus ARR (area ratio) for the 5x5 configuration (Clemente et.al., 2005) .....	41
Figure 2.25 Variation of settlement improvement factor with column stiffness (Domingues et.al., 2007) .....	42
Figure 3.1 Location of investigation boreholes and CPT soundings at the load test site (Özkeskin, 2004) .....	46
Figure 3.2 Variation of SPT N values with depth at the load test site (Özkeskin, 2004) .....	47

Figure 3.3 Variation of soil classification at the load test site based on CPT correlations (Özkeskin, 2004) .....	49
Figure 3.4 Location of aggregate piers at the load test site (Özkeskin, 2004) .....	50
Figure 3.5 Isometric view of the 3D finite element model .....	52
Figure 3.6 Comparison of surface load-settlement curves for untreated soil .....	55
Figure 3.7 Field test rammed aggregate pier group layout .....	57
Figure 3.8 Comparison of surface load-settlement curves for loading on Group A rammed aggregate piers (Normal 3D FEM Model).....	58
Figure 3.9 Comparison of surface load-settlement curves for loading on Group B rammed aggregate piers (Normal 3D FEM Model).....	58
Figure 3.10 Comparison of surface load-settlement curves for loading on Group C rammed aggregate piers (Normal 3D FEM Model).....	59
Figure 3.11 Mohr circle sequence and stress path EF during normal consolidation (Handy, 2001) .....	61
Figure 3.12 Mohr circle sequence and stress path FG as reductions in vertical stress created over consolidated soil (Handy, 2001) .....	62
Figure 3.13 Increasing horizontal stress on normally consolidated soil (Stress path AB) increases consolidation threshold stress from V1 to V2 (Handy, 2001) .....	62
Figure 3.14 Geometry of the assumed improved zones around the rammed aggregate piers .....	64
Figure 3.15 Comparison of surface load-settlement curves for loading on Group A rammed aggregate piers (Modified Ring Model) .....	65
Figure 3.16 Comparison of surface load-settlement curves for loading on Group B rammed aggregate piers (Modified Ring Model) .....	65

Figure 3.17 Comparison of surface load-settlement curves for loading on Group C rammed aggregate piers (Modified Ring Model) .....	66
Figure 3.18 Comparison of surface load-settlement curves for loading on Group A rammed aggregate piers (Composite Soil Model) .....	67
Figure 3.19 Comparison of surface load-settlement curves for loading on Group B rammed aggregate piers (Composite Soil Model) .....	68
Figure 3.20 Comparison of surface load-settlement curves for loading on Group C rammed aggregate piers (Composite Soil Model) .....	68
Figure 3.21 Comparison of vertical stress increase in the lower zone for Group A rammed aggregate piers ( $q/q_{ult} = 0.27$ ) .....	71
Figure 3.22 Comparison of vertical stress increase in the lower zone for Group A rammed aggregate piers ( $q/q_{ult} = 0.54$ ) .....	72
Figure 3.23 Comparison of vertical stress increase in the lower zone for Group A rammed aggregate piers ( $q/q_{ult} = 0.81$ ) .....	73
Figure 4.1 Schematic representation of composite soil model .....	77
Figure 4.2 Settlement improvement factor (IF) vs. area ratio (AR) charts for a rigid square footing ( $B=2.4\text{m}$ ) resting on end bearing rammed aggregate piers ( $L=5\text{m}$ , $E=36\text{ MPa}$ ) .....	79
Figure 4.3 Geometry and parameters of the design example .....	80
Figure 5.1 Effect of undrained shear strength of compressible clay layer ( $c_u$ ) on settlement improvement factor (IF) for footings resting on aggregate pier groups .....	86
Figure 5.2 Effect of elasticity modulus of rammed aggregate pier ( $E_{\text{column}}$ ) on settlement improvement factor (IF) for footings resting on aggregate pier groups .....	87
Figure 5.3 Effect of footing pressure ( $q$ ) on settlement improvement factor (IF) for footings resting on aggregate pier groups .....	88
Figure 5.4 Effect of compressible layer thickness ( $L_{\text{clay}}$ ) on settlement improvement factor (IF) for footings resting on aggregate pier groups .....	89

Figure 5.5 Effect of footing size (B) on settlement improvement factor (IF) for footings resting on aggregate pier groups .....	92
Figure 5.6 Comparison of settlement improvement factor (IF) values calculated by the finite element method (FEM) with the conventional methods in literature for footings resting on aggregate pier groups.....	93
Figure 5.7 Geometry of the cases used to investigate the effect of floating piers on the settlement improvement factor.....	94
Figure 5.8 Ratio of settlement improvement factor for floating pier group over end bearing pier group vs. area ratio (for selected case I) .....	95
Figure 5.9 Ratio of settlement improvement factor for floating pier group over end bearing pier group vs. area ratio (for selected case II) .....	96

## **CHAPTER 1**

### **INTRODUCTION**

#### **1.1 General**

As the world's population continues to grow, there is an increasing need to construct on marginal or inadequate soils. Traditionally, deep foundation methods such as piles and drilled concrete shafts have been used to transfer loads either deeper within these marginal or inadequate soils or to better materials below them. Recently, there has been a trend toward improving the load-carrying capacity of these soils using reinforcement, modification, or stabilization techniques. Stone columns are one of these soil improvement methods that are ideally suited for improving soft silts and clays and loose silty sands and offer a valuable technique under suitable conditions for (1) increasing bearing capacity, (2) reducing settlements, (3) increasing the time rate of settlement, (4) reducing the liquefaction potential of sands and (5) improving slope stability of both embankments and natural slopes.

Stone columns have been used successfully in a variety of applications such as a) avoiding stability and settlement problems of embankments and bridge approach fills over soft soils, b) improving soft foundation soils, in terms of bearing capacity and settlement control, under structures (buildings, bridge bents, storage tanks etc.) on shallow foundations, c) landslide stabilization projects, d) liquefaction mitigation projects.

Stone columns can be accomplished using various excavation, replacement and compaction techniques such as a) vibro-replacement (wet) process; in which a vibrating probe (vibroflot) opens a hole by jetting using large quantities of

water under high pressure. The uncased hole is flushed out and then the stone is added in 0.3-1.2 m increments and densified by means of an electrically or hydraulically actuated vibrator located near the bottom of the probe. b) vibro-replacement (dry) process; in which the probe, which may utilize air, displaces the native soil laterally as it is advanced into the ground. c) rammed stone columns; which are constructed by either driving an open or closed end pipe in the ground or boring a hole. A mixture of sand and stone is placed in the hole in increments, and rammed in using a heavy, falling weight. d) sand compaction piles; which are constructed by driving a steel casing down to the desired elevation using a heavy, vertical vibratory hammer located at the top of the pile. As the pile is being driven the casing is filled with sand. The casing is then repeatedly extracted and partially redriven using the vibratory hammer.

Stone columns can be constructed by the vibro-replacement technique in a variety of soils varying from gravels and sands to silty sands, silts, and clays. For embankment construction, the soils are generally soft to very soft, water deposited silts and clays. For bridge bent foundation support, silty sands having silts contents greater than about 15 percent and stiff clays are candidates for improvement with stone columns.

Stone columns should not be considered for use in soils having shear strengths less than  $7 \text{ kN/m}^2$ . Also stone columns in general should not be used in soils having sensitivities greater than about 5; experience is limited to this value of sensitivity (Baumann and Bauer, 1974). Caution should be exercised in constructing stone columns in soils having average shear strengths less than about  $19 \text{ kN/m}^2$  as originally proposed by Thorburn (1975).

For sites having shear strengths less than 17 to  $19 \text{ kN/m}^2$ , use of sand for stability applications should be given in consideration. Use of sand piles, however, generally results in more settlement than that for stone columns (Barksdale and Bachus, 1983).

For economic reasons, the thickness of the strata to be improved should in general be no greater than 9.0m and preferably about 6.0m. Usually, the weak layer should be underlain by a competent bearing stratum to realize optimum utility and economy (Barksdale and Bachus, 1983)

Design loads applied to each stone column typically vary depending on site conditions from about 15 to 60 tons.

Area replacement ratios used vary from 0.15 to 0.35 for most applications. The diameter of the constructed stone column depends primarily upon the type of soil present. It also varies to a lesser extent upon the quantity and velocity of water used in advancing the hole and the number of times the hole is flushed out by raising and dropping the vibroflot a short distance. Stone columns generally have diameters varying from 0.6m to 2.0m.

## **1.2 Aim of the Study**

This study uses a 3D finite element program (PLAXIS 3D Foundation), calibrated with the results of a full scale instrumented load test on a limited size footing (3.0mx3.5m). The full scale load tests were carried out both on untreated soil and on three different rammed aggregate pier groups of different lengths (floating to end-bearing) in soft silty clay. (Özkeskin, 2004) This calibrated 3D finite element model will be used to investigate the effects of area ratio, column modulus, column length, footing size, strength of compressible layer, bearing pressure and floating piers on the settlement reduction factor of rammed aggregate pier groups of limited size. The results will be compared with available analytical methods and similar studies. Design charts will also be produced for practical applications.

A comprehensive literature survey on the settlement of stone columns is given in Chapter 2. An explanation of the calibration procedure for the 3D finite element model is given in Chapter 3. Results of finite element analyses carried

out with the calibrated 3D model are presented in Chapter 4. The results of the finite element analyses are discussed in Chapter 5. Finally, Chapter 6 concludes the study by highlighting the findings.

## CHAPTER 2

### LITERATURE REVIEW ON SETTLEMENT OF STONE COLUMNS

#### 2.1 Introduction

Presently available methods for calculating settlement of stone columns can be classified as either (1) simple, approximate methods which make important simplifying assumptions or (2) sophisticated methods based on fundamental elasticity and/or plasticity theory (such as finite elements) which model material and boundary conditions. Several of the more commonly used approximate methods are presented first. Following this, a review is given of selected theoretically sophisticated elastic and elastic-plastic methods and design charts are presented. All of these approaches for estimating settlement assume an infinitely wide loaded area reinforced with stone columns having a constant diameter and spacing. For this condition of loading and geometry the unit cell concept is theoretically valid and has been used by the Aboshi et.al (1979), Barksdale and Takefumi (1990), Priebe (1990 and 1993), Goughnour and Bayuk (1979).

#### 2.2 Equilibrium Method

The equilibrium method described for example by Aboshi et.al.(1979) and Barksdale and Goughnour (1984), Barksdale and Takefumi (1990) is the method in Japanese practice for estimating the settlement of sand compaction piles. In applying this simple approach the stress concentration factor,  $n$ , must be estimated using past experience and the results of previous field measurements of stress.

The following assumptions are necessary in developing the equilibrium method: (1) the extended unit cell idealization is valid, (2) the total vertical load applied to the unit cell equals the sum of the force carried by the stone and the soil, (3) the vertical displacement of stone column and soil is equal, and (4) a uniform vertical stress due to external loading exists throughout the length of stone column, or else the compressible layer is divided into increments and the settlement of each increment is calculated using the average stress increase in the increment. Following this approach, as well as the other methods, settlement occurring below the stone column reinforced ground must be considered separately; usually these settlements are small and can often be neglected (Barksdale and Bachus, 1983).

For purposes of settlement and stability analysis, it is convenient to associate the tributary area of soil surrounding each stone column as illustrated in Figures 2.1 and 2.2. The tributary area can be closely approximated as an equivalent circle having the same total area.

For an equilateral triangular pattern of stone columns, the equivalent circle has an effective diameter of:

$$D_e = 1.05s \quad (2.1)$$

while for a square pattern ,

$$D_e = 1.13s \quad (2.2)$$

where  $s$  is the spacing of stone columns. The resulting equivalent cylinder of material having a diameter  $D_e$  enclosing the tributary soil and one stone column is known as the *unit cell*. The stone column is concentric to the exterior boundary of the unit cell (Fig.2.2a).

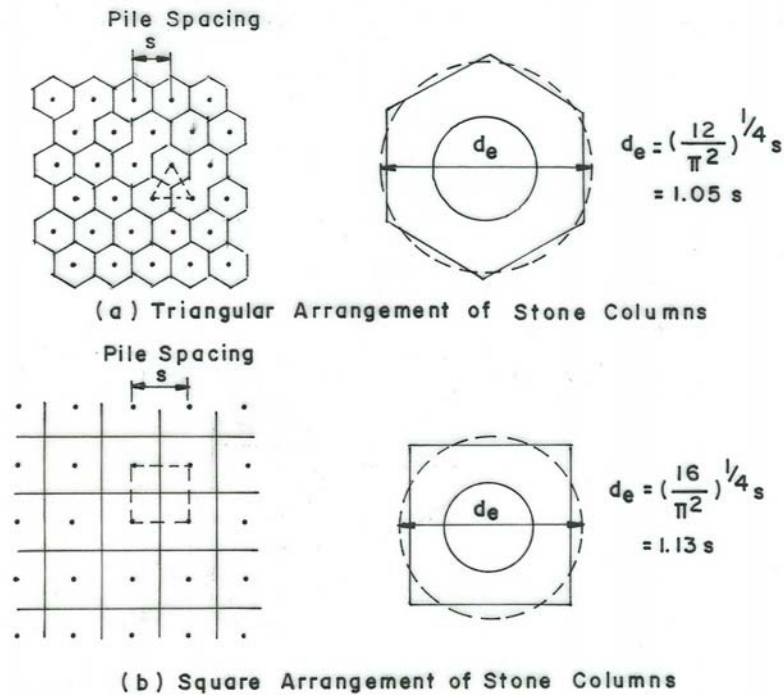


Figure 2.1 A typical layout of stone columns a) triangular arrangement b) square arrangement (Balaam and Booker, 1981)

For an infinitely large group of stone columns subjected to a uniform loading applied over the area; each interior column may be considered as a unit cell as shown in Figure 2.2b. Because of symmetry of load and geometry, lateral deformations cannot occur across the boundaries of the unit cell. Also from symmetry of load and geometry the shear stresses on the outside boundaries of the unit cell must be zero. Following these assumptions a uniform loading applied over the top of the unit cell must remain within the unit cell. The distribution of stress within the unit cell between the stone and soil could, however, change with depth. As discussed later, several settlement theories assume this idealized extension of the unit cell concept to be valid. The unit cell can be physically modeled as a cylindrical-shaped container having frictionless, rigid exterior wall symmetrically located around the stone column (Fig.2.2c).

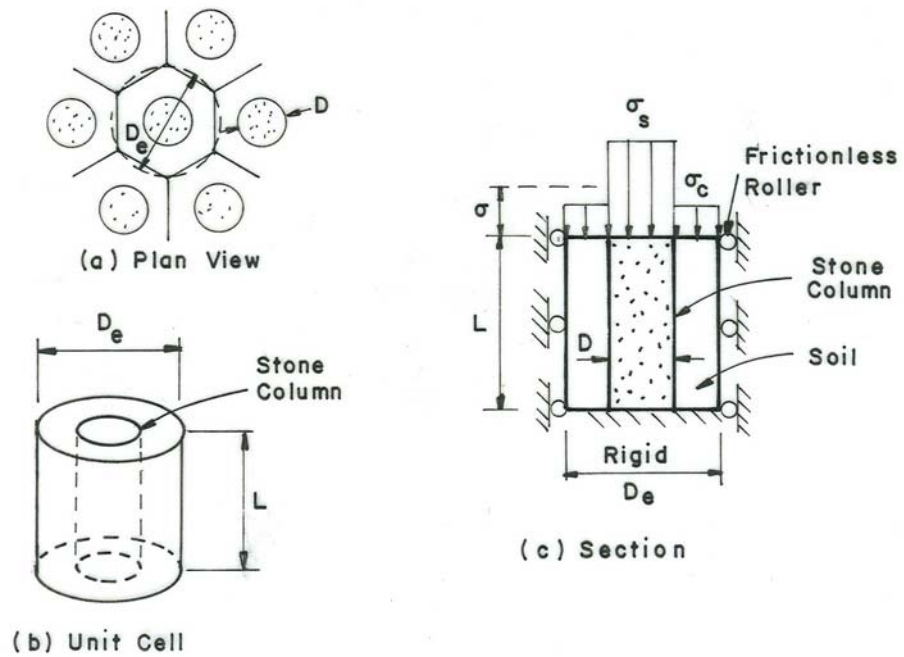


Figure 2.2 Unit cell idealizations (Bachus and Barksdale, 1989)

To quantify the amount of soil replaced by the stone, the *area replacement ratio* is introduced and defined as the ratio of the granular pile area over the whole area of the equivalent cylindrical unit within the unit cell and expressed as:

$$a_s = \frac{A_s}{A} \quad (2.3)$$

where  $a_s$  is the area replacement ratio,  $A_s$  is the area of the stone column and  $A$  is the total area within the unit cell. The area replacement ratio can be expressed in terms of the diameter and spacing of the stone columns as follows:

$$a_s = c_1 \left( \frac{D}{s} \right)^2 \quad (2.4)$$

where :      D = diameter of the compacted stone column  
                   s = center to center spacing of the stone columns  
                   c<sub>1</sub> = a constant dependent upon the pattern of stone columns  
                   used; for a square pattern c<sub>1</sub> = π/4 and for an equilateral  
                   triangular pattern c<sub>1</sub> = π/(2/√3).

After placing a uniform stress with an embankment or foundation load over stone columns and allowing consolidation, an important concentration of stress occurs in the stone column and an accompanying reduction in stress occurs in the surrounding less stiff soil (Aboshi et.al, 1979; Balaam et.al, 1977; Goughnour and Bayuk, 1979). Since the vertical settlement of the stone column and surrounding soil is approximately the same, stress concentration occurs in the stone column since it is stiffer than a cohesive or a loose cohesionless soil.

When a composite foundation is loaded for which the unit cell concept is valid such as a reasonably wide, relatively uniform loading applied to a group of stone columns having either a square or equilateral triangular pattern, the distribution of vertical stress within the unit cell (Fig.2.2c) can be expressed by a *stress concentration factor n* defined as:

$$n = \frac{\sigma_s}{\sigma_c} \quad (2.5)$$

where            σ<sub>s</sub> = stress in the stone column  
                   σ<sub>c</sub> = stress in the surrounding cohesive soil

The average stress  $\sigma$  which must exist over the unit cell area at a given depth must, for equilibrium of vertical forces to exist within the unit cell, be equal for a given area replacement ratio,  $a_s$ :

$$\sigma = \sigma_s a_s + \sigma_c (1 - a_s) \quad (2.6)$$

where all the terms have been previously defined. Solving Equation (2.6) for the stress in the clay and stone using the stress concentration factor  $n$  gives (Aboshi et.al., 1979):

$$\sigma_c = \sigma / [1 + (n - 1)a_s] = \mu_c \sigma \quad (2.7a)$$

and

$$\sigma_s = n\sigma [1 + (n - 1)a_s] = \mu_s \sigma \quad (2.7b)$$

From conventional one-dimensional consolidation theory

$$S_t = \left( \frac{C_c}{1 + e_0} \right) \log_{10} \left( \frac{\sigma'_0 + \sigma_c}{\sigma'_0} \right) H \quad (2.8)$$

where  $S_t$  = primary consolidation settlement occurring over a distance  $H$  of stone column treated ground  
 $H$  = vertical height of stone column treated ground over which settlements are being calculated.  
 $\sigma'_0$  = average initial effective stress in the clay layer  
 $\sigma_c$  = change in stress in the clay layer due to the externally applied loading, Equation (2.7a)  
 $C_c$  = compression index from one-dimensional consolidation test  
 $e_0$  = initial void ratio

From Equation (2.8) it follows that for normally consolidated clays, the ratio of settlements of the stone column improved ground to the unimproved ground,  $S_t/S$ , can be expressed as

$$S_t / S = \frac{\log_{10} \left( \frac{\sigma'_0 + \mu_c \sigma}{\sigma'_0} \right)}{\log_{10} \left( \frac{\sigma'_0 + \sigma}{\sigma'_0} \right)} \quad (2.9)$$

This equation shows that the level of improvement is dependent upon (1) the stress concentration factor  $n$ , (2) the initial effective stress in the clay, and (3) the magnitude of applied stress  $\sigma$ . Equation (2.9) indicates if other factors are constant, a greater reduction in settlement is achieved for longer columns and smaller applied stress increments.

For very large  $\sigma'_0$  (long length of stone column) and very small applied stress  $\sigma$ , the settlement ratio relatively rapidly approaches

$$S_t / S = 1 / [1 + (n - 1)a_s] = \mu_c \quad (2.10)$$

where all terms have been previously defined. Equation (2.10) is shown graphically in Figure 2.3.

The stress concentration factor  $n$  required calculating  $\sigma_c$  is usually estimated from the results of stress measurements made for full-scale embankments, but could be estimated from theory. From elastic theory assuming a constant vertical stress, the vertical settlement of the stone column can be approximately calculated as follows:

$$S_s = \frac{\sigma_s L}{D_s} \quad (2.11)$$

where  $S_s$  = vertical displacement of the stone column  
 $\sigma_s$  = average stress in the stone column  
 $L$  = length of the stone column  
 $D_s$  = constrained modulus of the stone column (the elastic modulus,  $E_s$ , could be used for an upper bound)

Using Equation (2.11) and its analogous form for the soil, the following equation is obtained by equating the settlement of the stone and soil:

$$\frac{\sigma_s}{\sigma_c} = \frac{D_s}{D_c} \quad (2.12)$$

where  $\sigma_s$  and  $\sigma_c$  are the stresses in the stone column and soil, respectively and  $D_s$  and  $D_c$  are the appropriate moduli of the two materials.

Use of Equation (2.12) gives values of the stress concentration factor  $n$  from 25 to over 500, which is considerably higher than that measured in the field. Field measurements for stone columns have shown  $n$  to generally be in the range of 2 to 5 (Goughnour and Bayuk, 1979). Therefore, use of the approximate compatibility method, Equation (2.12), for estimating the stress concentration factor is not recommended for soft clays (Barksdale and Bachus, 1983). For settlement calculations using the equilibrium method, a stress concentration factor  $n$  of 4.0 to 5.0 is recommended based on comparison of calculated settlement with observed settlements (Aboshi et.al. 1979).

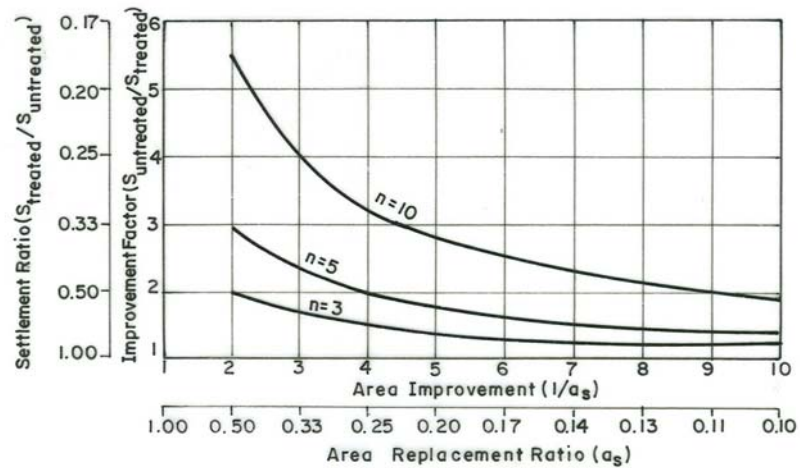


Figure 2.3 Maximum reductions in settlement that can be obtained using stone columns- equilibrium method of analysis (Barksdale and Bachus, 1983)

### 2.3 Priebe Method

The method proposed by Priebe (Bauman and Bauer, 1974; Priebe, 1988, 1993 and 1995; Mosoley and Priebe, 1993) for estimating reduction in settlement due to ground improvement with stone columns also uses the unit cell model. Furthermore the following idealized conditions are assumed:

- The column is based on a rigid layer
- The column material is incompressible
- The bulk density of column and soil is neglected

Hence, the column cannot fail in end bearing and any settlement of the load area results in a bulging of the column, which remains constant all over its length.

The improvement achieved at these conditions by the existence of stone columns is evaluated on the assumption that the column material shears from

beginning whilst the surrounding soil reacts elastically. Furthermore, the soil is assumed to be displaced already during the column installation to such an extent that its initial resistance corresponds to the liquid state, i.e. the coefficient of earth pressure equals to  $K=1$ . The results of evaluation, taking Poisson's ratio,  $\mu=1/3$ , which is adequate for the state of final settlement in most cases, is expressed as basic *improvement factor*  $n_0$ :

$$n_0 = 1 + \frac{A_c}{A} \left[ \frac{5 - A_c / A}{4K_{ac}(1 - A_c / A)} - 1 \right] \quad (2.13)$$

where  $A_c$  = cross section area of single stone column  
 $A$  = unit cell area  
 $K_{ac} = \tan^2 (45 - \phi_c / 2)$   
 $\phi_c$  = angle of internal friction angle of column material

The relation between the improvement factor  $n_0$ , the reciprocal area ratio  $A/A_c$  and the friction angle of the backfill material  $\phi_c$  is illustrated in Figure 2.4 by Barksdale and Bachus (1983) comparing the equilibrium method solution (equation 2.10) for stress concentration factors of  $n = 3, 5$  and  $10$ .

The Priebe curves generally fall between the upper bound equilibrium curves for  $n$  between  $5$  and  $10$ . The Priebe improvement factors are substantially greater than for the observed variation of the stress concentration factor from  $3$  to  $5$ . Measured improvement factors from two sites, also given in Figure 2.4, show good agreement with the upper bound equilibrium method curves, for  $n$  in the range of  $3$  to slightly less than  $5$ . Barksdale and Bachus (1983) underlined that the curves of Priebe appear, based on comparison with the equilibrium method and limited field data, to over predict the beneficial effects of stone columns in reducing settlement.

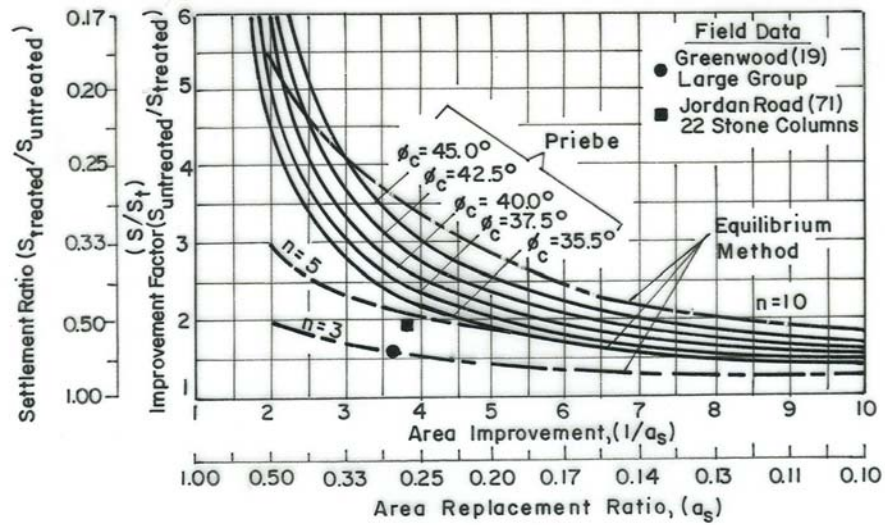


Figure 2.4 Settlement reduction due to stone column- Priebe and Equilibrium Methods (Barksdale and Bachus, 1983).

Later Priebe (1995) considered the compressibility of the backfill material and recommended the additional amount on the area ratio  $\Delta(A/A_c)$  depending on the ratio of the constrained moduli  $D_c/D_s$  which can be readily taken from Figure 2.5. Priebe (1995) also stated that weight of the columns and of the soil has to be added to the external loads. Under consideration of these additional loads (overburden), he defined the depth factor,  $f_d$  and illustrated in Figure 2.6. The improvement ratio  $n_0$  (corrected for consideration of the column compressibility, Fig. 2.5) should be multiplied by  $f_d$ .

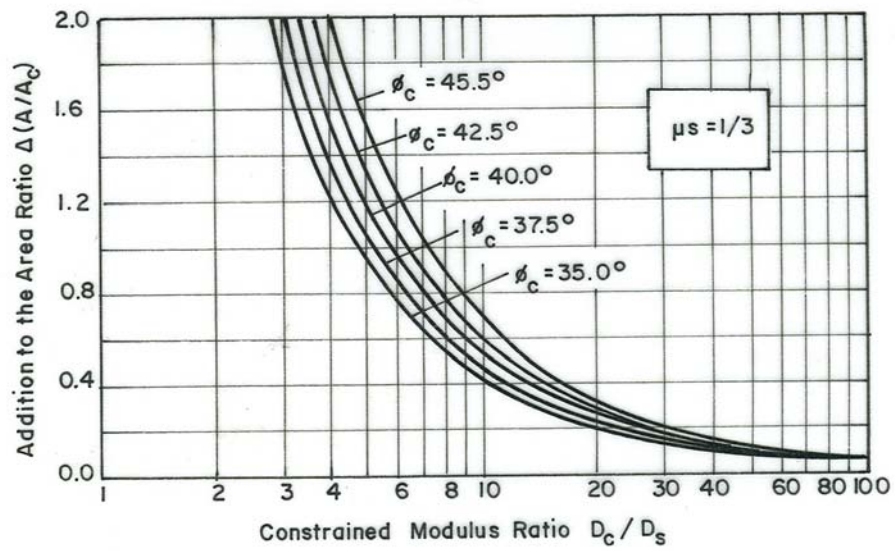


Figure 2.5 Consideration of column compressibility (Priebe, 1995)

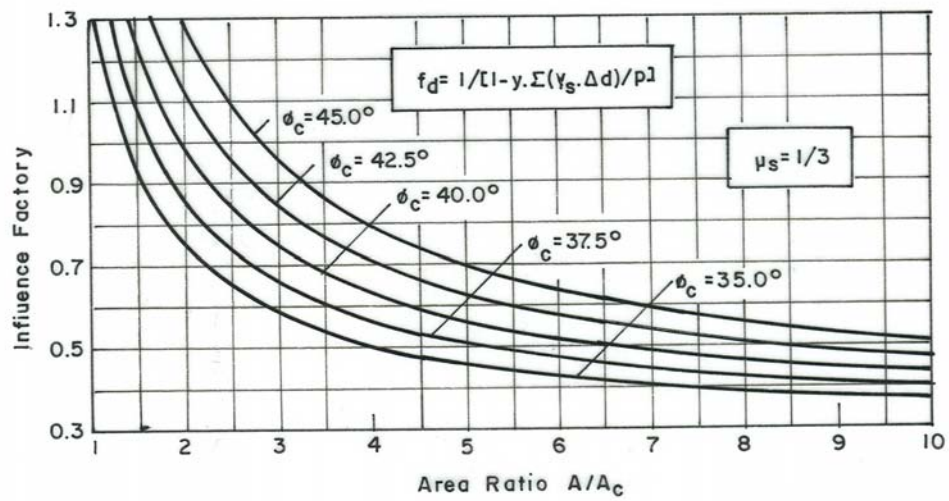


Figure 2.6 Determination of the depth factor (Priebe, 1995)

Due to the compressibility of the backfill material, the depth factor reaches a maximum value, which can be taken from the diagram given by Priebe (1995) in Figure 2.7.

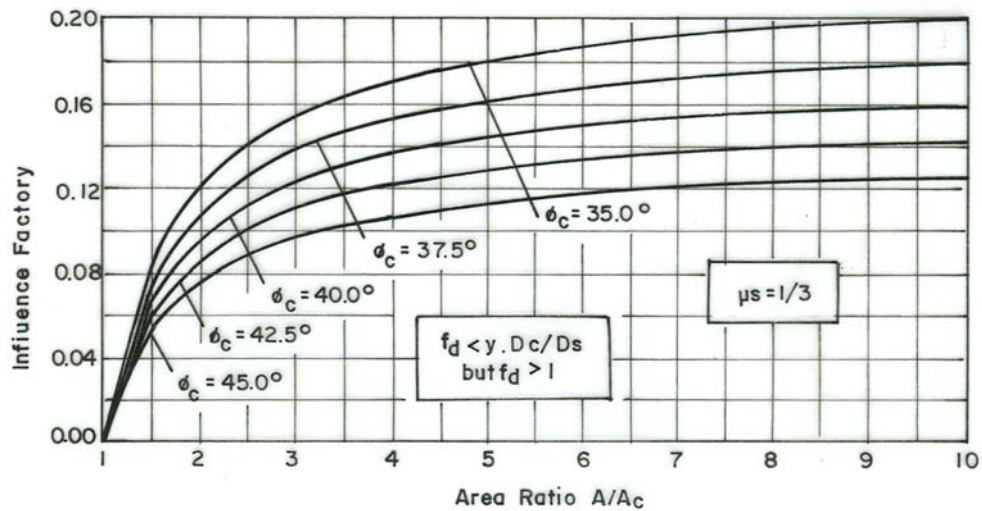
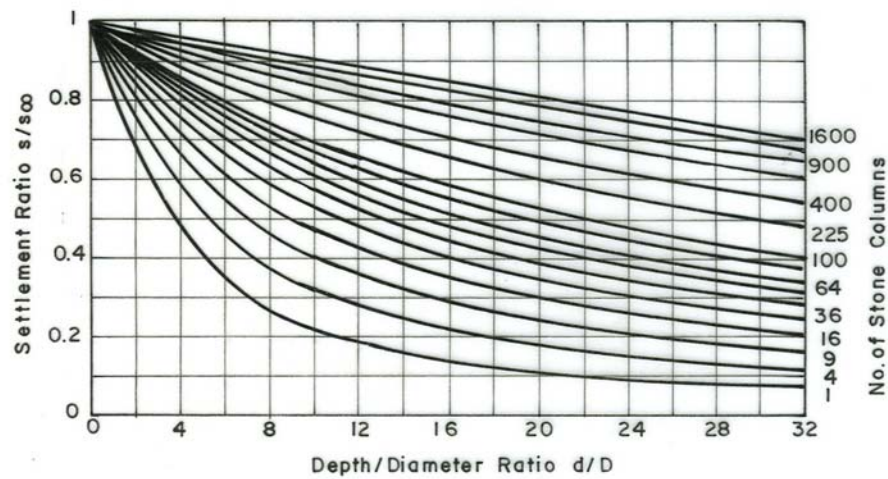
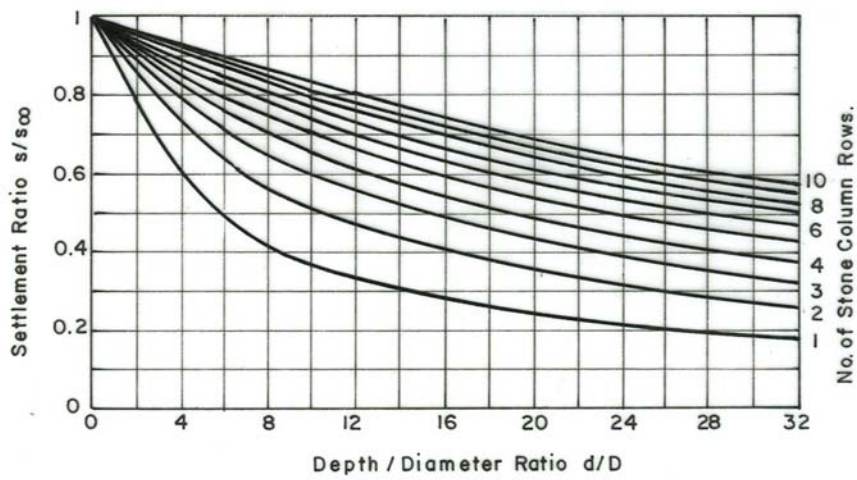


Figure 2.7 Limit value of the depth factor (Priebe, 1995)

The basic system of Priebe's Method discussed so far assumes improvement by a large grid of stone columns. Accordingly, it provides the reduction in the settlement of large slab foundation. For small foundations, Priebe (1995) offers diagrams, given in Figure 2.8a and 2.8b, which allow a simple way to determine the settlement performance of isolated single footings and strip foundations from the performance of a large grid. The diagrams are valid for homogeneous conditions only and refer to settlement  $s$  down to a depth  $d$  which is the second parameter counting from foundation level.



(a)



(b)

Figure 2.8 Settlement of small foundations a) for single footings b) for strip footings (Priebe, 1995)

## 2.4 Greenwood Method

Greenwood (1970) has presented empirical curves, which are based on field experience, giving the settlement reduction due to ground improvement with stone columns as a function of undrained soil strength and stone column spacing. These curves have been replotted by Bachus and Barksdale (1989) and presented in Figure 2.9 using area ratio and improvement factor rather than column spacing and settlement reduction as done in the original curves. The

curves neglect immediate settlement and shear displacement and columns assumed resting on firm clay, sand or harder ground. In replotting the curves a stone column diameter of 0.9m was assumed for the  $c_u = 40 \text{ kN/m}^2$  upper bound curve and a diameter of 1.07m for the  $c_u = 20 \text{ kN/m}^2$  lower bounds curve. Also superimposed on the figure is the equilibrium method upper bounds solution, Equation 2.10 for stress concentration factors of 3, 5, 10 and 20. The Greenwood curve for vibro-replacement and shear strength of  $20 \text{ kN/m}^2$  generally corresponds to stress concentration factors of about 3 to 5 for the equilibrium method and hence appears to indicate probable levels of improvement for soft soils for area ratio less than about 0.15. For firm soils and usual levels of ground improvement ( $0.15 \leq a_s \leq 0.35$ ), Greenwood's suggested improvement factors on Figure 2.9 appear to be high. Stress concentration  $n$  decreases as the stiffness of the ground being improved increases relative to the stiffness of the column. Therefore, the stress concentration factors greater than 15 required developing the large level of improvement is unlikely in the firm soil.

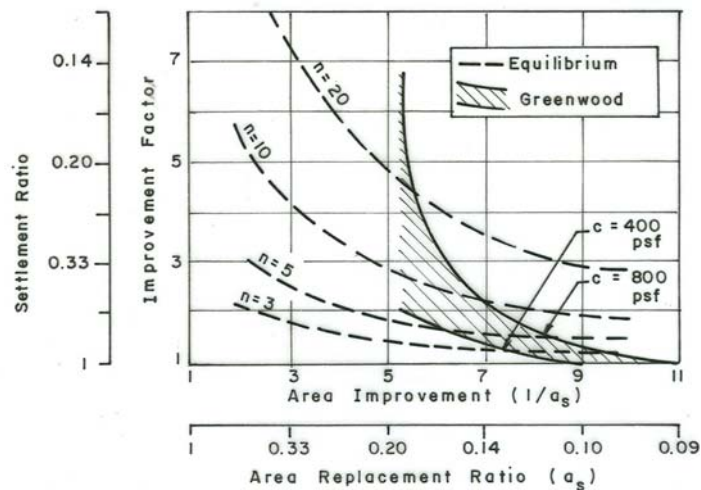


Figure 2.9 Comparison of Greenwood and Equilibrium Methods for predicting settlement of stone column reinforced soil (Bachus and Barksdale, 1989)

## 2.5 Incremental Method

The method for predicting settlement developed by Goughnour and Bayuk (1979b) is an important extension of methods presented earlier by Hughes et al. (1975), Bauman and Bauer (1974). The unit cell model is used together with an incremental, iterative, elastic-plastic solution. The loading is assumed to be applied over a wide area. The stone is assumed to be incompressible so that all volume change occurs in the clay. Both vertical and radial consolidations are considered in the analysis. The unit cell is divided into small, horizontal increments. The vertical strain and vertical and radial stresses are calculated for each increment assuming all variables are constant over the increment.

Both elastic and plastic responses of the stone column are considered. If stress levels are sufficiently low the stone column remains in the elastic range. For most design stress levels, the stone column bulges laterally yielding plastically over at least a portion of its length. Because of the presence of the rigid unit cell boundaries, a contained state of plastic equilibrium of the stone column in general exists.

The assumption is also made that the vertical and, radial and tangential stresses at the interface between the stone and soil are principle stresses. Therefore no shear stresses are assumed to act on the vertical boundary between the stone column and the soil. Both Goughnour and Bayuk (1979b) and Barksdale and Bachus (1983) noted that because of the occurrence of relatively small shear stresses at the interface (generally less than about 10 to 20 kN/m<sup>2</sup>), this assumption appears acceptable.

In the elastic range the vertical strain is taken as the increment of vertical stress divided by the modulus of elasticity. The apparent stiffness of the material in the unit cell should be equal to or greater than that predicted by dividing the vertical stress by the modulus of elasticity since some degree of constraint is provided by the boundaries of the unit cell. The vertical strain calculated by

this method therefore tends to be an upper (conservative) bound in the elastic range.

Upon failure of the stone within an increment; the usual assumption (Hughes and Withers, 1974, Bauman and Bauer, 1974, Aboshi et.al. 1979) is made that the vertical stress in the stone equals the radial stress in the clay at the interface times the coefficient of passive pressure of the stone. Radial stress in the cohesive soil is calculated following the plastic theory considering equilibrium within the clay. This gives the change in radial stress in the clay as a function of the change in vertical stress in the clay, the coefficient of lateral stress in the clay applicable for the stress increment, the geometry and the initial stress state in the clay. In solving the problem the assumption is made that when the stone column is in a state of plastic equilibrium the clay is also in a plastic state.

Radial consolidation of the clay is considered using a modification of Terzaghi one-dimensional consolidation theory. Following this approach the Terzaghi one-dimensional equations are still utilized, but the vertical stress in the clay is increased to reflect greater volume change due to radial consolidation. For typical lateral earth pressure coefficients, this vertical stress increase is generally less than about 25 percent, the stress increasing with an increase in the coefficient of lateral stress applicable for the increment in stress under consideration.

For a realistic range of stress levels and other conditions the incremental method was found to give realistic results.

## **2.6 Granular Wall Method**

A simple way of estimating the improvement of the settlement behavior of a soft cohesive layer due to the presence of stone columns has been presented by Van Impe and De Beer (1983) by considering the stone columns to deform, at their limit of equilibrium, at constant volume. The only parameters to be

known are the geometry of the pattern of the stone columns, their diameter, the angle of shearing strength of the stone material, the oedometer modulus of the soft soil and its Poisson's ratio. They also presented a diagram for estimating effective vertical stress in the stone material.

In order to express the improvement on the settlement behavior of the soft layer reinforced with the stone columns, the following parameters are defined:

$$m = \frac{F_1}{F_{\text{tot}}} = \alpha \frac{\sigma'_{v,1}}{P_0} \quad (2.14)$$

$$\beta = \frac{S_v}{S_{v,0}} \quad (2.15)$$

where  $F_1$  = the vertical load transferred to the stone column  
 $F_{\text{tot}}$  = the total vertical load on the area a, b (Fig. 2.10).  
 $S_v$  = the vertical settlement of the composite layer of soft cohesive soil and stone columns  
 $S_{v,0}$  = the vertical settlement of the natural soft layer without stone columns

In Figure 2.11, the relationship between m and  $\alpha$  is given for different values of  $\phi_1$  and for chosen values of the parameters  $P_0/E$  and  $\mu$ .

In the Figure 2.12, the  $\beta$  (settlement improvement factor) values as a function of  $\alpha$  are given for some combination of  $P_0/E$  and  $\mu$  and for different  $\phi_1$  values.

The vertical settlement of the composite layer of soft cohesive soil and stone columns,  $s_v$  is expressed as:

$$s_v = \beta H (1 - \mu^2) \left[ 1 - \frac{\mu^2}{1 - \mu^2} \right] \frac{P_0}{E} \quad (2.16)$$

where  $\beta = f(a, b, \phi_s, \mu, P_0/E)$ , obtained from Fig. 2.10  
 $\mu$  = Poisson's ratio of the soft soil  
 $\phi_1$  = angle of shearing strength of the stone material  
 $E$  = oedometer modulus of the soft soil  
 $P_0$  = vertical stress

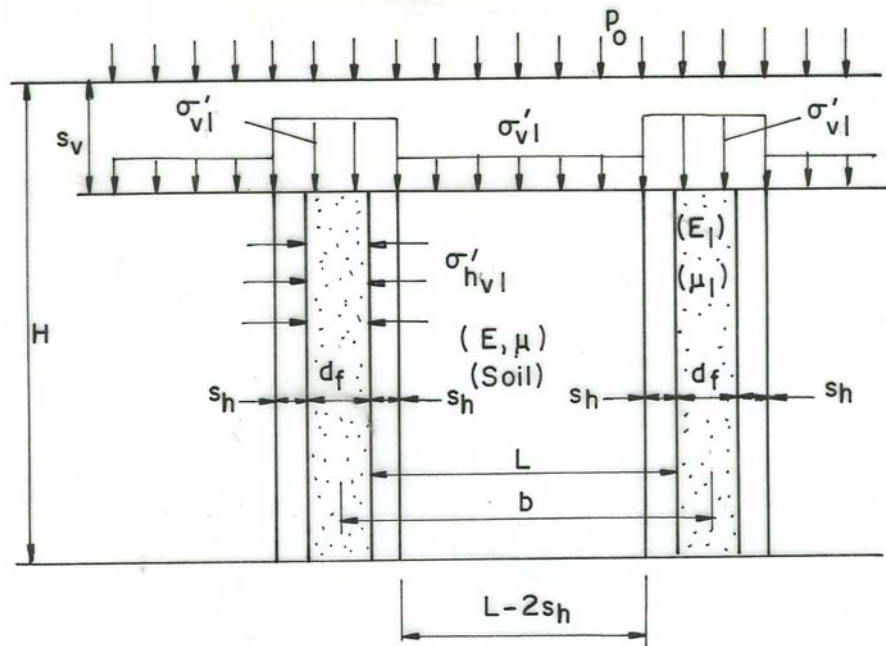


Figure 2.10 Definitions for Granular Wall Method  
 (Van Impe and De Beer, 1983)

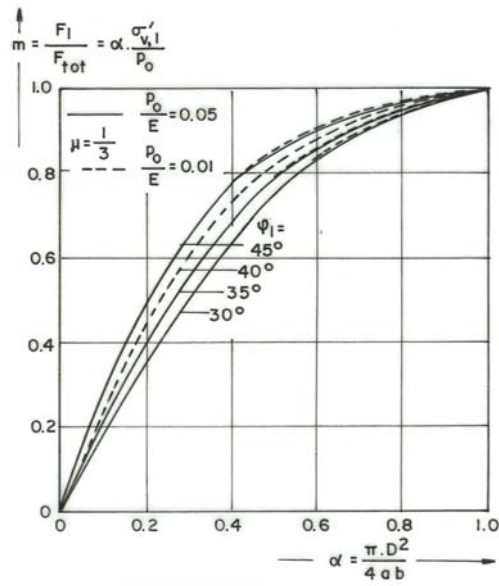


Figure 2.11 Stress distribution of stone columns (Van Impe and De Beer, 1983)

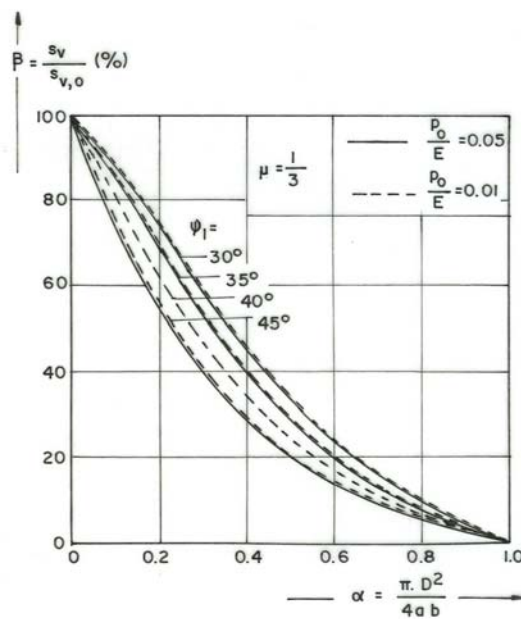


Figure 2.12 Improvement on the settlement behavior of the soft layer reinforced with the stone columns (Van Impe and De Beer, 1983)

## 2.7 Finite Element Method

The finite element method offers the most theoretically sound approach for modeling stone column improved ground. Nonlinear material properties, interface slip and suitable boundary conditions can all be realistically modeled using the finite element technique. Although 3-D modeling can be used, from a practical standpoint either axisymmetric or plane strain model is generally employed. Most studies have utilized the axisymmetric unit cell model to analyze the conditions of either uniform load on a large group of stone columns (Balaam et.al. 1977, Balaam and Booker, 1981) or a single stone column (Balaam and Poulos, 1983); Aboshi et.al.(1979) have studied a plane strain loading condition.

Balaam et.al.(1977) analyzed large groups of stone columns by finite elements using the unit cell concept. Undrained settlements were found to be small and neglected. The ratio of modulus of the stone to that of the clay was assumed to vary from 10 to 40, and the Poisson's ratio of each material was assumed to be 0.3. A coefficient of at rest earth pressure  $K_0 = 1$  was used. Only about 6% difference in settlement was found between elastic and elastic-plastic response. The amount of stone column penetration into the soft layer and the diameter of the column were found to have a significant effect on settlement (Figure 2.13); the modular ratio of stone column to soil was of less importance.

Balaam and Poulos (1983) found for a single pile that slip at the interface increases settlement and decreases the ultimate load of a single pile. Also assuming adhesion at the interface equal to the cohesion of the soil gave good results when compared to those obtained from field measurements.

Balaam and Booker (1981) found, for the unit cell model using linear elastic theory for a rigid loading (equal vertical strain assumption), that vertical stresses were almost uniform on horizontal planes in the stone column and also uniform in the cohesive soil. Also stress state in the unit cell was essentially

triaxial. Whether the underlying firm layer was rough or smooth made little difference. Based upon these findings, a simplified, linear elasticity theory was developed and design curves were given for predicting performance. Their analysis indicates that as drainage occurs, the vertical stress in the clay decreases and the stress in the stone increases as the clay goes from the undrained state. This change is caused by a decrease with drainage both the modulus and Poisson's ratio of the soil.

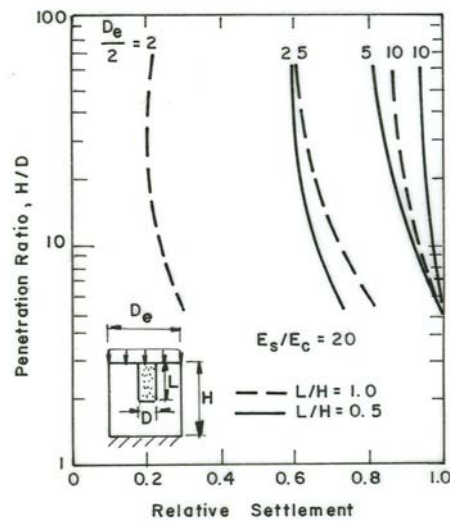


Figure 2.13 Effect of stone column penetration length on elastic settlement  
(Balaam et.al., 1977)

Barksdale and Bachus (1983) presented some design curves for predicting primary consolidation settlement. The finite element program was used in their study. For a nonlinear analysis load was applied in small increments and computation of incremental and total stresses were performed by solving a system of linear, incremental equilibrium equations for the system.

Curves for predicting settlement of *low compressibility soils* such as stone column reinforced sands, silty sands and some silts were developed using

linear elastic theory. Low compressibility soils are defined as those soils having modular ratios  $E_s/E_c \leq 10$  where  $E_s$  and  $E_c$  are the average modulus of elasticity of the stone column and soil, respectively. The settlement curves for area ratios of 0.1, 0.15 and 0.25 are given in Figure 2.14.

The elastic finite element study utilizing the unit cell model shows a nearly linear increase in stress concentration in the stone column with increasing modular ratio (Figure 2.15, Barksdale and Bachus, 1983). The approximate linear relation exists for area replacement ratios  $a_s$  between 0.1 and 0.25, and length to diameter ratios varying from 4 to 20. For a modular ratio  $E_s/E_c$  of 10, a stress concentration factor  $n$  of 3 exists. For modular ratios greater than about 10, Barksdale and Bachus (1983) noted that elastic theory underestimates drained settlements due to excessively high stress concentration that theory predicts to occur in the stone and lateral spreading in soft soils. For large stress concentrations essentially all of the stress according to elastic theory is carried by stone column. Since the stone column is relatively stiff, small settlements are calculated using elastic theory when using excessively high stress concentrations.

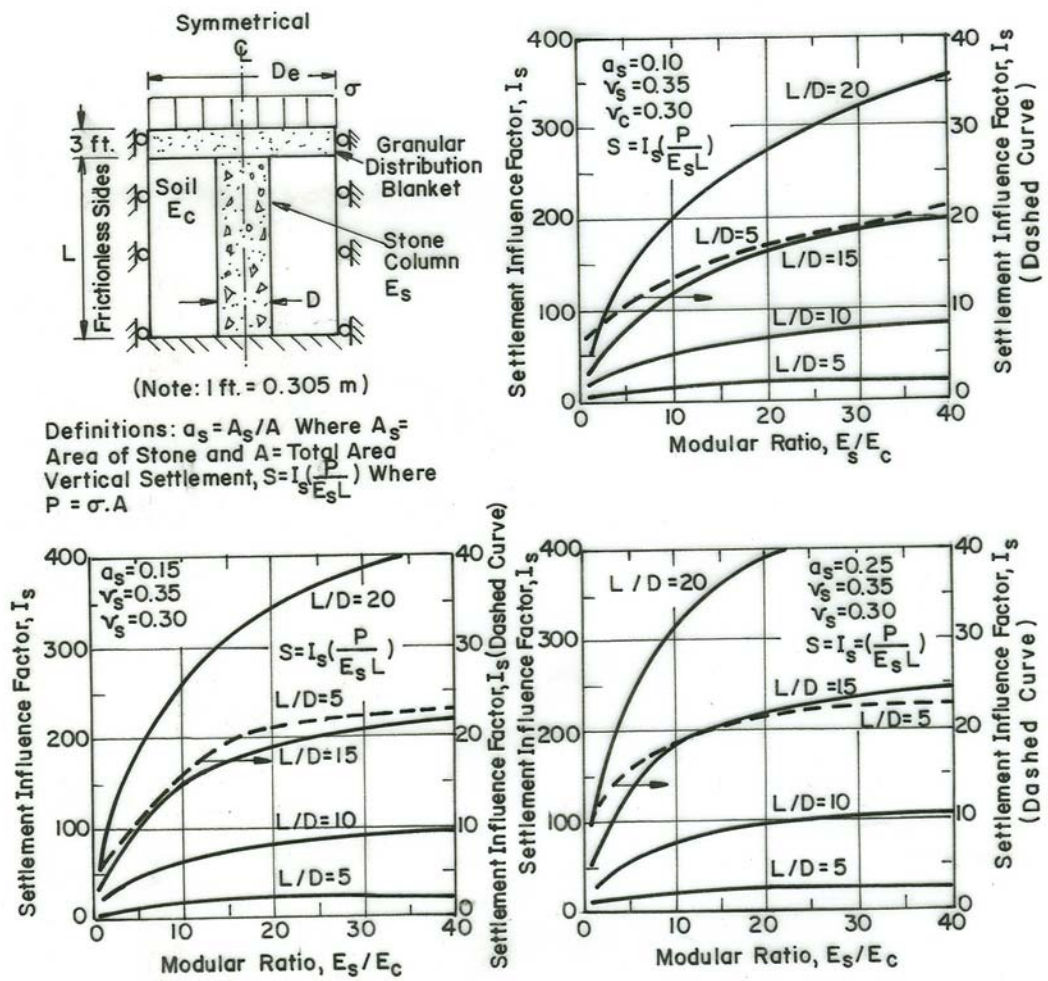


Figure 2.14 Notations used in unit cell linear elastic solutions and linear elastic settlement influence factors for area ratios,  $a_s = 0.10, 0.15, 0.25$  (Barksdale and Bachus, 1983).

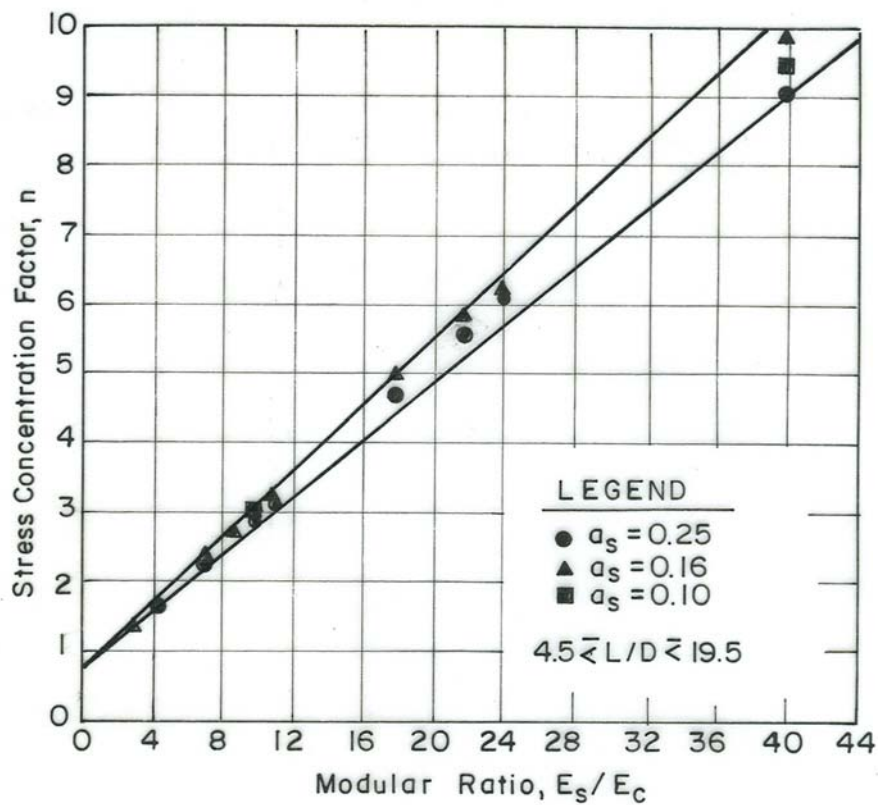


Figure 2.15 Variation of stress concentration factor with modular ratio- Linear elastic analysis (Barksdale and Bachus, 1983)

To calculate the consolidation settlement in *compressible cohesive soils* ( $E_s/E_c \geq 10$ ), design curves were developed assuming the clay to be elastic-plastic and the properties of the stone to be stress dependent (non-linear stress-strain properties). The non-linear stress-strain properties were obtained from the results of 305mm diameter triaxial test results. In soft clays not reinforced with stone columns, it was observed that lateral bulging can increase the amount of vertical settlement beneath the fill by as much as 50 percent. Therefore, to approximately simulate lateral bulging effects, a soft boundary was placed around the unit cell to allow lateral deformation. Based on the field measurements, a boundary 25mm thick having an elastic modulus of 83 kN/m<sup>2</sup> was used in the model, which causes maximum lateral deformations due to

lateral spreading, which should occur across the unit cell. To obtain the possible variation in the effect of boundary stiffness (lateral spreading), a relatively rigid boundary was also used, characterized by a modulus of 6900 kN/m<sup>2</sup>.

The unit cell model and notation used in the analysis is summarized in Figure 2.16. The design charts developed using this approach is presented in Figure 2.17. Settlement is given as a function of the uniform, average applied pressure  $\sigma$  over the unit cell, modulus of elasticity of the soil  $E_c$ , area replacement ratio  $a_s$ , length to diameter ratio,  $L/D$ , and boundary rigidity. The charts were developed for a representative angle of internal friction of the stone  $\phi_s = 42^\circ$ , and a coefficient of at rest earth pressure  $K_0$  of 0.75 for both the stone and soil. For soils having a modulus  $E_c$  equal to or less than 1100 kN/m<sup>2</sup>, the soil was assumed to have a shear strength of 19 kN/m<sup>2</sup>. Soils having greater stiffness did not undergo an interface or soil failure; therefore, soil shear strength did not affect the settlement.

Figure 2.18 is given by Barksdale and Bachus (1983), which shows the theoretical variation of the stress concentration factor  $n$  with the modulus of elasticity of the soil and length to diameter ratio,  $L/D$ . Stress concentration factors in the range of about 5 to 10 are shown for short to moderate length columns reinforcing very compressible clays ( $E_c < 1380$  to 2070 kN/m<sup>2</sup>). These results conclude that the nonlinear theory may predict settlements smaller than those observed (Barksdale and Bachus, 1983).

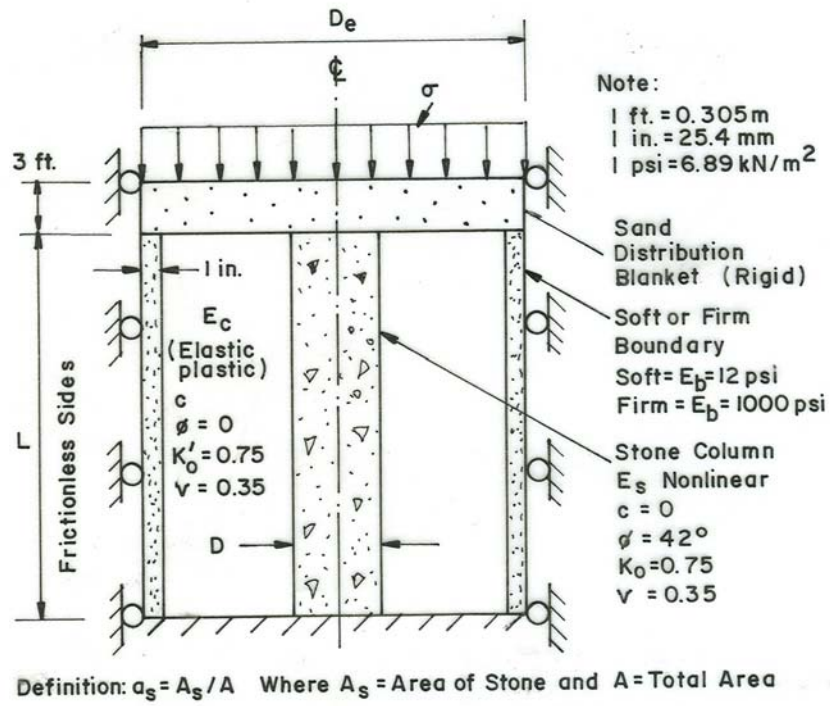


Figure 2.16 Notation used in unit cell nonlinear solutions given in Figure 2.17

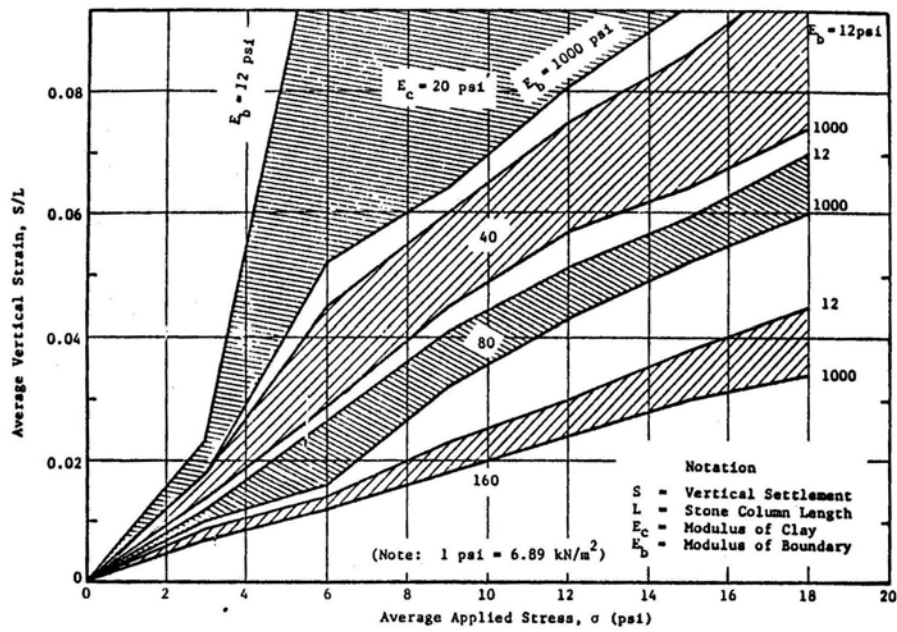
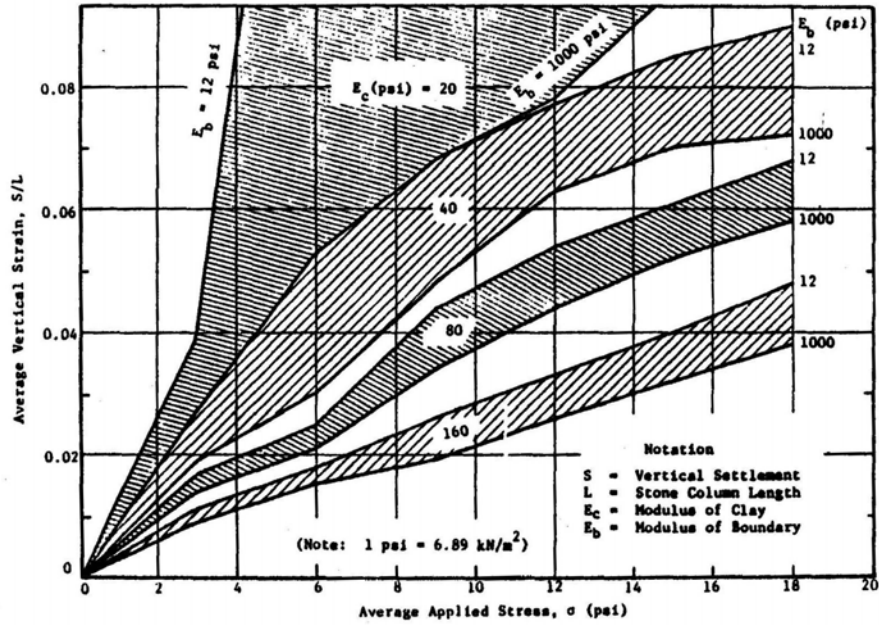


Figure 2.17 Nonlinear Finite Element unit cell settlement curves (Barksdale and Bachus, 1983).

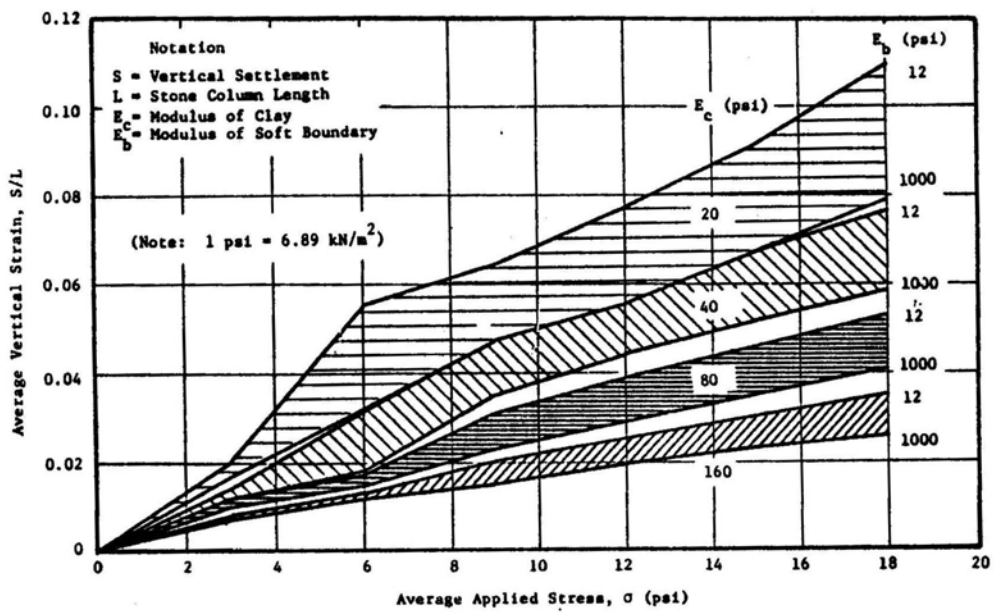
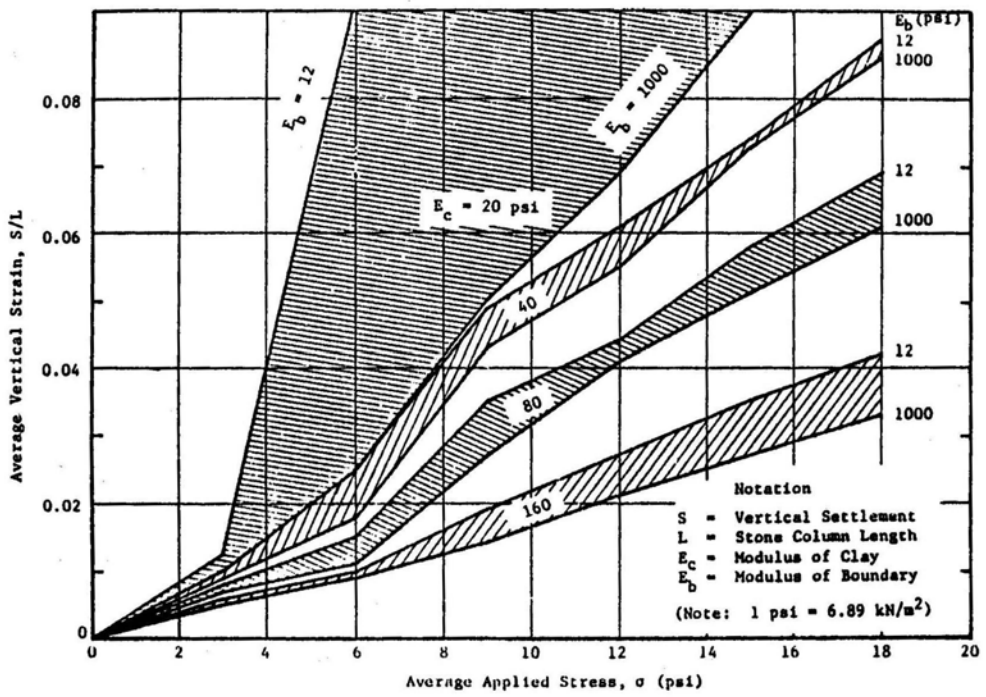
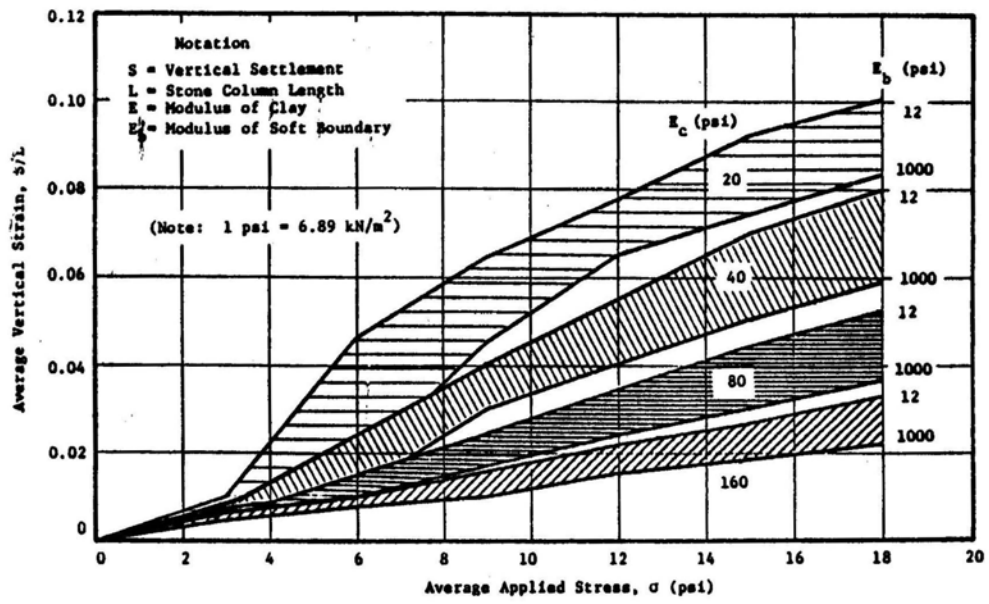
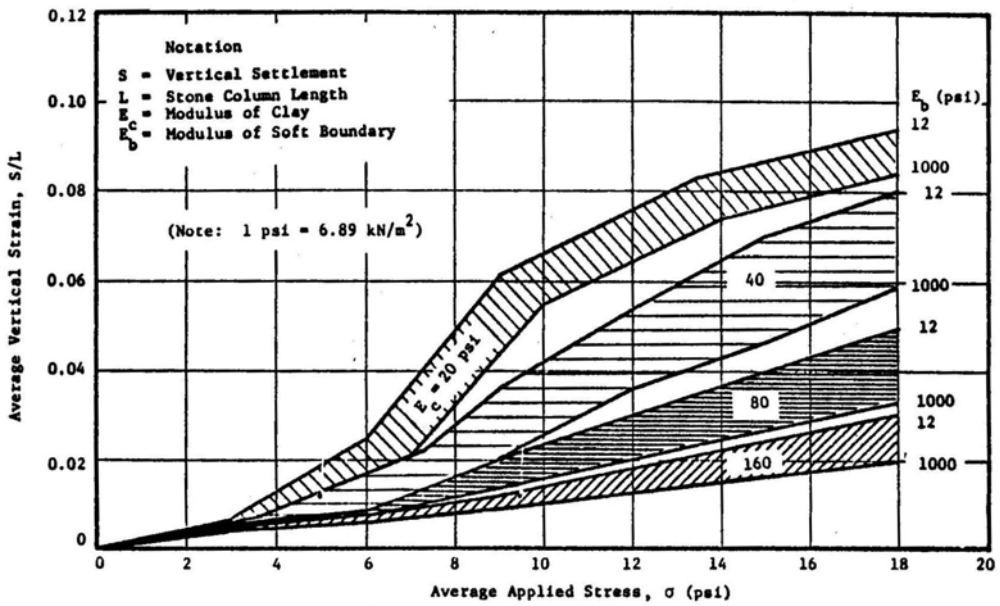


Figure 2.17 (Cont.)

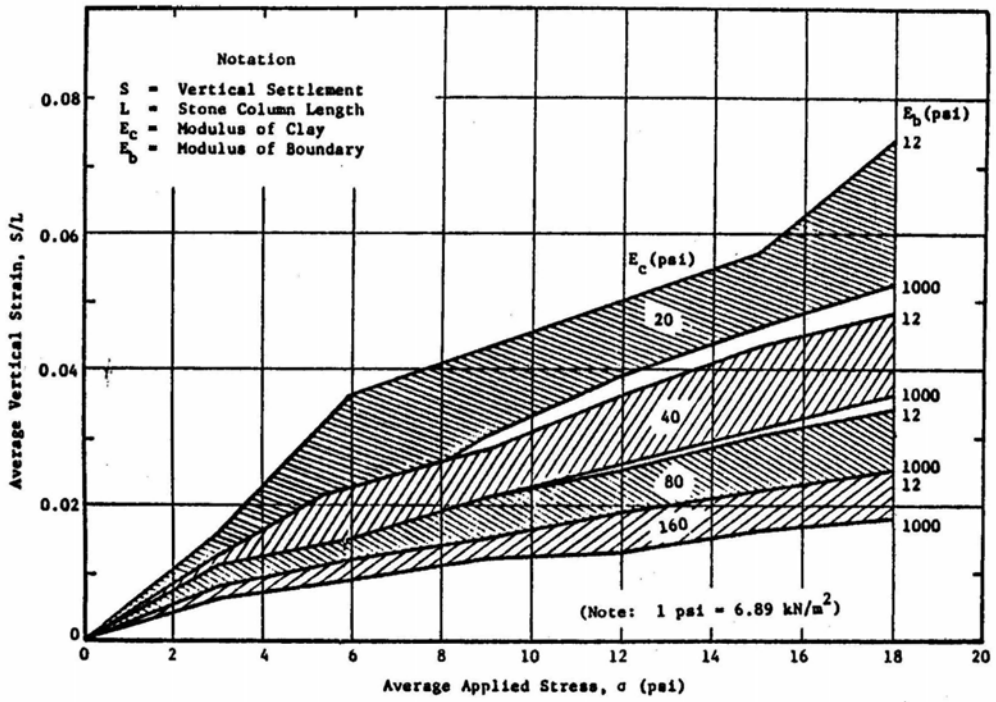


$a_s = 0.25, L/D = 10$

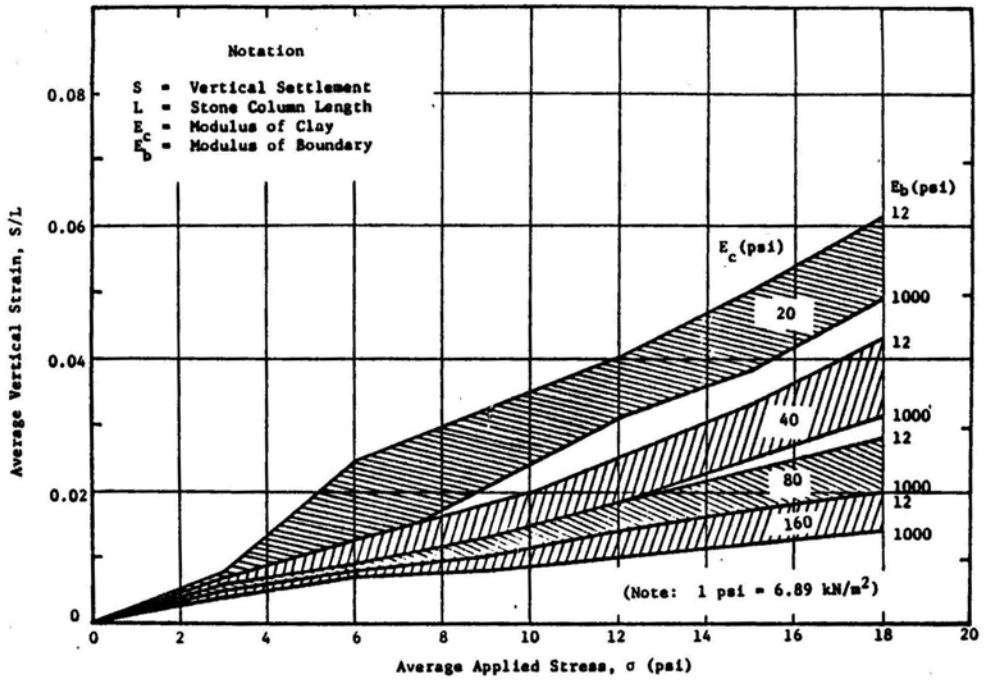


$a_s = 0.25, L/D = 20$

Figure 2.17 (Cont.)

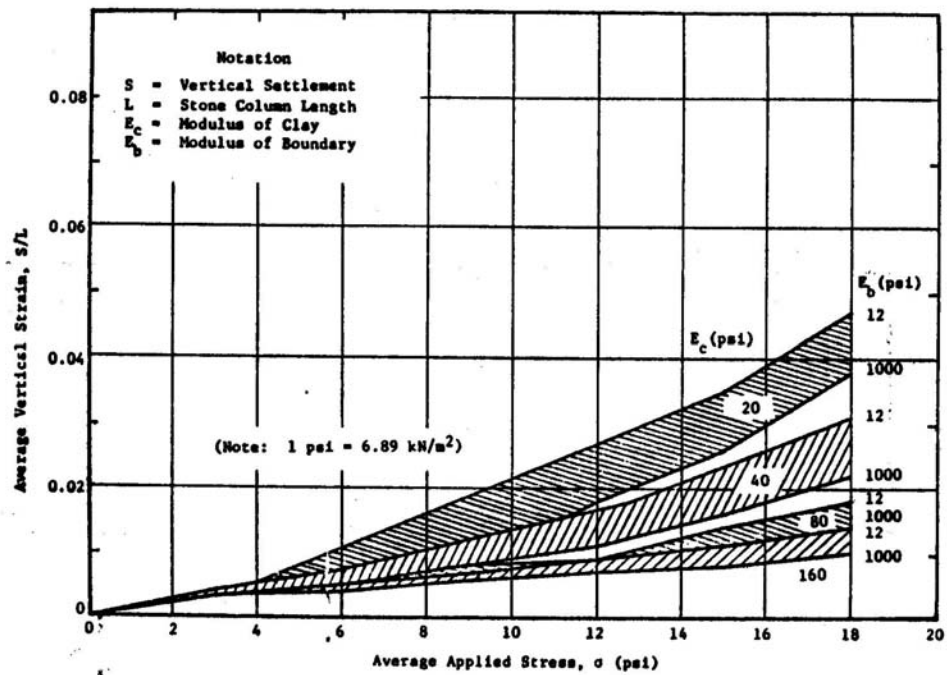


$a_s = 0.35, L/D = 5$



$a_s = 0.35, L/D = 10$

Figure 2.17 (Cont.)



$a_s = 0.35, L/D = 20$

Figure 2.17 (Cont.)

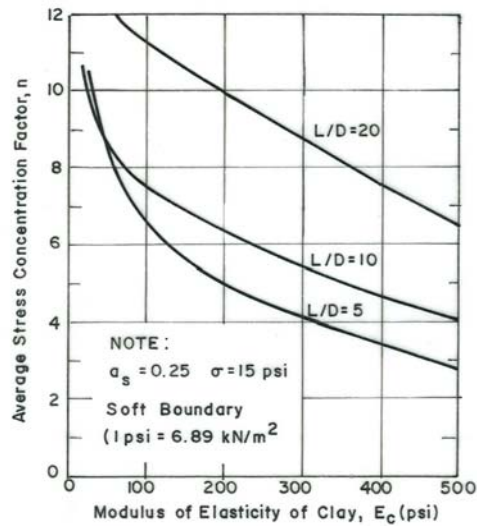


Figure 2.18 Variation of stress concentration with modular ratio-nonlinear analysis (Barksdale and Bachus, 1983)

Ambily and Gandhi (2007) carried out experimental and finite element analyses to study the effect of shear strength of soil, angle of internal friction of stones, and spacing between the stone columns on the behavior of stone columns. Model experiments were carried out on a 100mm diameter stone column surrounded by soft clay in cylindrical tanks of 500mm high and a diameter varying from 210 to 835mm to represent the required unit cell area of soft clay around each column assuming triangular pattern of installation of columns. For single column tests the diameter of the tank was varied from 210 to 420mm and for group tests on 7 columns, 835mm diameter was used. Tests had been carried out with shear strength of 30, 14, and 7 kPa. The stone column was extended to the full depth of the clay placed in the tank for a height of 450mm so that L/D ratio was 4.5.

Finite element program PLAXIS was used to simulate the results of the model tests and to carry out further parametric analyses. Axisymmetric analyses were carried out using Mohr-Coulomb's criterion considering elastoplastic behavior for soft clay and stones. Load settlement curves obtained from finite element analyses usually match well with the measured values from the model tests. As a result of the finite element analyses carried out in line with the model tests the following conclusions were drawn:

- Single column behavior with a unit cell concept can simulate the field behavior for an interior column when a large number of columns is simultaneously loaded.
- Stiffness improvement factor was found to be independent of the shear strength of surrounding clay. (Figure 2.19)
- Stiffness improvement factor depends mainly on column spacing and on the angle of internal friction of the stones. (Figure 2.20) Improvement factor increases with decreasing column spacing and increasing internal angle of friction of stones. For column spacing to diameter of stone column ratios of  $s/d$  greater than 3, there is no significant improvement in the stiffness.
- Figure 2.21 compares the stiffness improvement factor obtained from this study with the existing theories such as Priebe (1995) and Balaam et.al. (1977)

for different area ratio (area of unit cell/area of stone column) and angle of internal friction of stones. It can be concluded that, this study predicts a slightly higher stiffness improvement factor for an area ratio more than 4 and a lower value for an area ratio less than 4 compared to Priebe (1995).

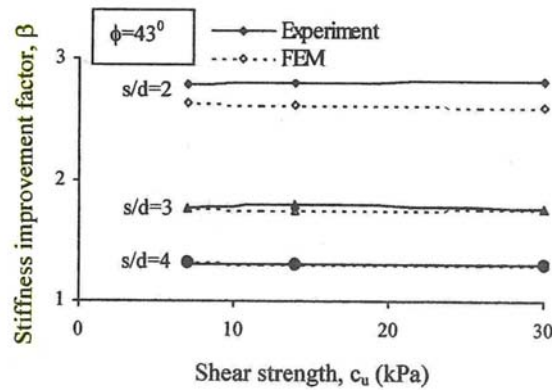


Figure 2.19 Effect of  $c_u$  on stiffness improvement factor (Ambily and Gandhi, 2007)

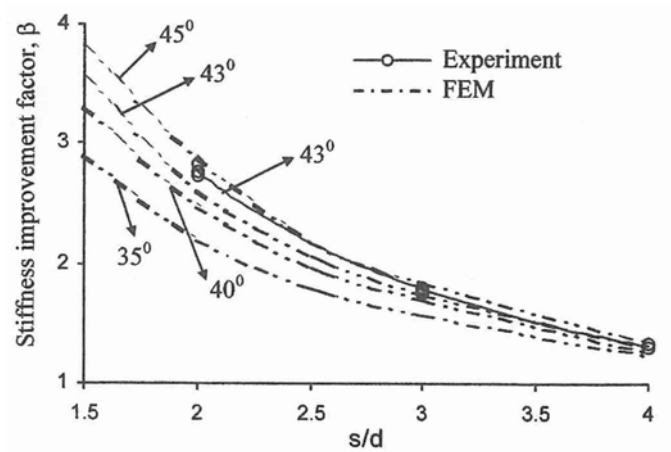


Figure 2.20 Effect of  $s/d$  and  $\phi$  on stiffness improvement factor (Ambily and Gandhi, 2007)

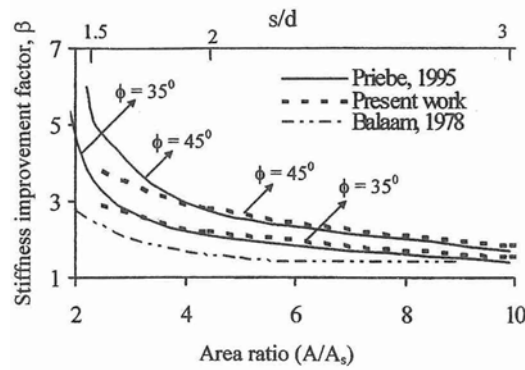


Figure 2.21 Comparison of stiffness improvement factor with existing theories (Ambily and Gandhi, 2007)

Clemente et.al. (2005) carried out three-dimensional numerical analyses, using the finite difference software FLAC-3D to numerically develop relationships between settlement improvement factor (IF) and area ratio (ARR) that take into account the actual subsurface and stone column mechanical properties, as well as the effects of bearing pressure and foundation size. The geometry consisted of square spacing of stone columns with different  $s/d$  (1.5, 2.0 and 3.0) and  $L/d$  (3.0, 6.0 and 9.0) ratios, loaded by rigid square footings of different sizes. Finite difference mesh terminated at the tip of the stone columns, hence the columns were end-bearing. Both the soil and stone columns are modeled as Mohr Coulomb materials having a modulus ratio of  $E_c/E_s = 6.9$ . Settlement improvement factor (IF) versus area ratio (ARR) graphs obtained from the results of the 3-D finite difference analyses are shown in Figures 2.22, 2.23 and 2.24 for different stone column groups. Comparison with one of the existing theories, i.e. Priebe (1993), is also present on the figures. As can be seen from the figures the settlement improvement factor decreases with increasing area ratio, and the decrease in improvement is negligible after a certain area ratio level. Another important calculation derived from this study is the bearing stress dependence of the improvement factor. The improvement factor tends to increase with increasing bearing pressure.

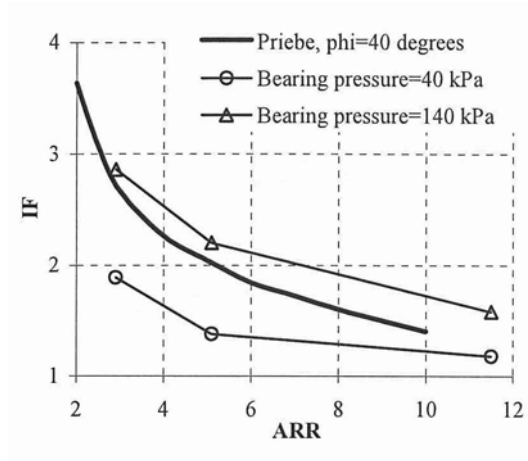


Figure 2.22 Comparison of Priebe 1993 and FLAC IF (improvement factor) versus ARR (area ratio) for the 1x1 configuration (Clemente et.al., 2005)

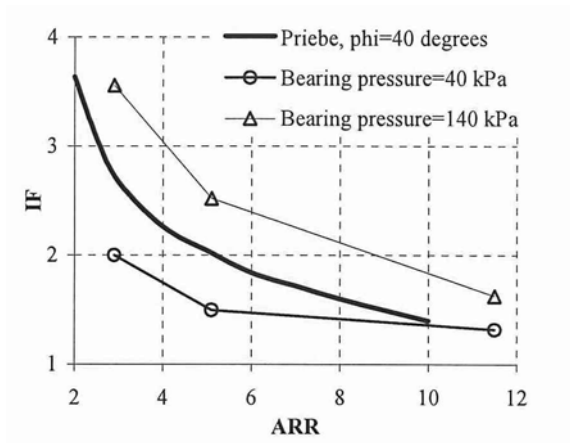


Figure 2.23 Comparison of Priebe 1993 and FLAC IF (improvement factor) versus ARR (area ratio) for the 2x2 configuration (Clemente et.al., 2005)

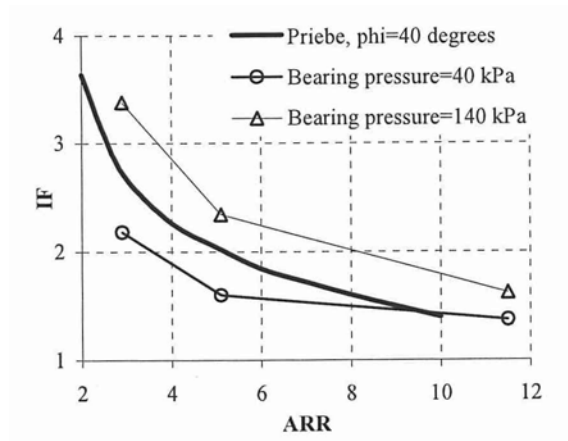


Figure 2.24 Comparison of Priebe 1993 and FLAC IF (improvement factor) versus ARR (area ratio) for the 5x5 configuration (Clemente et.al., 2005)

Domingues et.al. (2007) carried out a parametric study in an embankment on soft soils reinforced with stone columns using a computer program based on finite element method to investigate the effect of stiffness of the column material on the settlement improvement factor. Embankment height was 2.0 meters and the soft soil thickness was 5.5m. The column depth was equal to the thickness of the soft stratum. The diameter of the column was 1.0 meter and the replacement area ratio was 0.19. The unit cell formulation is used considering one column and its surrounding soil with confined axisymmetric behaviour. The computer program incorporates the Biot consolidation theory (coupled formulation of the flow and equilibrium equations) with constitutive relations simulated by the p-q- $\theta$  critical state model. As it is shown in Figure 2.25, it is concluded that the settlement improvement factor increases as the stiffness of the column increases as a result of this parametric analysis.

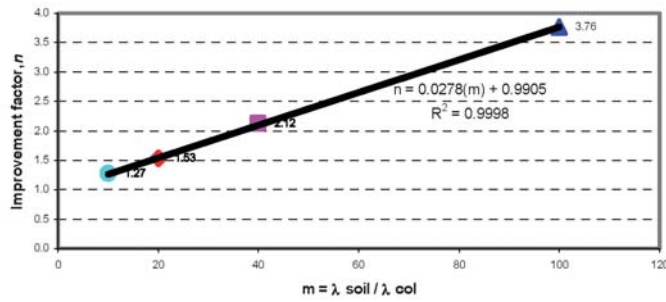


Figure 2.25 Variation of settlement improvement factor with column stiffness  
(Domingues et.al., 2007)

## 2.8 Subgrade Modulus Approach

Lawton and Fox (1994) uses the subgrade modulus approach for settlement analyses of rigid footings and rafts supported by rammed aggregate piers. They state that the total settlement under the footing is a summation of the settlement of the upper zone (UZ) and lower zone (LZ). Upper zone (UZ) is defined as the composite soil zone plus the soil beneath the composite soil zone that is densified and prestressed during the construction process. The thickness of this densified soil zone is usually assumed equal to the diameter of the rammed aggregate piers. Lower zone (LZ) is defined as the untreated soil zone below the upper zone. They state that by assuming that the footing is perfectly rigid and using the subgrade modulus, the following equations apply for calculating the upper zone settlement:

$$q_p = q \cdot R_s / (R_a \cdot R_s - R_a + 1) \quad (2.17)$$

$$q_m = q_p / R_s \quad (2.18)$$

$$S_{UZ} = q_p / k_p = q_m / k_m \quad (2.19)$$

where  $q_p$  = bearing stress applied to the aggregate piers  
 $q$  = average design bearing pressure

$q_m$  = bearing stress applied to matrix soil

$R_s$  = subgrade modulus ratio

$R_a$  = area ratio

$k_p$  = subgrade modulus for aggregate piers

$k_m$  = subgrade modulus for matrix soil

Values of subgrade moduli for the aggregate piers are determined either by static load tests on individual piers or by estimation from previously performed static load tests within similar soil conditions and similar aggregate pier materials and installation methods. Subgrade moduli for the matrix soils are either determined from static load tests or estimated from boring data and allowable bearing pressures provided by geotechnical consultants.

Özkeskin (2004) proposes a method which modifies the method given by Lawton and Fox (1994), stating that using subgrade modulus of composite soil,  $k_{comp}$ , in equation (2.19) yields better results for estimating the upper zone settlement. It is suggested that the subgrade reaction of the composite soil,  $k_{comp}$ , can be estimated from the following equations:

$$k_{comp} = a_s \cdot k_s / (1 - a_s)k_c \quad (2.20)$$

or

$$k_{comp} = n \cdot k_c \quad (2.21)$$

where  $k_{comp}$  = subgrade reaction of the composite soil

$a_s$  = area ratio

$k_s$  = subgrade reaction of the aggregate piers

$k_c$  = subgrade reaction of the native soil

Another approach to estimate the settlement of the upper zone (pier-soil composite) is presented by White et.al (2007). Their approach is to divide the footing stress by the stiffness of the pier-soil composite. They state that the stiffness of the pier-soil composite can be determined by a full scale load test

or by using a scaling relationship proposed by Terzaghi (1943) that uses the stiffness of an isolated pier to estimate the stiffness of the pier-soil composite as follows:

$$k_{\text{comp}} = k_g (B_g / B_f) \quad (2.22)$$

where  $k_{\text{comp}}$  = stiffness of the pier-soil composite  
 $B_g$  = diameter of the pier  
 $B_f$  = footing width  
 $k_g$  = stiffness of the isolated pier

Lawton and Fox (1994) state that the settlement of the lower zone can be calculated using the conventional settlement estimation methods given in the literature. For this purpose, an estimation of the applied stresses transmitted to the interface between the upper zone (UZ) and the lower zone (LZ) is needed. The authors state that, since the presence of a stiffer upper layer substantially reduces the stresses transmitted to the lower layer, the use of Boussinesq type equations are inappropriate and they usually use a modification of the 2:1 method, and use a stress dissipation slope of 1.67:1 through the upper zone (UZ) by engineering judgement. Tekin (2005) also confirms this assumption, by observing the slope of the stress dissipation to vary from 1.53:1 to 1.69:1 in her experimental study of the floating pier groups

## CHAPTER 3

### CALIBRATION OF THE FINITE ELEMENT MODEL

#### 3.1 Introduction

The finite element model that is going to be used for the parametric studies that will be presented in the proceeding chapters of this study is calibrated with the results of full-scale field load tests detailed in Özkeskin (2004). The full scale field tests consist of load tests on both untreated soil and on three different groups of rammed aggregate piers with different lengths on the same site, and therefore offers the unique opportunity of calibrating geotechnical parameters for a finite element model. Once calibrated by these field data, the finite element model can be used as a powerful tool to investigate the effect of rammed aggregate piers on different foundation geometries and material properties.

#### 3.2 Details of the Full-Scale Load Test

The test area which is approximately 10 m x 30 m is located around Lake Eymir, Ankara. Site investigation at the test area included five boreholes which are 8 m to 13.5 m in depth, SPT, sampling and laboratory testing, and four CPT soundings. (Figure 3.1) The borehole, CPT logs and laboratory test results are presented at Appendix A.

The variation of SPT-N values with depth is given in Figure 3.2. It can be seen that, N values are in the range of 6 to 12 with an average of 10 in the first 8 m, after 8 m depth, N values are greater than 20.

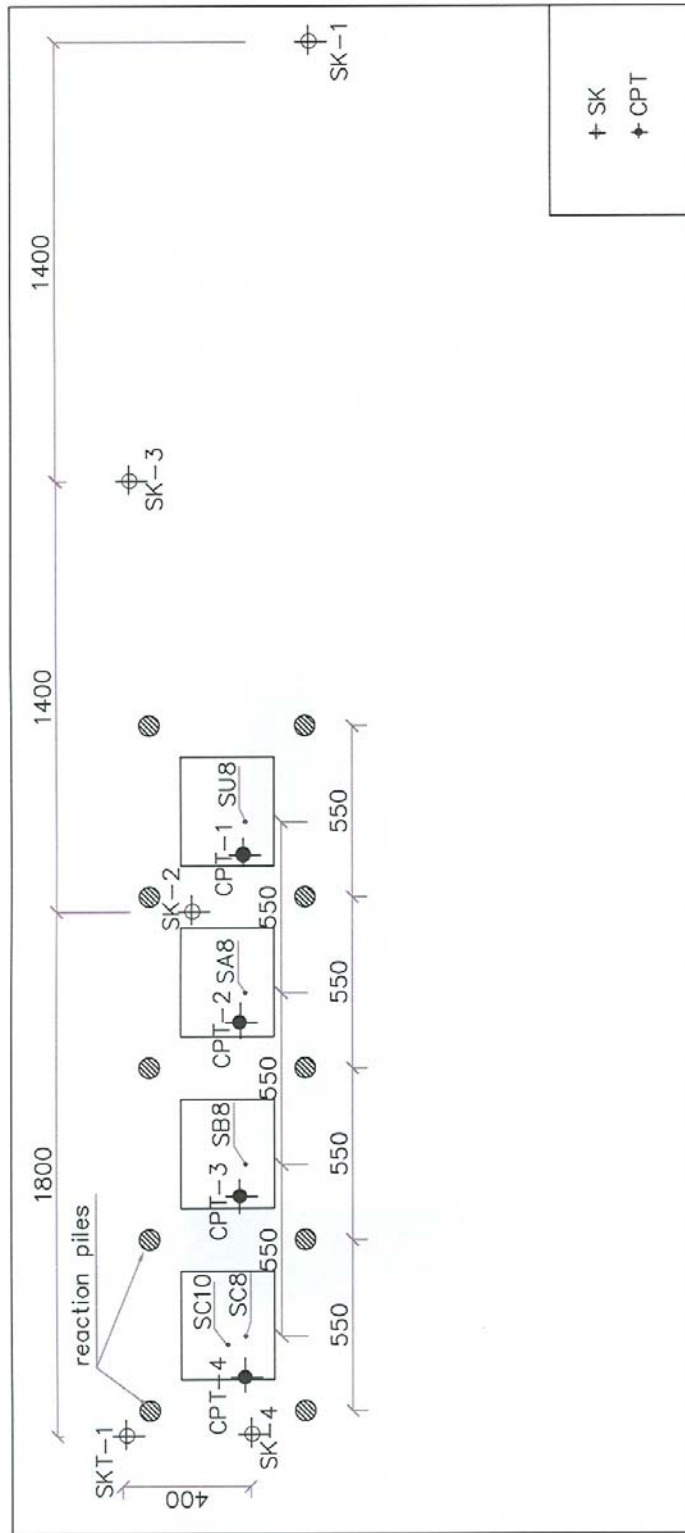


Figure 3.1 Location of investigation boreholes and CPT soundings at the load test site (Özkeskin, 2004)

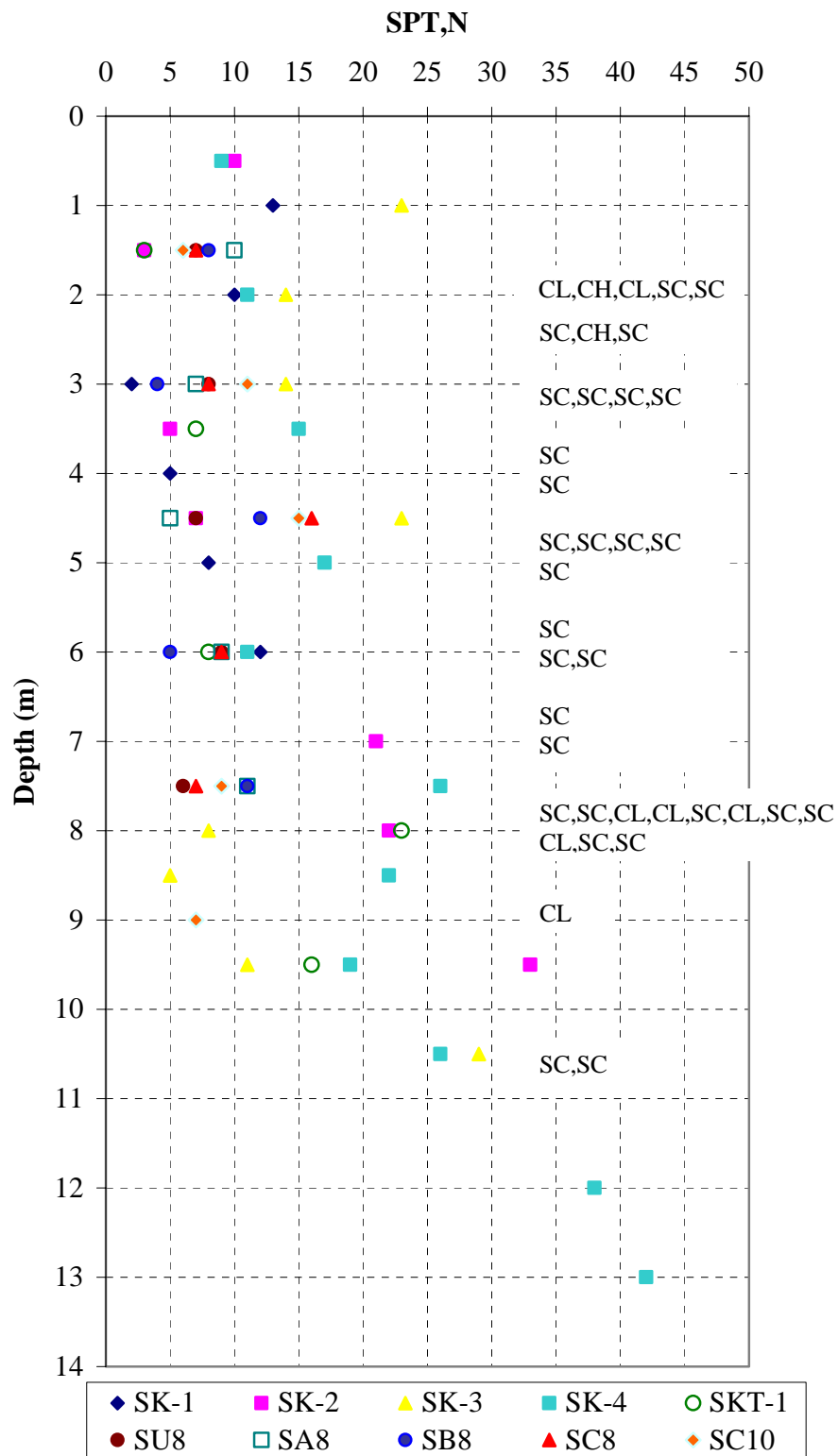


Figure 3.2 Variation of SPT N values with depth at the load test site (Özkeskin, 2004)

Based on the laboratory test results, the compressible layer, first 8 m, is classified as CL and SC according to USCS. The fine and coarse content of the compressible layer change in the range of 25% to 40% and 10% to 25% respectively. As liquid limit of the compressible layer changes predominantly in the range of 27% to 43% with an average of 30%, the plastic limit changes in the range of 14% to 20% with an average of 15%.

Based on the CPT soundings, the average of the tip and friction resistance of the compressible soil strata can be taken as 1.1 MN/m<sup>2</sup> and 53 kN/m<sup>2</sup>, respectively. The variation of soil classification based on CPT correlations is given in Figure 3.3.

The bearing stratum under the weak stratum is weathered graywacke. The ground water is located near the surface.

Four large plate load tests were conducted at the load test site. Rigid steel plates having plan dimensions of 3.0 m by 3.5 m were used for loading. First load test was on untreated soil. Second load test was Group A loading on improved ground with aggregate piers of 3.0 m length, third load test was Group B loading on improved ground with aggregate piers of 5.0 m length and finally fourth load test was Group C loading on improved ground with aggregate pier lengths of 8.0 m. Each aggregate pier groups, i.e. Group A, Group B, and Group C, consisted of 7 piers installed with a spacing of 1.25 m in a triangular pattern. The pier diameter was 65cm. (Figure 3.4)

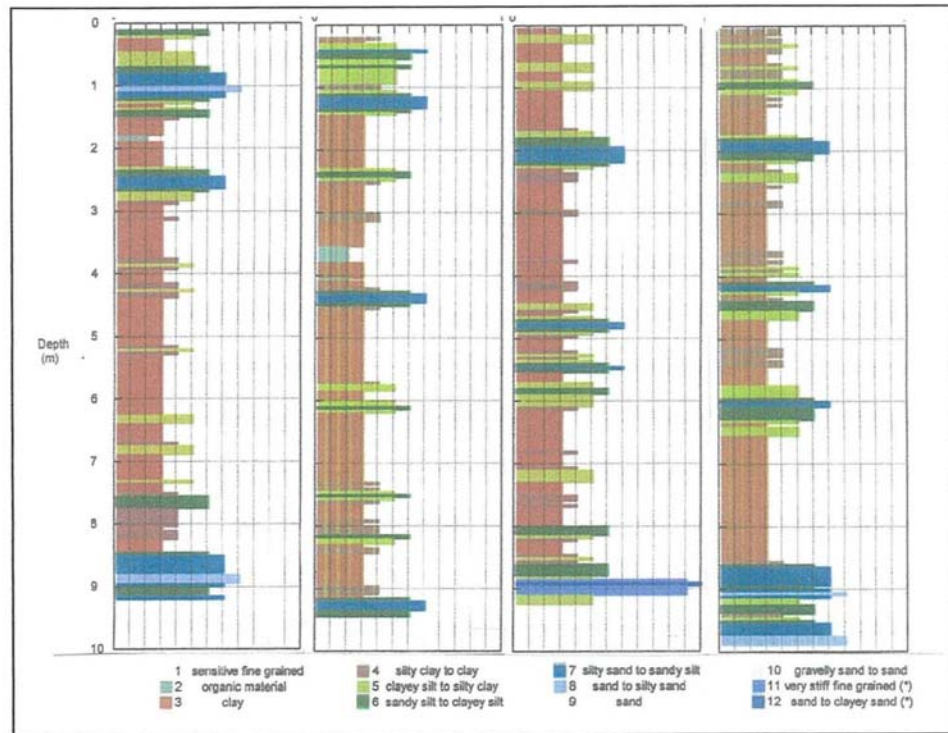


Figure 3.3 Variation of soil classification at the load test site based on CPT correlations (Özkeskin, 2004)

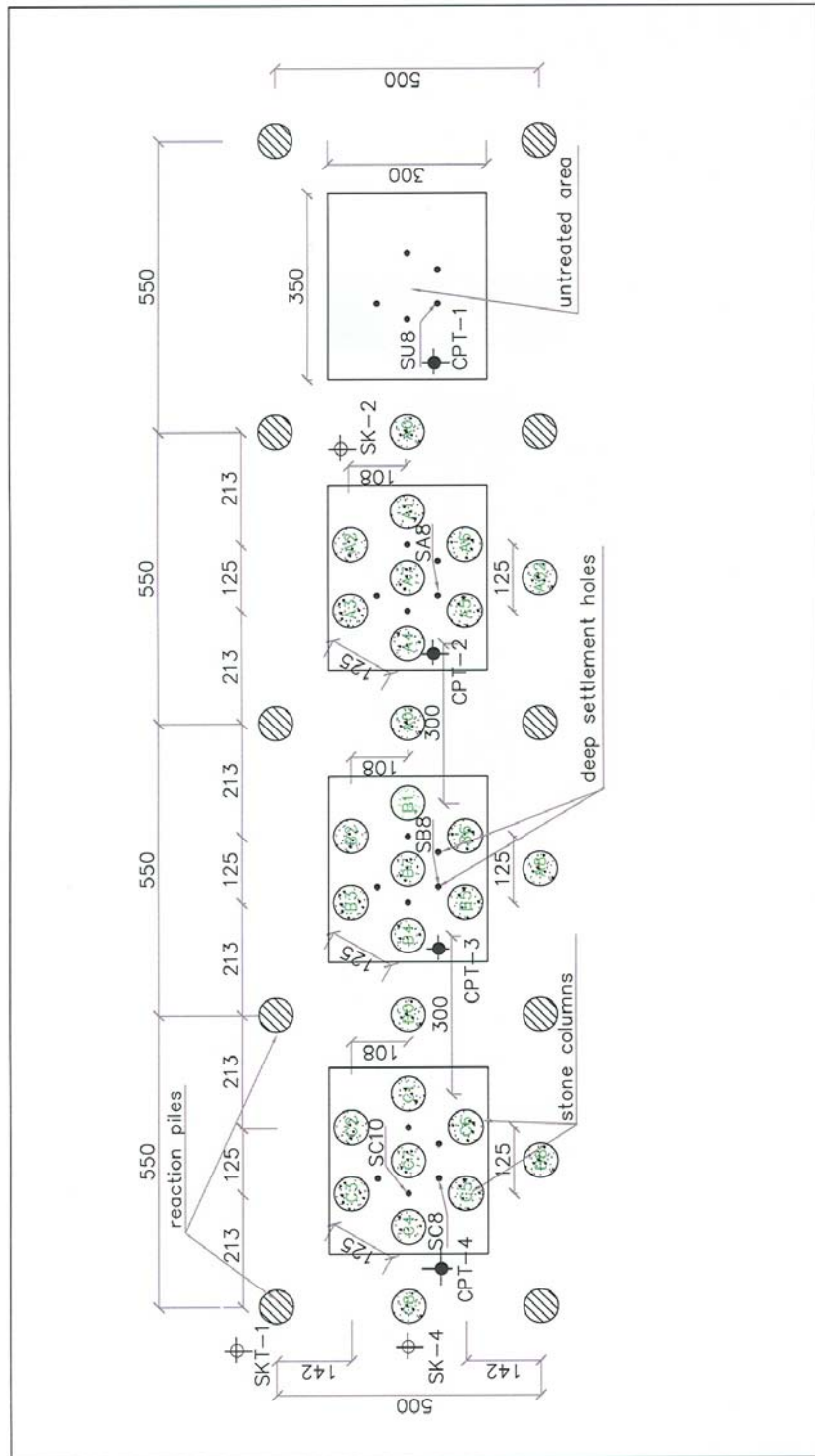


Figure 3.4 Location of aggregate piers at the load-test site (Özkeskin, 2004)

For each group of aggregate piers, deep settlement plates were installed at 1.5 m, 3 m, 5 m, 8 m and 10 m depths. 10 cm thick fine sand layers were laid and compacted to level the surface before placing the total pressure cell on top of the center aggregate pier. The loading sequence for untreated soil load test was cyclic and at each increment and decrement, load was kept constant until the settlement rate was almost zero. For aggregate pier groups, the loading sequence was 50, 100, 150, 200, 250, 150, 0 kPa. Two surface movements, one at the corner and one at the center of the loading plate, and five deep movement measurements were taken with respect to time.

### **3.3 Details of the Finite Element Model**

Geotechnical finite element software PLAXIS 3D which offers the possibility of 3D finite element modeling was used for the analysis. Loading plate, which has dimensions of 3.0m x 3.5m, was modeled as a rigid plate and the loading was applied as a uniformly distributed vertical load on this plate according to the loading scheme used during the actual field test. The boundaries of the 3D finite element mesh was extended 4 times the loading plate dimensions in order to minimize the effects of model boundaries on the analysis. The height of the finite element model was selected as 12 meters. The first 8 meters was the compressible silty clay layer and the remaining 4 meters was the relatively incompressible stiff clayey sand layer. An isometric view of the 3D model is given in Figure 3.5.

Both the compressible and incompressible soil layers was modeled using the elastic-perfectly plastic Mohr-Coulomb soil model. Groundwater level was defined at the surface. The parameters of the incompressible layer was set to relatively high values, and various geotechnical parameters was assigned to the compressible layer until the surface load-settlement curve calculated from the finite element model matches with the field test data carried on untreated soil. The closest match, which is shown in Figure 3.6, was obtained with the following parameters:

Silty clay ( 0-8m depth)

$$\gamma = 18 \text{ kN/m}^3$$

$$c = 22 \text{ kPa}$$

$$\phi = 0^\circ$$

$$E = 4500 \text{ kPa}$$

$$\nu = 0.35$$

Clayey sand ( 8-12m depth)

$$\gamma = 20 \text{ kN/m}^3$$

$$c' = 0 \text{ kPa}$$

$$\phi' = 40^\circ$$

$$E = 50000 \text{ kPa}$$

$$\nu = 0.30$$

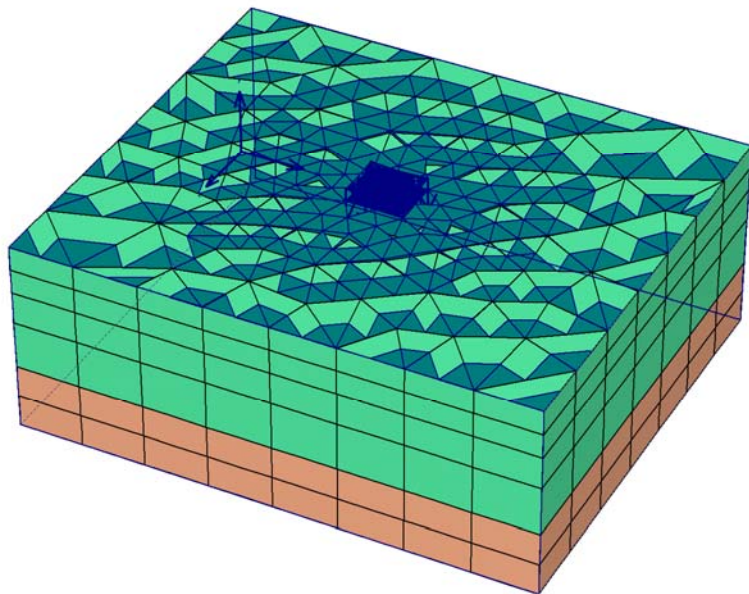


Figure 3.5 Isometric view of the 3D finite element model

The back calculated parameters (cohesion and deformation modulus values) for the compressible silty clay layer is verified using the results of load test carried out at the site as follows:

- The ultimate bearing capacity value of the untreated soil is determined from the measured surface pressure-settlement curve (Figure 3.6) by multiplying the pressure corresponding to a surface settlement of 25mm, i.e. the allowable bearing capacity, by three. The ultimate bearing capacity values for untreated soil is determined as  $q_{ult}=186\text{kPa}$ , by using this approach. This value is also verified by the double tangent method. The undrained cohesion value of the compressible silty clay layer corresponding to this ultimate bearing capacity value can be back-calculated as :

$$c_u = q_{ult} / 5.7 (1+0.3 (B/L)) \text{ (Terzaghi, 1943)}$$

$$c_u = 186 / 5.7 (1+0.3 (3/3.5))$$

$$c_u = 25 \text{ kPa}$$

The estimated value above is very near to the used value,  $c = 22 \text{ kPa}$  at the finite element analyses.

- The deformation modulus value of compressible silty clay layer can be estimated from the measured surface pressure-settlement curve (Figure 3.6) as follows:

$$\rho_z = \beta \cdot p \cdot L / E_u \text{ (Sovinc, 1969)}$$

$\rho_z$  = vertical displacement of a uniformly loaded rigid rectangle area resting on a finite layer with smooth frictionless interface at the base. This value is measured as 0.030m for a uniform load of  $p=75\text{kPa}$  as it can be seen from Figure 3.6.

$$\rho_z = \text{dimensionless constant (identified as 0.58 from Sovinc, 1969)}$$

$p$  = foundation load (=75 kPa)

$L$  = foundation length (=3.5m)

$E_u$  = undrained elasticity modulus of the silty clay layer.

From here,  $E_u$  value for the silty clay layer is back calculated as

$E_u=5075$  kPa.

Therefore, the drained elasticity modulus value for the silty clay layer can be calculated as :

$$E = E_u \cdot (1 + \nu') / (1 + \nu_u)$$

$$E = 5075 (1 + 0.35) / (1 + 0.5)$$

$$E = 4568 \text{ kPa}$$

The back calculated value above fits to the used value,  $E = 4500$  kPa at the finite element analyses.

To investigate the effect of silty sand layers that were observed at the CPT soundings, those silty sand layers were modeled in the 3D finite element analysis at a separate model. The silty sand layers were defined as two layers at depths 0.75m to 1.25m and 2.5m to 2.75m. The silty sand layers were also modeled by Mohr-Coulomb soil model and the geotechnical parameters were assigned as follows:

#### Silty Sand Layers

$$\gamma = 20 \text{ kN/m}^3$$

$$c' = 5 \text{ kPa}$$

$$\phi' = 33^\circ$$

$$E = 10000 \text{ kPa}$$

$$\nu = 0.30$$

Surface load-settlement curve computed by this model is also presented in Figure 3.6. As it can be seen from the figure, the presence of silty sand layers have no significant effect on the computed load-settlement curve. Therefore, the analysis were continued with the homogeneus silty clay layer as the compressible layer.

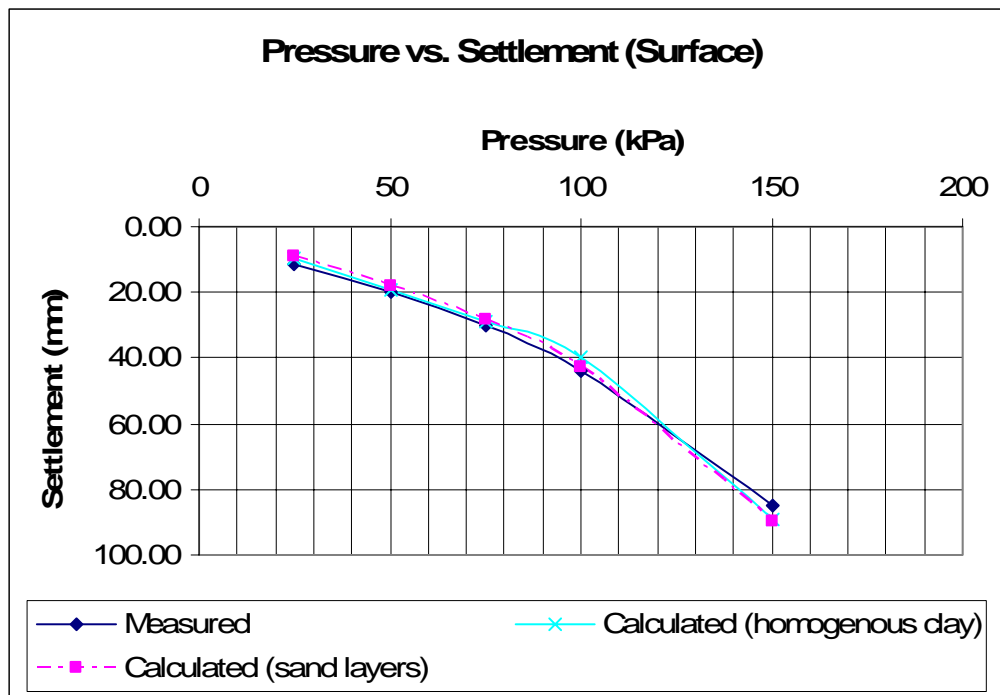


Figure 3.6 Comparison of surface load-settlement curves for untreated soil

### 3.4 Modeling of Field Tests on Rammed Aggregate Pier Groups

Once the geotechnical parameters of the native soil was determined, the next step was to model the field tests on three different rammed aggregate pier groups (i.e. Group A, Group B and Group C). In all three tests the rammed aggregate pier layout was similar (Figure 3.7) and the lengths of the aggregate piers were 3m, 5m and 8m for Group A, Group B and Group C, respectively.

The size of the loading plate was 3.0mx3.5m, as it was the case at the field test on untreated soil.

The field load tests on rammed aggregate pier groups were again modeled by PLAXIS 3D. The size of the finite element mesh was kept the same as the model for the test on untreated soil for comparison purposes. Material model and geotechnical parameters derived from the calibration process detailed in Section 3.2 was used for the native soil. Rammed aggregate piers were modeled with linear elastic material model and modulus of elasticity value was given as  $E = 39 \text{ MPa}$ , as recommended by Özkeskin (2004), after backcalculating the single pier loading tests carried out at the site with the finite element method. Loading plate, which has dimensions of 3.0mx3.5m, was modeled as a rigid plate and the loading was applied as a uniformly distributed vertical load on this plate according to the loading scheme used during the actual field test. Calculated surface pressure-settlement curves for each aggregate pier groups are compared with the field measurements in Figure 3.8, Figure 3.9 and Figure 3.10. Surface pressure values are normalized with respect to the ultimate bearing capacity,  $q_{ult}$ , of the untreated soil. The ultimate bearing capacity value of the untreated soil is determined from the measured surface pressure-settlement curve (Figure 3.6) by multiplying the pressure corresponding to a surface settlement of 25mm, i.e. the allowable bearing capacity, by three. The ultimate bearing capacity values for untreated soil is determined as  $q_{ult}=186\text{kPa}$ , by using this approach. Investigating Figure 3.8, Figure 3.9 and Figure 3.10, the following conclusions can be drawn:

- Measured surface load-settlement curves show near-linear-elastic behaviour.
- Calculated load-settlement curve for Group A shows plastic behaviour, after a normalized surface pressure of  $q/q_{ult} = 0.50$  whereas calculated load settlement curves for Group B and Group C loading are more close to the near-linear-elastic behaviour. This difference may be attributed to the fact that Group A rammed aggregate piers are floating piers and

plastification occurs in the unimproved soil beneath the floating columns at high stress levels.

- Calculated surface settlements are larger than the measured settlements for all cases. But the calculated values get closer to the measured ones from Group A to Group C. (i.e. from floating pier to end bearing pier)

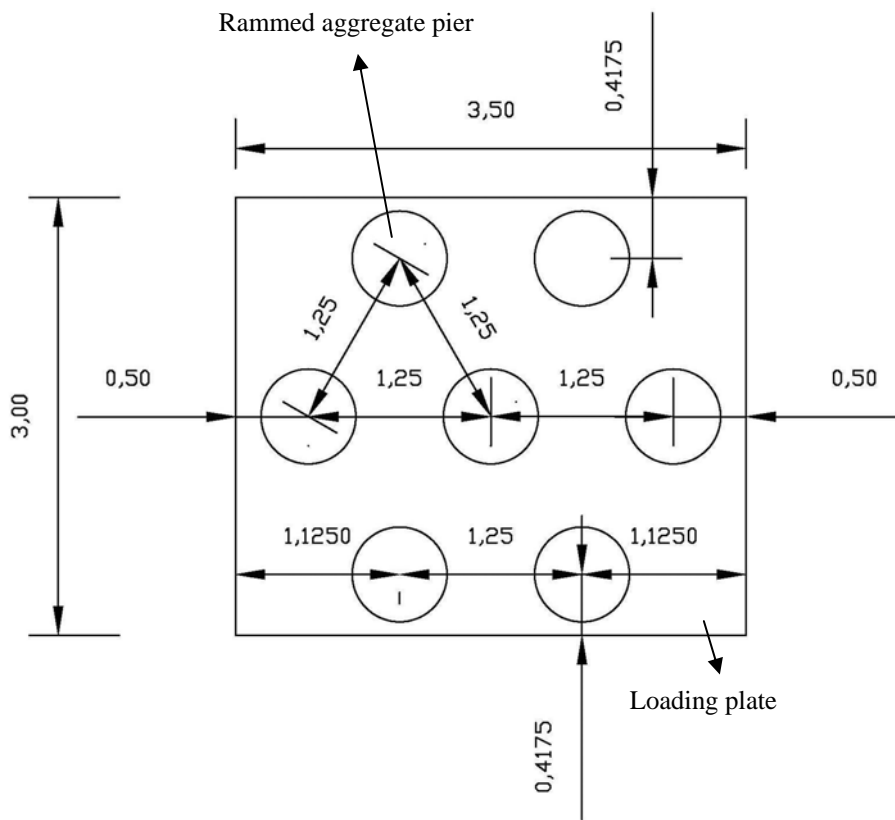


Figure 3.7 Field test rammed aggregate pier group layout

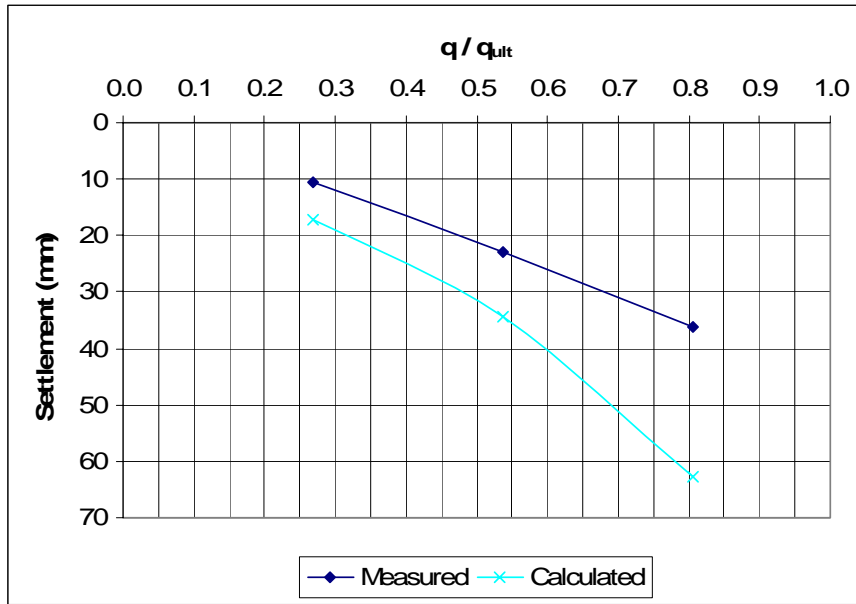


Figure 3.8 Comparison of surface load-settlement curves for loading on Group A rammed aggregate piers (Normal 3D FEM Model)

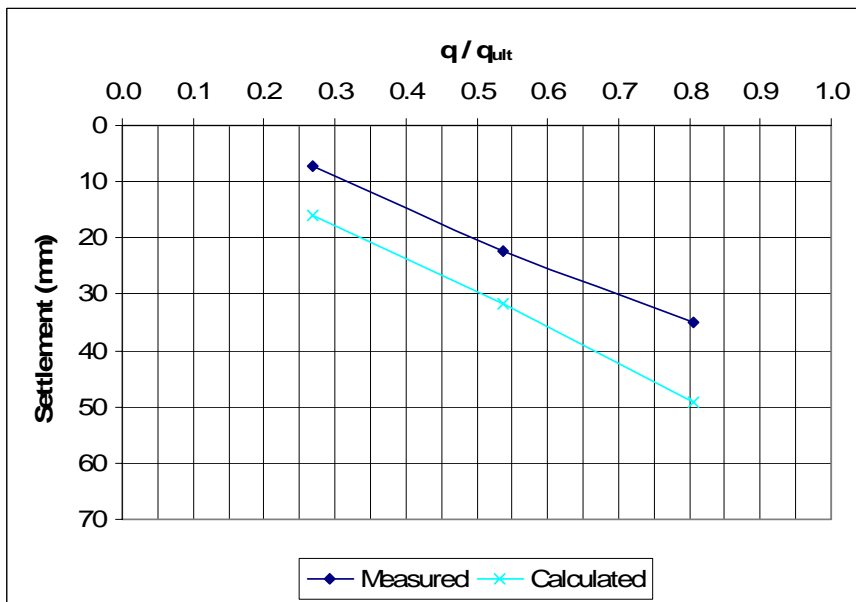


Figure 3.9 Comparison of surface load-settlement curves for loading on Group B rammed aggregate piers (Normal 3D FEM Model)

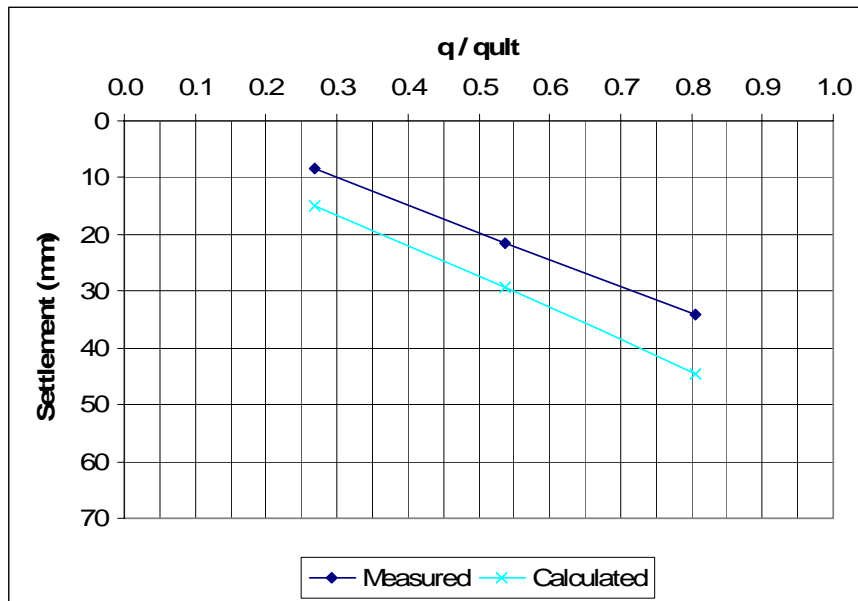


Figure 3.10 Comparison of surface load-settlement curves for loading on Group C rammed aggregate piers (Normal 3D FEM Model)

The observed stiffer and near-linear-elastic behaviour of aggregate pier groups can be explained by the increase of lateral stress in the matrix soil around the rammed aggregate piers caused by the ramming action during the installation of the piers. This increase in lateral stress of matrix soil results in improved stiffness characteristics as explained by Handy (2001). Handy (2001) investigates this situation by the help of Mohr circles. Figure 3.11 shows Mohr circle sequence and stress path during normal consolidation. An increase in vertical stress that causes a soil to consolidate yields a proportionate increase in horizontal stress so that the Mohr circle remains tangent to the consolidation envelope, according to stress path EF in Figure 3.11. On the other hand, a reduction in vertical stress leaves the horizontal stress mostly intact, and therefore approximately follows stress path FG in Figure 3.12. On reloading, the path approximately reverses along path GF. Because the soil behavior during unloading and reloading up to the preconsolidation pressure is near-linear-elastic, the stress zone enclosed by the consolidation envelopes is

referred to as the near-linear-elastic zone. Because unloading may extend the stress path past the consolidation envelope into an area between the consolidation and shear envelopes, this is referred to as the extended near-linear-elastic zone, or simply the extended zone. (Handy, 2001)

Lateral stresses indicative of passive conditions have been measured close to and between rammed aggregate piers (Handy, 2001). Lateral stress imposed on a normally consolidated soil gives stress path AB in Figure 3.13, and can proceed as high as the passive limit. Subsequent foundation loading then follows a stress path BC, which is in the near-linear-elastic zone. At C the Mohr circle intersects the consolidation envelope, ending the expanded near-linear-elastic response and initiating consolidation. Foundation loads on a normally consolidated soil confined by high lateral stress therefore should elicit a near-linear-elastic response instead of immediately initiating consolidation. (Handy, 2001)

The theoretical maximum vertical stress before consolidation can begin is obtained from definitions of  $K_p=H_2/V_1$  and  $K_0=H_2/V_2$  (Figure 3.13), where H and V represent horizontal and vertical stresses and the subscripts denote before-and-after loading. Solving each for  $H_2$  and equating gives

$$\begin{aligned} V_2/V_1 &= K_p/K_0 = K_r & (3.1) \\ K_r &= (1+\sin\phi') / (1-\sin\phi')^2 \end{aligned}$$

where,

$V_2$  = vertical effective stress required for consolidation

$V_1$  = in situ vertical effective stress or overburden pressure

$K_p$  = passive coefficient

$K_0$  = at-rest coefficient

$K_r$  = reinforcement factor

In an ideal undrained situation with a friction angle of zero and the soil at incipient failure, the analogous chain of Mohr circles gives;

$$K_r = 1 + (4c / V_1) \quad (3.2)$$

where:

$c$  = cohesion on a total stress basis

$V_1$  = initial vertical stress

Thus using equation 3.1, it can be stated that, for example, for the normally consolidated soil of Figure 3.13 with a friction angle of  $28^\circ$  subjected to passive lateral stress, the overburden pressure at any depth may be exceeded by a factor of 5.2 before consolidation can begin. Without the additional lateral stress, consolidation settlement would initiate as soon as additional load is applied.

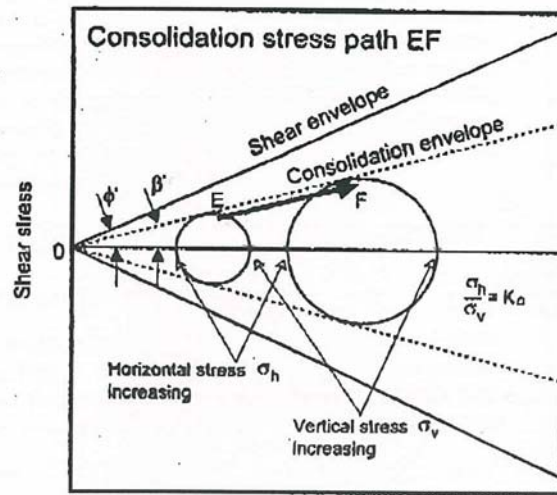


Figure 3.11 Mohr circle sequence and stress path EF during normal consolidation (Handy, 2001)

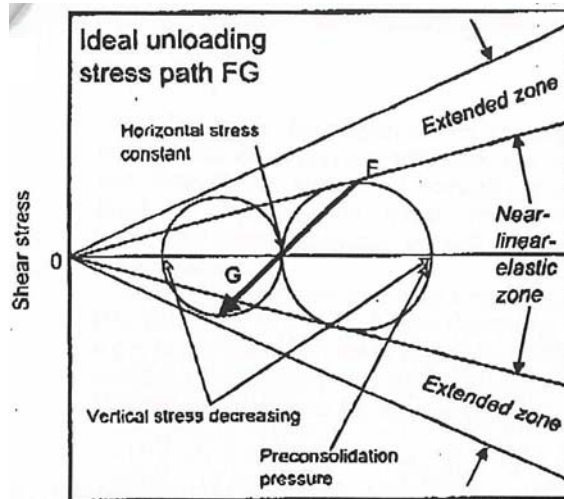


Figure 3.12 Mohr circle sequence and stress path FG as reductions in vertical stress created over consolidated soil (Handy, 2001)

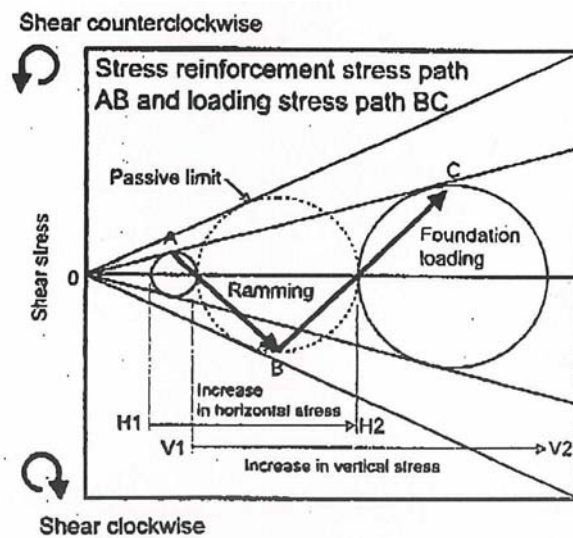


Figure 3.13 Increasing horizontal stress on normally consolidated soil (Stress path AB) increases consolidation threshold stress from  $V_1$  to  $V_2$  (Stress path BC) (Handy, 2001)

In order to match the observed stiffer and near-linear-elastic behaviour of actual field test measurements, it is decided to define linear elastic improved zones around the rammed aggregate piers at the 3D finite element model. Two different improvement assumptions are made for comparison purposes. In both trials, it is assumed that a circular zone with a radius equal to two times of the rammed aggregate pier radius is improved around the rammed aggregate piers. This circular zone is also divided into two zones. (Figure 3.14) For both trials, it is assumed that the material model for the rammed aggregate piers and the improved zones are linear elastic. For the first trial (which will be called Modified Ring Model 1) it is assumed that the modulus of elasticity value of the improved soil around the rammed aggregate pier increases to 1/2 of the modulus of elasticity value of the rammed aggregate pier at the first improved zone -  $r = 1.5r_{\text{aggregate pier}}$  -, and to 1/4 of the modulus of elasticity value of the rammed aggregate pier at the second improved zone -  $r = 2.0r_{\text{aggregate pier}}$  -. For the second trial (which will be called Modified Ring Model 2), these improved modulus of elasticity values were selected as 2/3 of the modulus of elasticity value of the rammed aggregate pier at the first improved zone -  $r = 1.5r_{\text{aggregate pier}}$  -, and to 1/3 of the modulus of elasticity value of the rammed aggregate pier at the second improved zone -  $r = 2.0r_{\text{aggregate pier}}$  -. It must be mentioned that these improved values are related to the ramming energy value imposed at the site. To give an idea about the ramming energy level, it can be stated that the granular material used for the aggregate piers were compacted in 1.0m to 1.5m thick lifts by dropping a weight of 1.5tons from a height of 1.0m for 10 times for each lift. (Özkeskin, 2004) Calculated surface pressure-settlement curves for each aggregate pier groups are compared with the field measurements in Figure 3.15, Figure 3.16 and Figure 3.17. Surface pressure values are normalized with respect to the ultimate bearing capacity,  $q_{\text{ult}}$ , of the untreated soil, as explained before. Investigating the figures, the following conclusions can be drawn:

- Calculated load-settlement curves fit to the expected near-linear-elastic behavior much better than before.

- The agreement with the measured surface settlement values are quite satisfactory for Group B and Group C loadings. For Group A loading, although the calculated values get closer to the measured values than before, agreement with the measured values is not as good as Group B and Group C loadings, especially at higher load levels.
- Investigating the analysis results, it is decided that best match with the measured values are achieved with the Modified Ring Model 2.

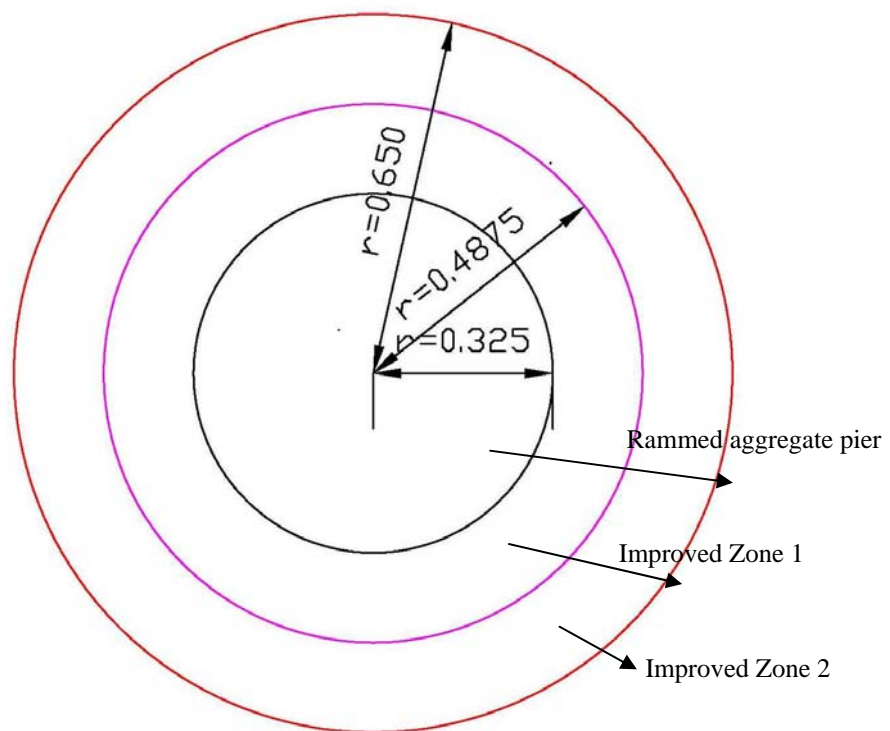


Figure 3.14 Geometry of the assumed improved zones around the rammed aggregate piers

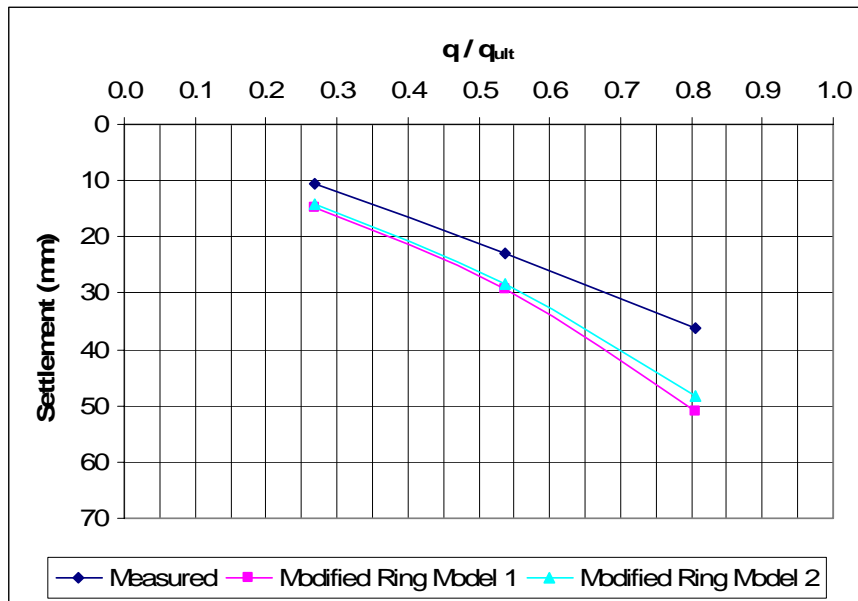


Figure 3.15 Comparison of surface load-settlement curves for loading on Group A rammed aggregate piers (Modified Ring Model)

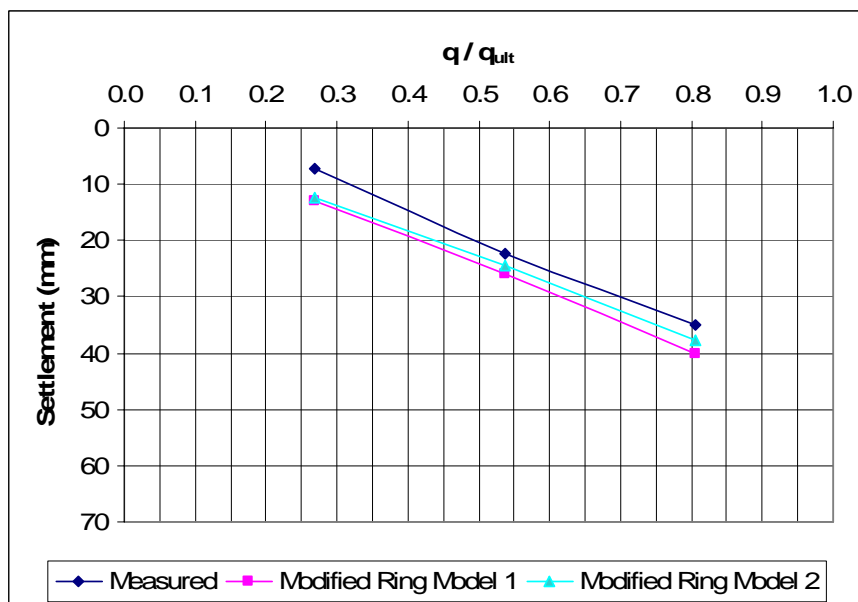


Figure 3.16 Comparison of surface load-settlement curves for loading on Group B rammed aggregate piers (Modified Ring Model)

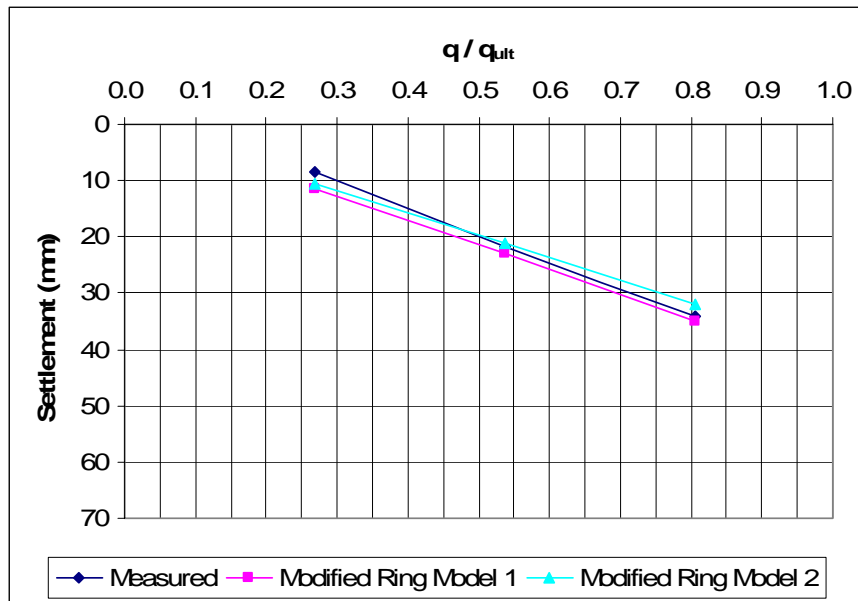


Figure 3.17 Comparison of surface load-settlement curves for loading on Group C rammed aggregate piers (Modified Ring Model)

The next step is to try to simplify this improved near-linear-elastic zone assumption (Modified Ring Model) so that it can be easily used for practical analyses. For this purpose, the area under the loading plate with the rammed aggregate piers is modeled as a composite soil block (Composite Soil Model). Linear elastic material model is used for the composite soil block and the modulus of elasticity of this composite zone is calculated as the weighted average of the rammed aggregate pier, improved zones around the rammed aggregate pier, and native soil, according to their respective areas. The improved modulus of elasticity values were selected as  $2/3$  of the modulus of elasticity value of the rammed aggregate pier at the first improved zone -  $r = 1.5r_{\text{aggregate pier}}$  -, and to  $1/3$  of the modulus of elasticity value of the rammed aggregate pier at the second improved zone -  $r = 2.0r_{\text{aggregate pier}}$  -, as concluded before. Calculated surface pressure-settlement curves for this case are compared with the field measurements in Figure 3.18, Figure 3.19 and Figure

3.20. The results of Modified Ring Model 2 are also given in the figures for comparison purposes.

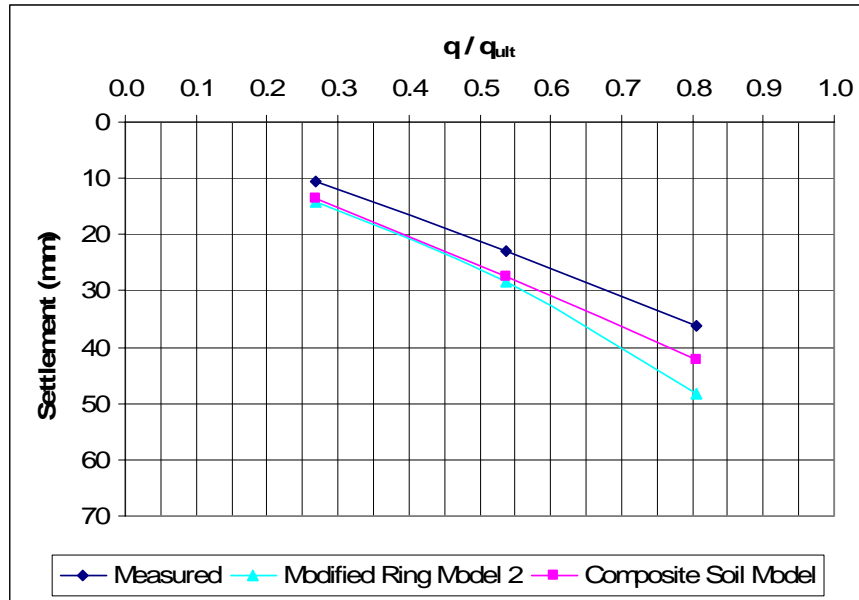


Figure 3.18 Comparison of surface load-settlement curves for loading on Group A rammed aggregate piers (Composite Soil Model)

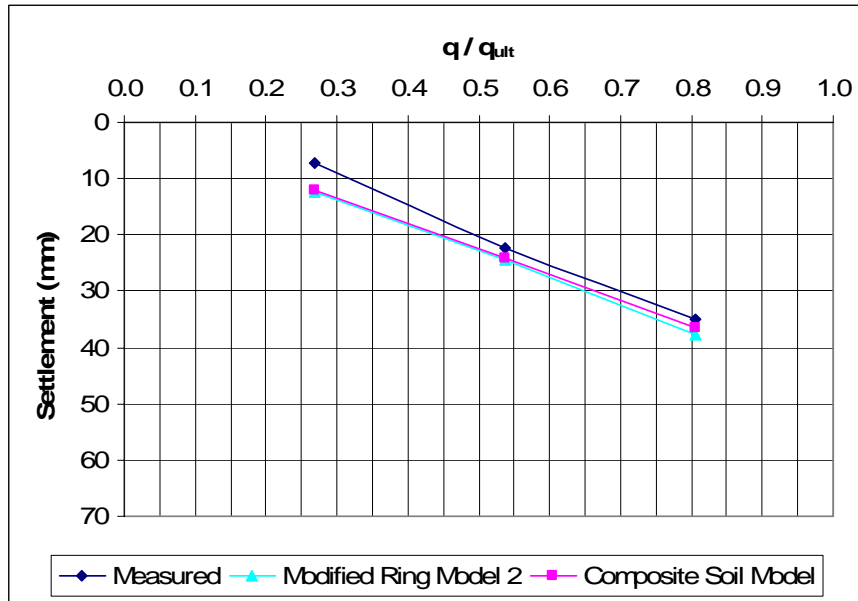


Figure 3.19 Comparison of surface load-settlement curves for loading on Group B rammed aggregate piers (Composite Soil Model)

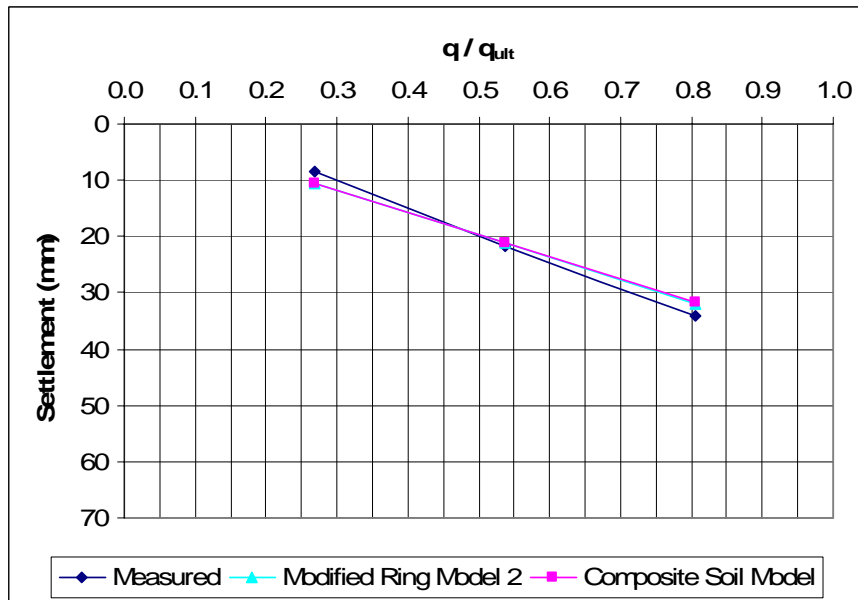


Figure 3.20 Comparison of surface load-settlement curves for loading on Group C rammed aggregate piers (Composite Soil Model)

Investigating Figure 3.18, Figure 3.19 and Figure 3.20, the following conclusions can be drawn:

- Calculated load-settlement curves with the Composite Soil Model yield more close results to the measured values than the Modified Ring Model, especially for floating pier groups. (i.e. Group A and Group B)
- The agreement with the measured values get worse for floating pile group (Group A) at higher stress levels.

In order to understand the reason of this discrepancy between the calculated and measured surface settlement values at floating pier group (Group A), it was decided to compare the increase in vertical stress with depth at the center of the footing, with the analytical elastic solutions at the literature. Three theoretical elastic solutions were used for this purpose. These are:

- i) Giroud (1970); which gives the distribution of vertical stress increase with depth under a rectangular flexible footing on an elastic soil of infinite depth.
- ii) Burmister (1956); which gives the distribution of vertical stress increase with depth under a rectangular flexible footing on an elastic soil of finite depth underlain by a rigid layer.
- iii) Fox (1948); which gives the distribution of vertical stress increase with depth under a rectangular flexible footing on a two layer elastic soil with  $E_1 > E_2$ .

It is to be noted that all of the analytical solutions were derived for flexible footings, while the full scale load test was on a rigid footing. Unfortunately, no reliable analytical solutions exist at the literature for the vertical stress increase with depth under rectangular rigid footings. Besides, all of the analytical solutions assume a homogenous soil layer under the footing and none of the solutions is able to model the stress concentration that occurs under the footing because of the stone columns. Therefore, primarily the the vertical stress increase at the lower zone (untreated zone under the

floating piers) were compared as shown in Figure 3.21, Figure 3.22 and Figure 3.23 for different surface pressure levels. Surface pressure values are normalized with respect to the ultimate bearing capacity,  $q_{ult}$ , of the untreated soil, as explained before.

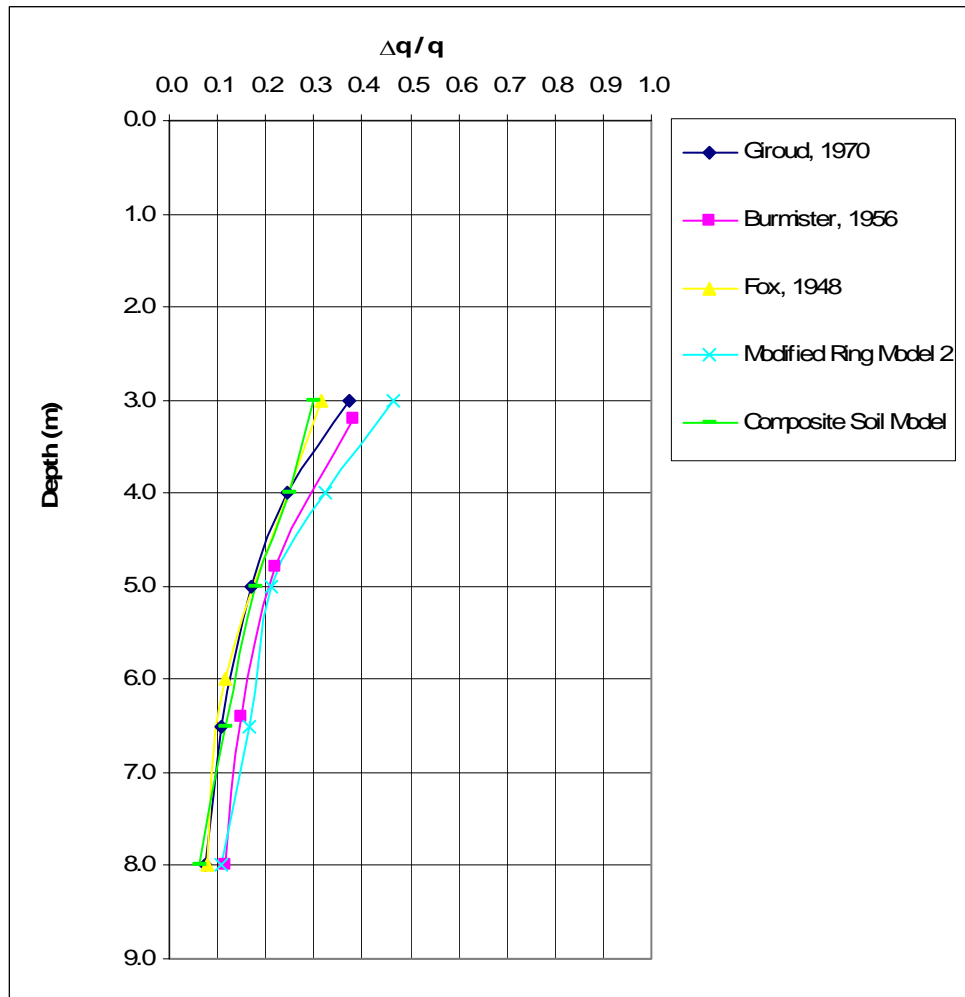


Figure 3.21 Comparison of vertical stress increase in the lower zone for Group A rammed aggregate piers ( $q / q_{ult} = 0.27$ )

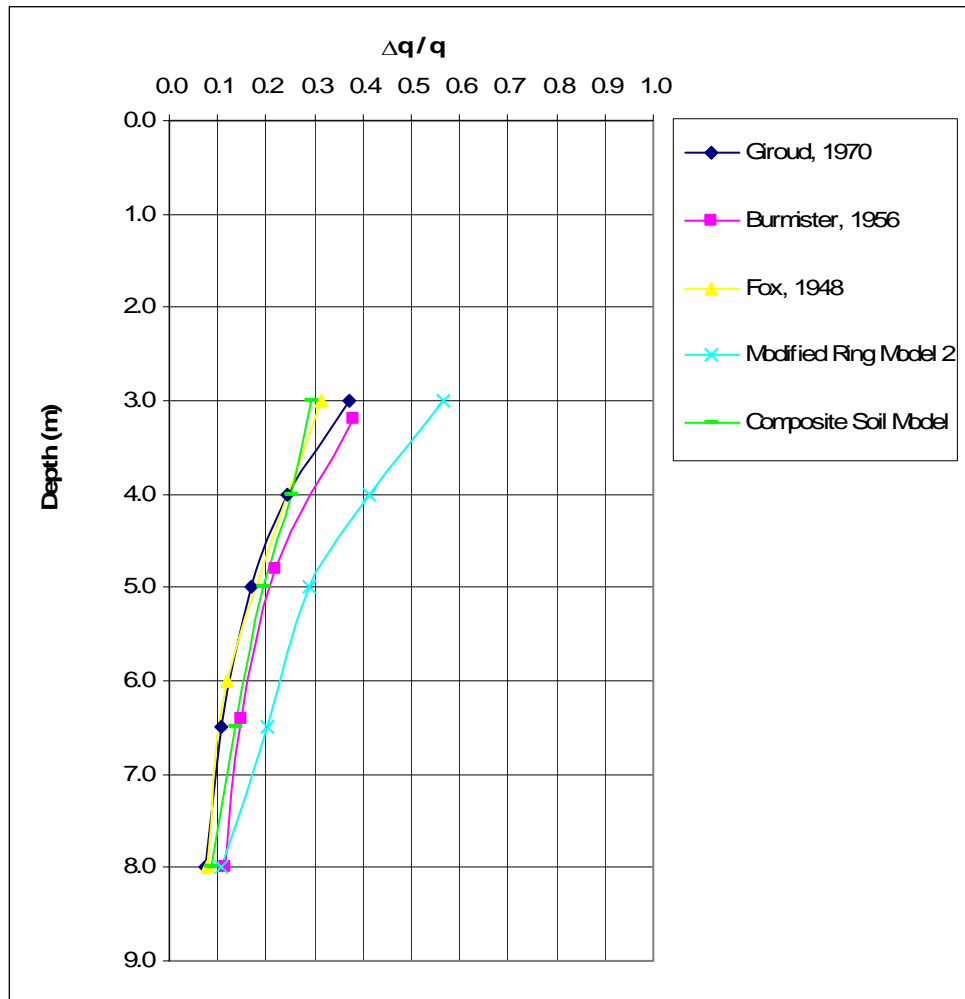


Figure 3.22 Comparison of vertical stress increase in the lower zone for Group A rammed aggregate piers ( $q / q_{ult} = 0.54$ )

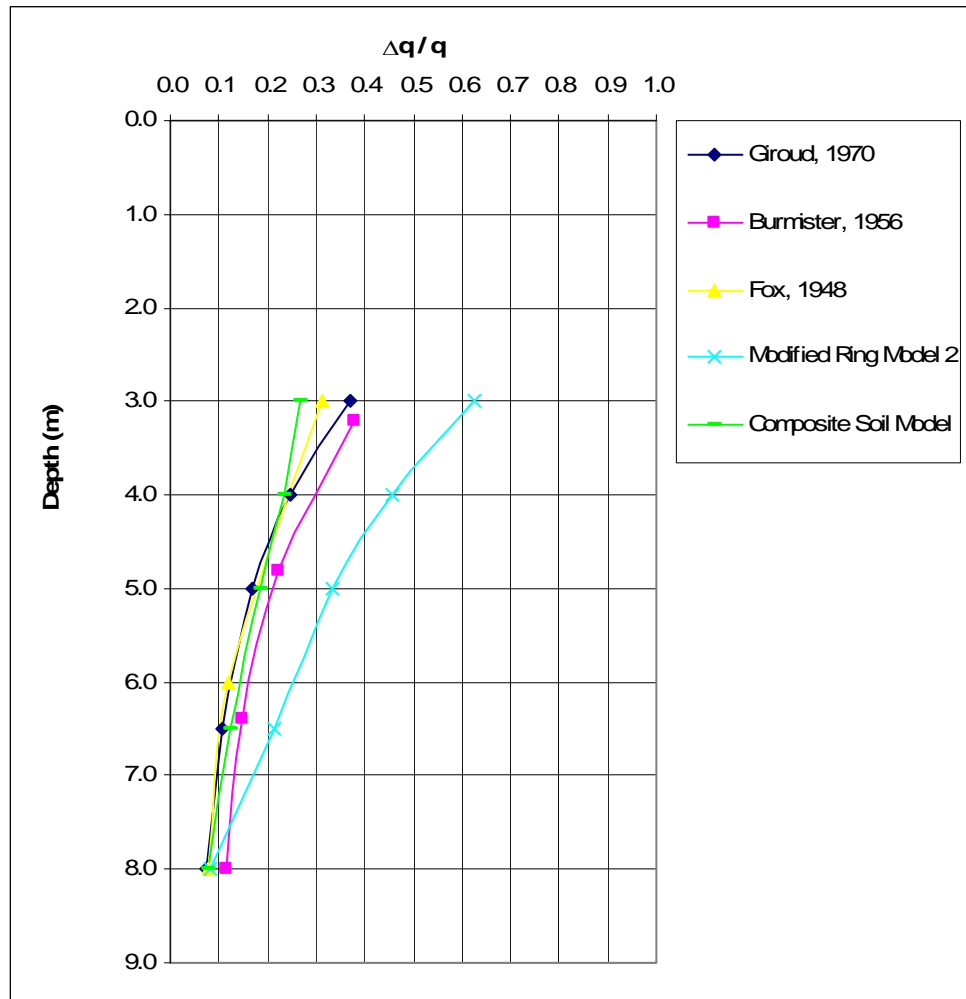


Figure 3.23 Comparison of vertical stress increase in the lower zone for Group A rammed aggregate piers ( $q / q_{ult} = 0.81$ )

Investigating Figure 3.21, Figure 3.22 and Figure 3.23, it is noted that Modified Ring Model yields higher vertical stress increase in the lower zone for floating pier Group A than the analytical solutions and the Composite Soil Model. The difference increases with increasing surface pressure level. It is believed that, this results in additional plastification and settlements in the lower zone, which explains the reason of the discrepancy between the measured and calculated surface settlement values for floating pier Group A, especially at higher load levels.

As a result of the calibration process detailed in this chapter, it is concluded that the 3D finite element model, i.e. the Composite Soil Model, in which the area under the loading plate with the rammed aggregate piers is modeled as a composite soil block with equivalent linear elastic soil properties taking the stiffness increase around the piers during the installation process into account, satisfactorily models the surface pressure-settlement curves of uniformly loaded footings supported by rammed aggregate piers. It is to be mentioned that the model should be used cautiously for floating pier groups with pier lengths less than  $1.5B$  ( $B$  = width of the footing), especially at high surface pressure levels, i.e.  $q / q_{ult} > 0.5$ , where  $q_{ult}$  = ultimate bearing capacity of the native soil.

## CHAPTER 4

### RESULTS OF THE PARAMETRIC STUDY

#### 4.1 Introduction

Once the 3D finite element model (Composite Soil Model) to be used for the analysis of rigid footings resting on rammed aggregate piers was calibrated using the results of full-scale load tests as presented in the previous chapter, the next step is to carry out a parametric study using this finite element model to investigate the effect of both geometric parameters (area ratio of rammed aggregate piers, foundation load, width of foundation, rammed aggregate pier length) and material parameters (strength of foundation material, modulus of elasticity value of rammed aggregate piers) on the settlement improvement factor. Design charts to estimate settlement improvement factors for footings resting on rammed aggregate piers will also be presented as a result of this parametric study.

#### 4.2 Details of the Parametric Study

Three different footing sizes (2.4m×2.4m, 3.6m×3.6m and 4.8m×4.8m) were used for the parametric study. The thickness of the compressible clay layer under these footings was varied as  $L_{\text{clay}} = 5\text{m}$ , 10m and 15m for each different footing size. Four different area ratios (AR= 0.087, 0.136, 0.230 and 0.349) were used for the rammed aggregate pier groups under each different footing and compressible layer combination. Foundation pressures,  $q$ , were selected as  $q=25-50-75-100-125-150$  kPa. Schematic representation of these parameters can be seen in Figure 4.1. The strength and deformation modulus values of the compressible clay layer were varied as shown at Table 4.1. The deformation

modulus value of the rammed aggregate piers were selected as  $E_{column} = 36$  MPa and 72MPa.

Table 4.1 Strength and deformation properties of the compressible clay layer used at the parametric study.

$\gamma$ (kN/m <sup>3</sup> )	$c$ (kN/m <sup>2</sup> )	$\phi$ (°)	$\nu$	$E_{clay}$ (kN/m <sup>2</sup> )
18	20	0	0.35	4500
18	25	0	0.35	5625
18	30	0	0.35	6750
18	40	0	0.35	9000
18	60	0	0.35	13500

For each case, first the untreated case is analyzed by modelling the uniformly loaded rigid footing on compressible clay using PLAXIS 3D. Untreated soil settlements were obtained by this way. Next, the rigid footings resting on rammed aggregate piers were modeled by PLAXIS 3D using the Composite Soil Block approach that was explained in detail in Chapter 3. This approach, which was calibrated with the results of the full scale loading tests, takes into account the increase in stiffness around the rammed aggregate piers that results from the installation process. Two circular improved zones are assumed around the rammed aggregate piers (Figure 3.14) and it is assumed that the elasticity modulus value of the soil in these improved zones are 2/3 and 1/3 of the elasticity modulus value of the rammed aggregate pier. The soil perimeter under the footing improved by the rammed aggregate piers is modelled as a linear elastic composite soil block. The elasticity modulus of this composite soil block is calculated as the weighted average of the elasticity modulus values of the rammed aggregate piers, improved zones around the rammed aggregate

piers, and native soil, according to their respective areas. (Figure 4.1) Once the settlement values for the footings resting on rammed aggregate pier groups are calculated using this method, settlement improvement factors are calculated as:

$$IF = S_{\text{untreated}} / S_{\text{treated}}$$

where:

IF = settlement improvement factor

$S_{\text{untreated}}$  = settlement of rigid footing resting on untreated soil.

$S_{\text{treated}}$  = settlement of rigid footing resting on soil treated with rammed aggregate pier group.

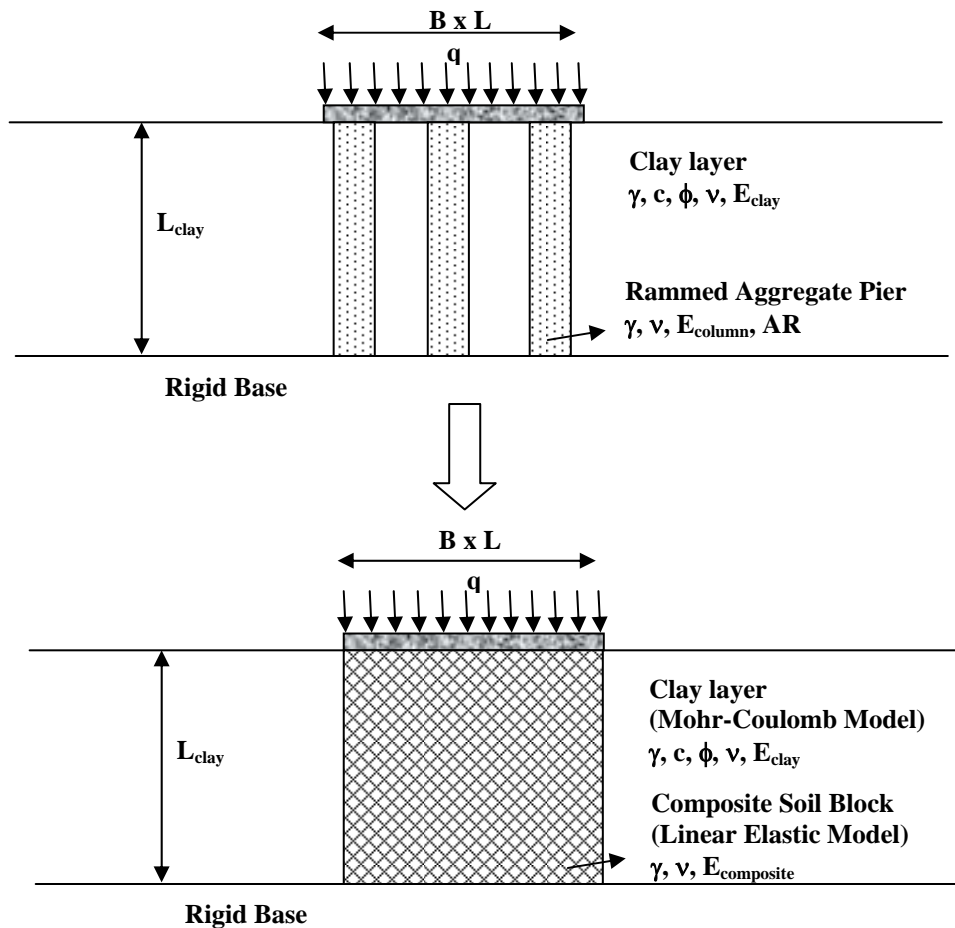


Figure 4.1 Schematic representation of composite soil model

### **4.3 Presentation of the Results of the Parametric Study**

The results of the parametric study detailed in Section 4.2 are presented as design charts at Appendix B. A sample design chart is shown in Figure 4.2. Since, the calculated values of settlement improvement factors were unreasonably large under footing pressures of  $q = 125$  kPa and  $q = 150$  kPa for compressible clay layer with  $c_u = 20$  kPa, these values were excluded from design charts.

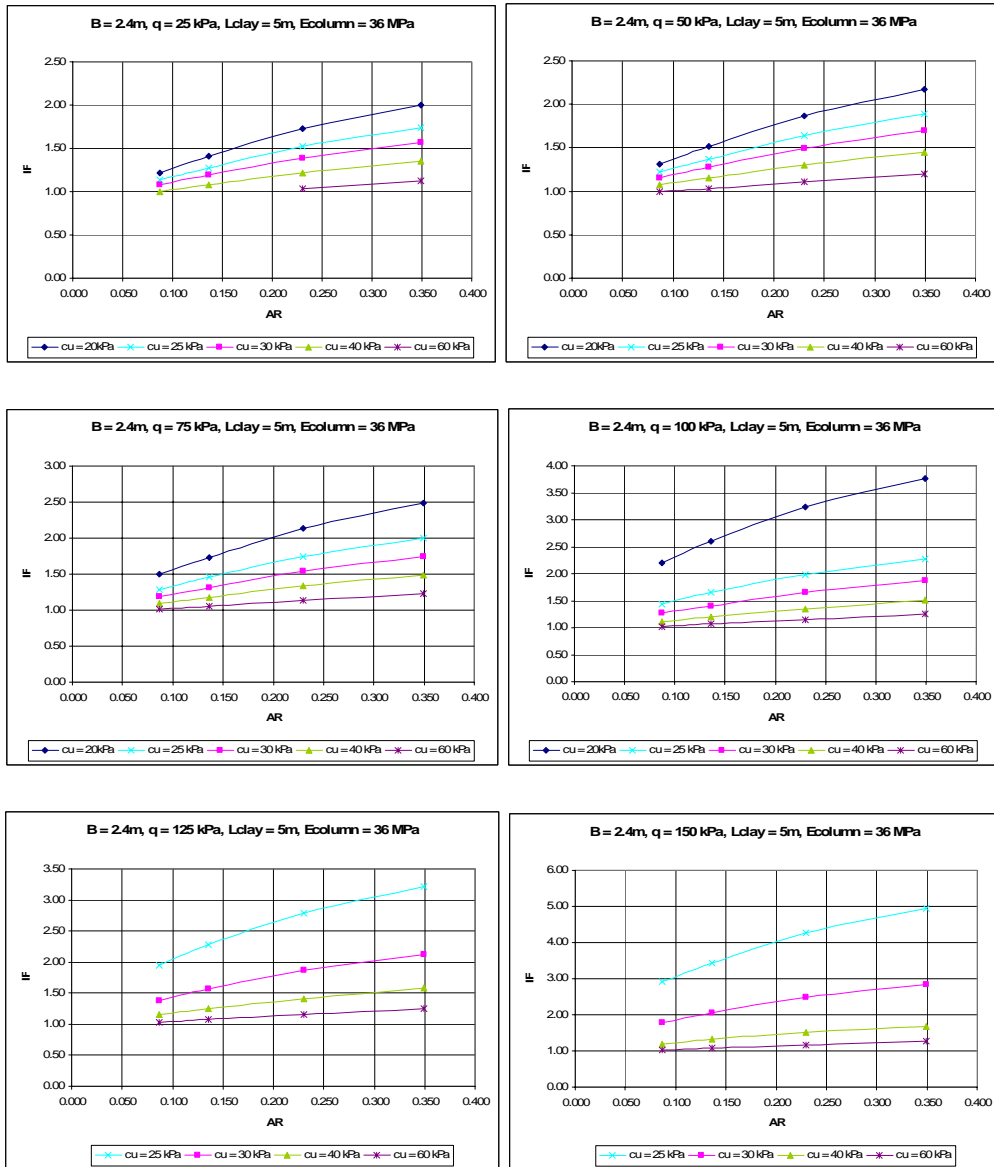


Figure 4.2 Settlement improvement factor (IF) vs. area ratio (AR) charts for a rigid square footing (B=2.4m) resting on end bearing rammed aggregate piers (L=5m, E=36 MPa)

#### 4.4 Design Example

To illustrate the use of the design charts given in Appendix B, a design example will be solved in this section. The geometry and the parameters of the problem are given in Figure 4.3 and it consists of a square footing ( $3.0\text{m} \times 3.0\text{m}$ ) resting on a compressible clay layer of  $8\text{m}$  thickness. The footing is uniformly loaded with a load of  $q=75\text{ kPa}$ , and the total untreated soil settlement under this load is calculated as  $4.5\text{cm}$ . Since the permissible total settlement for the footing is  $2.5\text{cm}$ , the soil under the footing will be improved by rammed aggregate piers with a column elastic modulus of  $E_{\text{column}} = 60\text{ MPa}$ .

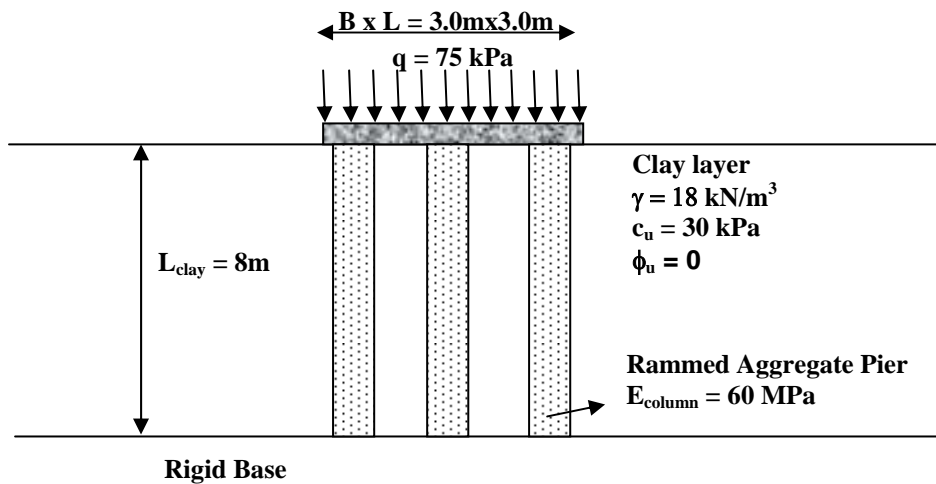


Figure 4.3 Geometry and the parameters of the design example

The required area ratio for the rammed aggregate piers will be calculated using the design charts given in Appendix B as follows:

The required settlement improvement factor can be calculated as :

$$\text{IF} = 4.5 / 2.5 = 1.80$$

For a square footing with B=2.4m, q=75kPa and a compressible layer thickness L=5m,

$$\text{for } E_{\text{column}} = 36 \text{ MPa and } AR = 0.230 ; IF = 1.54 \text{ (From Figure B1)} \quad (4.1)$$

$$\text{for } E_{\text{column}} = 72 \text{ MPa and } AR = 0.230 ; IF = 2.30 \text{ (From Figure B2)} \quad (4.2)$$

$$\text{for } E_{\text{column}} = 60 \text{ MPa and } AR = 0.230 ; IF = 2.05 \text{ (by linear interpolation of 4.1 and 4.2)} \quad (4.3)$$

For a square footing with B=2.4m, q=75kPa and a compressible layer thickness L=10m,

$$\text{for } E_{\text{column}} = 36 \text{ MPa and } AR = 0.230 ; IF = 1.36 \text{ (From Figure B7)} \quad (4.4)$$

$$\text{for } E_{\text{column}} = 72 \text{ MPa and } AR = 0.230 ; IF = 1.84 \text{ (From Figure B8)} \quad (4.5)$$

$$\text{for } E_{\text{column}} = 60 \text{ MPa and } AR = 0.230 ; IF = 1.68 \text{ (by linear interpolation of 4.4 and 4.5)} \quad (4.6)$$

For a square footing with B=2.4m, q=75kPa and a compressible layer thickness L=8m,

$$\text{for } E_{\text{column}} = 60 \text{ MPa and } AR = 0.230 ; IF = 1.83 \text{ (by linear interpolation of 4.3 and 4.6)} \quad (4.7)$$

For a square footing with B=3.6m, q=75kPa and a compressible layer thickness L=5m,

$$\text{for } E_{\text{column}} = 36 \text{ MPa and } AR = 0.230 ; IF = 1.69 \text{ (From Figure B3)} \quad (4.8)$$

$$\text{for } E_{\text{column}} = 72 \text{ MPa and } AR = 0.230 ; IF = 2.70 \text{ (From Figure B4)} \quad (4.9)$$

$$\text{for } E_{\text{column}} = 60 \text{ MPa and } AR = 0.230 ; IF = 2.36 \text{ (by linear interpolation of 4.8 and 4.9)} \quad (4.10)$$

For a square footing with B=3.6m, q=75kPa and a compressible layer thickness L=10m,

$$\text{for } E_{\text{column}} = 36 \text{ MPa and } AR = 0.230 ; IF = 1.44 \text{ (From Figure B9)} \quad (4.11)$$

$$\text{for } E_{\text{column}} = 72 \text{ MPa and } AR = 0.230 ; IF = 2.08 \text{ (From Figure B10)} \quad (4.12)$$

$$\text{for } E_{\text{column}} = 60 \text{ MPa and } AR = 0.230 ; IF = 1.87 \text{ (by linear interpolation of 4.11 and 4.12)} \quad (4.13)$$

For a square footing with B=3.6m, q=75kPa and a compressible layer thickness L=8m,

$$\text{for } E_{\text{column}} = 60 \text{ MPa and } AR = 0.230 ; IF = 2.07 \text{ (by linear interpolation of 4.10 and 4.13)} \quad (4.14)$$

For a square footing with B=3.0m, q=75kPa and a compressible layer thickness L=8m,

for Ecolumn = 60 MPa and AR = 0.230 ; IF = 1.95 (by linear interpolation of 4.7 and 4.14) (4.15)

For a square footing with B=2.4m, q=75kPa and a compressible layer thickness L=5m,

for Ecolumn = 36 MPa and AR = 0.136 ; IF = 1.31 (From Figure B1) (4.16)

for Ecolumn = 72 MPa and AR = 0.136 ; IF = 1.80 (From Figure B2) (4.17)

for Ecolumn = 60 MPa and AR = 0.136 ; IF = 1.64 (by linear interpolation of 4.16 and 4.17) (4.18)

For a square footing with B=2.4m, q=75kPa and a compressible layer thickness L=10m,

for Ecolumn = 36 MPa and AR = 0.136 ; IF = 1.20 (From Figure B7) (4.19)

for Ecolumn = 72 MPa and AR = 0.136 ; IF = 1.53 (From Figure B8) (4.20)

for Ecolumn = 60 MPa and AR = 0.136 ; IF = 1.42 (by linear interpolation of 4.19 and 4.20) (4.21)

For a square footing with B=2.4m, q=75kPa and a compressible layer thickness L=8m,

for Ecolumn = 60 MPa and AR = 0.136 ; IF = 1.51 (by linear interpolation of 4.18 and 4.21) (4.22)

For a square footing with B=3.6m, q=75kPa and a compressible layer thickness L=5m,

for Ecolumn = 36 MPa and AR = 0.136 ; IF = 1.40 (From Figure B3) (4.23)

for Ecolumn = 72 MPa and AR = 0.136 ; IF = 2.03 (From Figure B4) (4.24)

for Ecolumn = 60 MPa and AR = 0.136 ; IF = 1.82 (by linear interpolation of 4.23 and 4.24) (4.25)

For a square footing with B=3.6m, q=75kPa and a compressible layer thickness L=10m,

for Ecolumn = 36 MPa and AR = 0.136 ; IF = 1.25 (From Figure B9) (4.26)

for Ecolumn = 72 MPa and AR = 0.136 ; IF = 1.66 (From Figure B10) (4.27)

for  $E_{\text{column}} = 60 \text{ MPa}$  and  $AR = 0.136$  ;  $IF = 1.52$  (by linear interpolation of 4.26 and 4.27) (4.28)

For a square footing with  $B=3.6\text{m}$ ,  $q=75\text{kPa}$  and a compressible layer thickness  $L=8\text{m}$ ,

for  $E_{\text{column}} = 60 \text{ MPa}$  and  $AR = 0.136$  ;  $IF = 1.64$  (by linear interpolation of 4.25 and 4.28) (4.29)

For a square footing with  $B=3.0\text{m}$ ,  $q=75\text{kPa}$  and a compressible layer thickness  $L=8\text{m}$ ,

for  $E_{\text{column}} = 60 \text{ MPa}$  and  $AR = 0.136$  ;  $IF = 1.58$  (by linear interpolation of 4.22 and 4.29) (4.30)

For the required settlement improvement factor of  $IF=1.80$ , the required area ratio of rammed aggregate piers is calculated as:

**AR = 0.192** (by linear interpolation of 4.15 and 4.30)

## **CHAPTER 5**

### **DISCUSSION OF THE ANALYSIS RESULTS**

#### **5.1 Introduction**

Key parameters (i.e. area ratio of rammed aggregate pier group, undrained shear strength of compressible clay layer, elastic modulus of rammed aggregate pier, footing pressure, thickness of compressible layer and footing size) effecting the settlement improvement factor for footings resting on compressible clay improved by end bearing rammed aggregate piers will be discussed in this chapter, using the results of the parametric analyses presented at Chapter 4. Also, settlement improvement factors derived from the method presented at Chapter 4 will be compared with some conventional methods presented in the literature. Finally, the effect of floating rammed aggregate pier groups on the settlement improvement factor will be discussed on some selected cases.

#### **5.2 Effect of Area Ratio on Settlement Improvement Factor**

As it can be seen from the design charts presented at Appendix B, the settlement improvement factor increases as the area ratio of the rammed aggregate pier group, AR, increases. The effect is more pronounced for smaller values of undrained shear strength of the compressible clay layer and higher values of the modulus of elasticity values of the rammed aggregate piers.

### **5.3 Effect of Undrained Shear Strength of Compressible Clay Layer on Settlement Improvement Factor**

The settlement improvement factor increases as undrained shear strength of the compressible clay layer,  $c_u$ , decreases, as it can be seen from Figure 5.1. The effect is more pronounced for higher values of footing pressure.

### **5.4 Effect of Elasticity Modulus of Rammed Aggregate Pier on Settlement Improvement Factor**

The settlement improvement factor increases as the elasticity modulus of the rammed aggregate pier,  $E_{\text{column}}$ , increases, as it can be seen from Figure 5.2. The effect is more pronounced for higher values of area ratio of rammed aggregate piers.

### **5.5 Effect of Footing Pressure on Settlement Improvement Factor**

The settlement improvement factor increases as the footing pressure,  $q$ , increases, as it can be seen from Figure 5.3. The effect is more pronounced for higher pressure levels and lower undrained shear strength values of compressible clay layer.

### **5.6 Effect of Compressible Layer Thickness on Settlement Improvement Factor**

The settlement improvement factor decreases as the compressible layer thickness under the footing,  $L_{\text{clay}}$ , increases, as it can be seen from Figure 5.4. The effect is more pronounced for higher pressure levels and lower undrained shear strength values of compressible clay layer and is not very significant for low footing pressures and comparatively high undrained shear strength values of compressible clay layer.

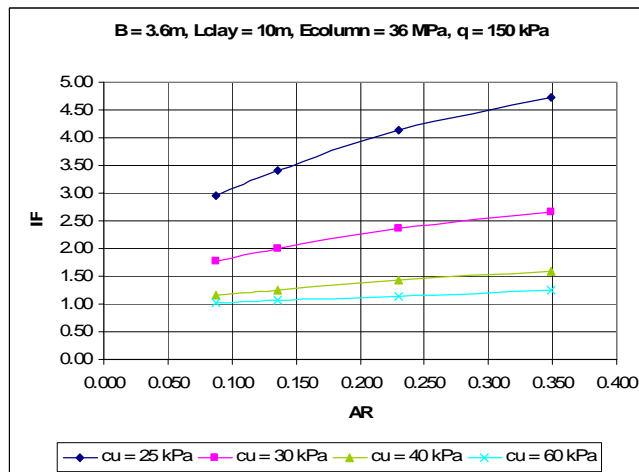
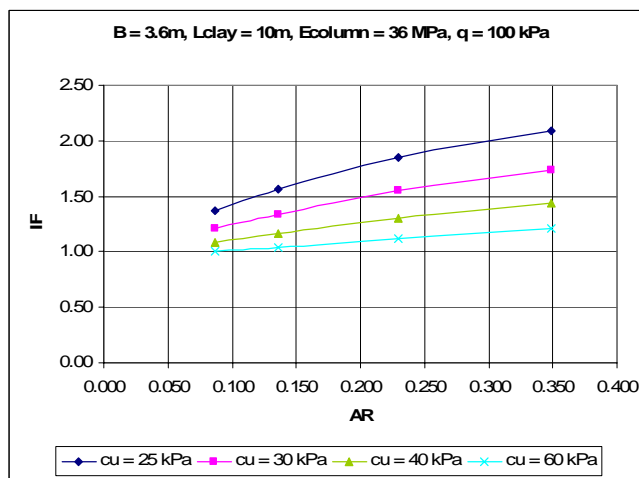
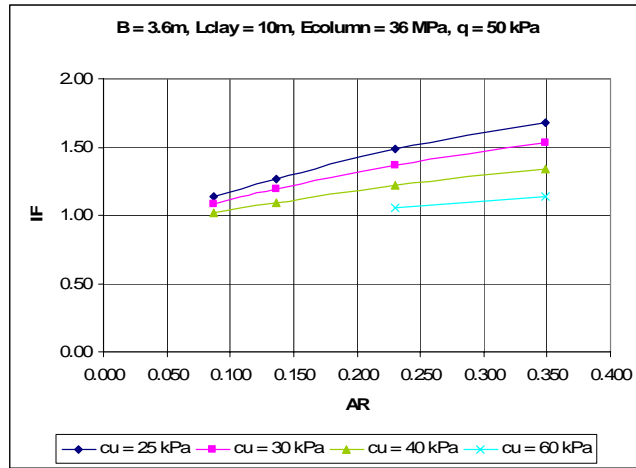


Figure 5.1 Effect of undrained shear strength of compressible clay layer ( $c_u$ ) on settlement improvement factor (IF) for footings resting on aggregate pier groups

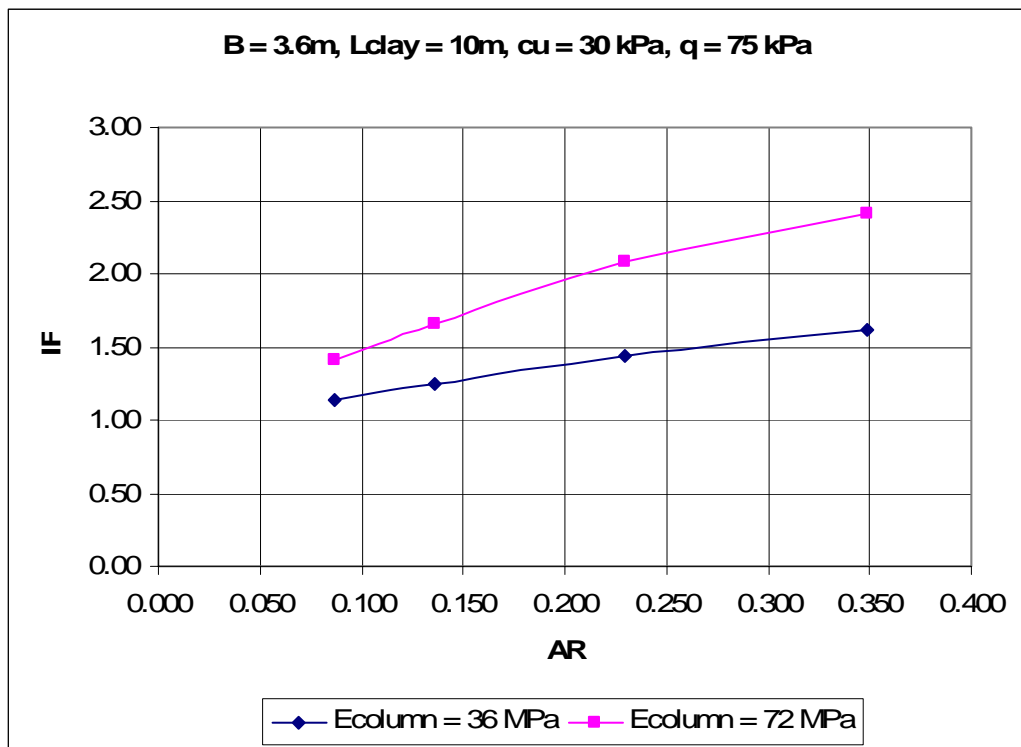


Figure 5.2 Effect of elasticity modulus of rammed aggregate pier ( $E_{column}$ ) on settlement improvement factor (IF) for footings resting on aggregate pier groups

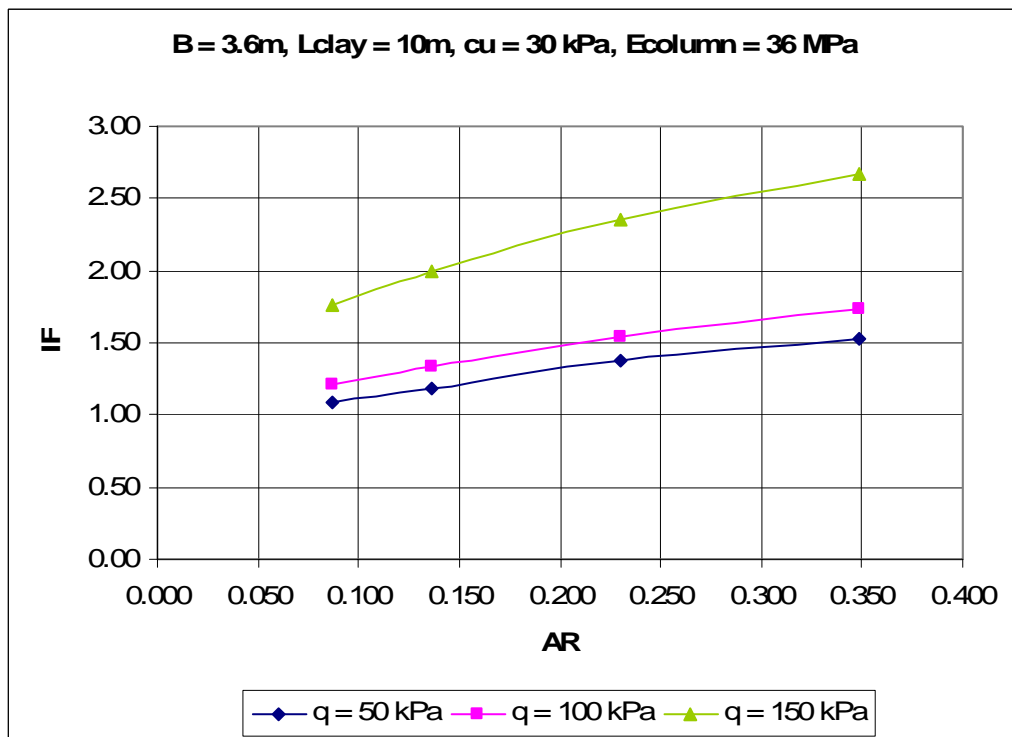
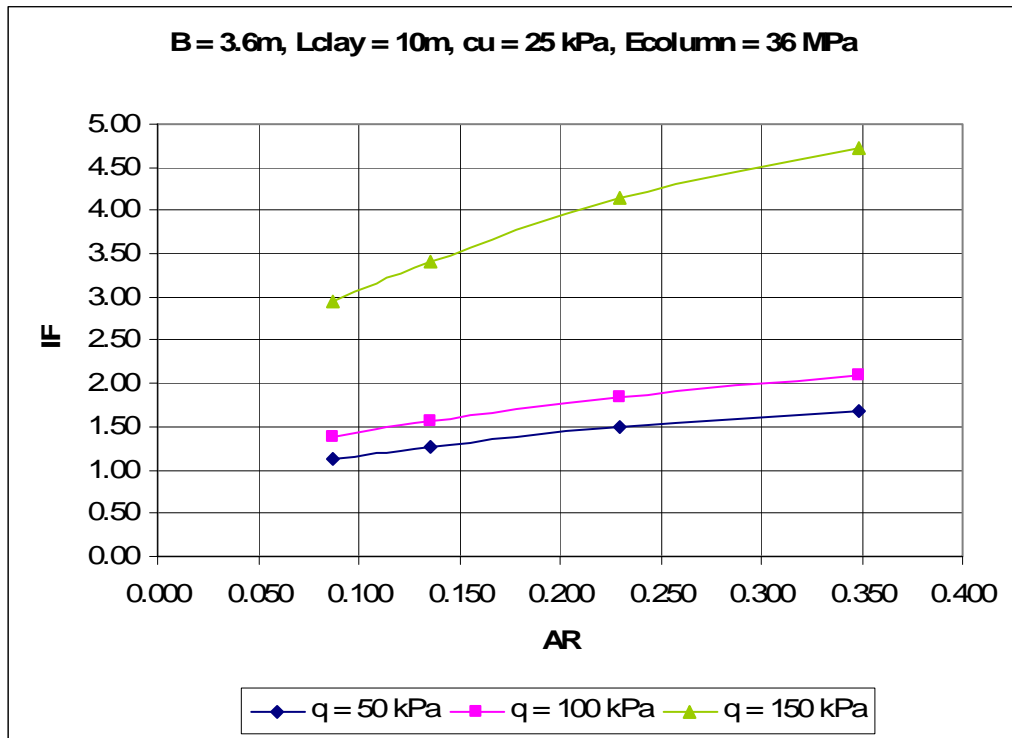


Figure 5.3 Effect of footing pressure (q) on settlement improvement factor (IF) for footings resting on aggregate pier groups

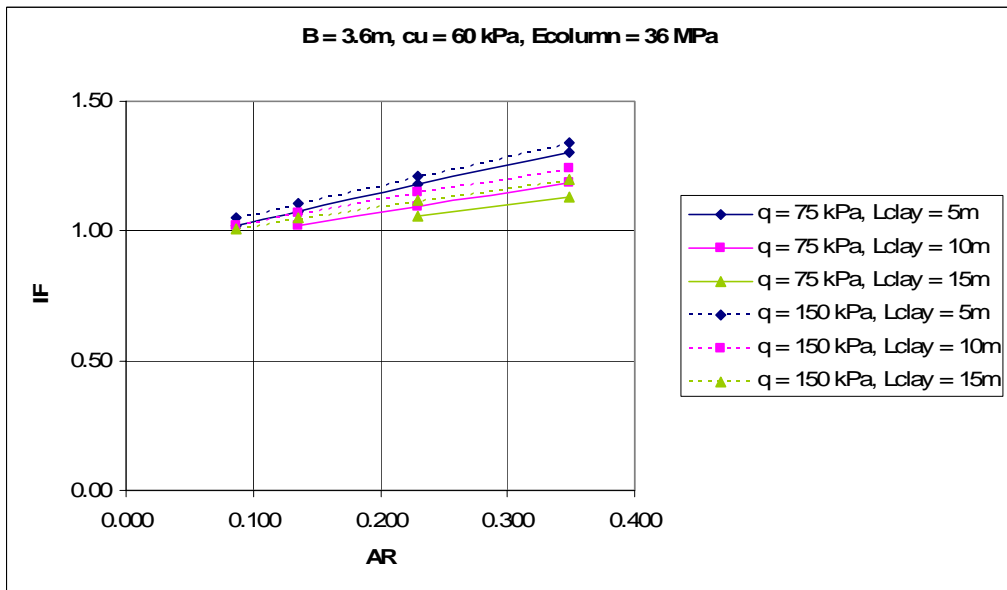
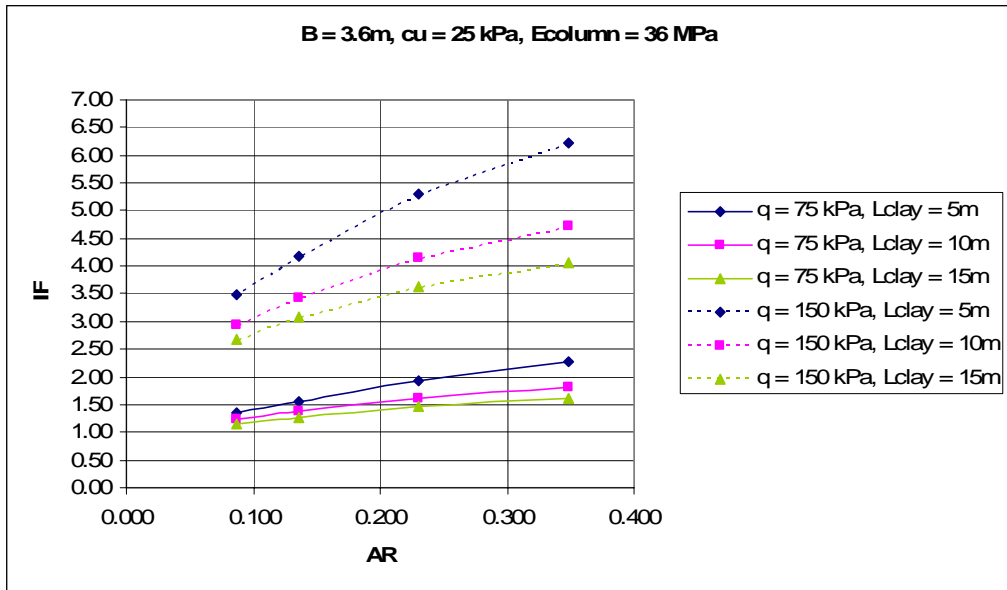


Figure 5.4 Effect of compressible layer thickness ( $L_{clay}$ ) on settlement improvement factor (IF) for footings resting on aggregate pier groups

### **5.7 Effect of Footing Size on Settlement Improvement Factor**

The settlement improvement factor increases as the footing size,  $B$ , increases, as it can be seen from Figure 5.5. The effect is more pronounced for higher pressure levels and lower undrained shear strength values of compressible clay layer and is not very significant for low footing pressures and comparatively high undrained shear strength values of compressible clay layer.

### **5.8 Comparison of Calculated Settlement Improvement Factors with Conventional Methods**

The settlement improvement factors calculated from the 3D finite element analyses described in Chapter 4 are compared with two of the conventional methods (i.e. Equilibrium method and Priebe method) in the literature. (Figure 5.6) The comparison is made for a selected square footing size ( $B=3.6\text{m}$ ), under a footing pressure of  $q=100\text{kPa}$ , resting on end bearing rammed aggregate piers with a length of  $10\text{m}$  and elasticity modulus values of  $E_{\text{column}} = 36\text{ MPa}$  and  $72\text{ MPa}$ . The undrained cohesion value of the compressible clay layer is selected as  $c_u = 25\text{ kPa}$  and  $40\text{ kPa}$ . Settlement improvement factors calculated from the Priebe method usually gives higher values than those obtained by the finite element method, especially for higher area ratio (AR) of rammed aggregate piers and higher elasticity modulus values of rammed aggregate piers ( $E_{\text{column}}$ ). The settlement improvement factors calculated from the Equilibrium method depends heavily on the selected value of the stress concentration factor  $n$ . Settlement improvement factor values for stress concentration factor values of  $n=3$  and  $n=10$  are plotted on Figure 5.6 for comparison values. Settlement improvement factor values calculated with stress concentration factor of  $n=10$  forms an upper bound to the problem and is significantly higher than the calculated values by the finite element method, especially for lower values of elasticity modulus of rammed aggregate piers. ( $E_{\text{column}}$ ). Settlement improvement factors calculated with stress concentration factor of  $n=3$ , yields closer results to the calculated values by the

finite element method. It must be kept in mind that both Priebe method and Equilibrium method are derived for loading on wide areas and contains important simplifying assumptions as described at Chapter 2.

### **5.9 Effect of Floating Columns on Settlement Improvement Factor**

Two cases are selected to investigate the effect of using floating rammed aggregate pier groups instead of end bearing pier groups as shown in Figure 5.7. The length of the floating piers is selected equal to the width of the square footing for both cases. The undrained cohesion value of the compressible clay layer is selected as  $c_u = 25$  kPa and 40 kPa. The elasticity modulus value of the rammed aggregate piers is varied as  $E_{\text{column}} = 36$  MPa and 72 MPa. The floating pier groups are also modelled by 3D finite element model (Composite Soil Model) described in Chapter 3. To investigate the effectiveness of using floating piers instead of end bearing piers, the ratio of settlement improvement factor for floating pier groups over settlement improvement factor for end bearing groups (IF floating / IF end bearing) are plotted against area ratio of rammed aggregate pier groups (AR), as shown in Figure 5.8 and Figure 5.9. These figures can be used in combination with the design charts for end-bearing piers which are presented at Appendix B to judge the feasibility of using floating pier groups for selected cases.

As it can be seen from Figure 5.8 and Figure 5.9, the advantage of using end bearing piers instead of floating piers for reducing settlements increases as the area ratio of piers increases, the elasticity modulus value of the piers increases, the thickness of the compressible clay layer decreases and the undrained shear strength of the compressible clay decreases.

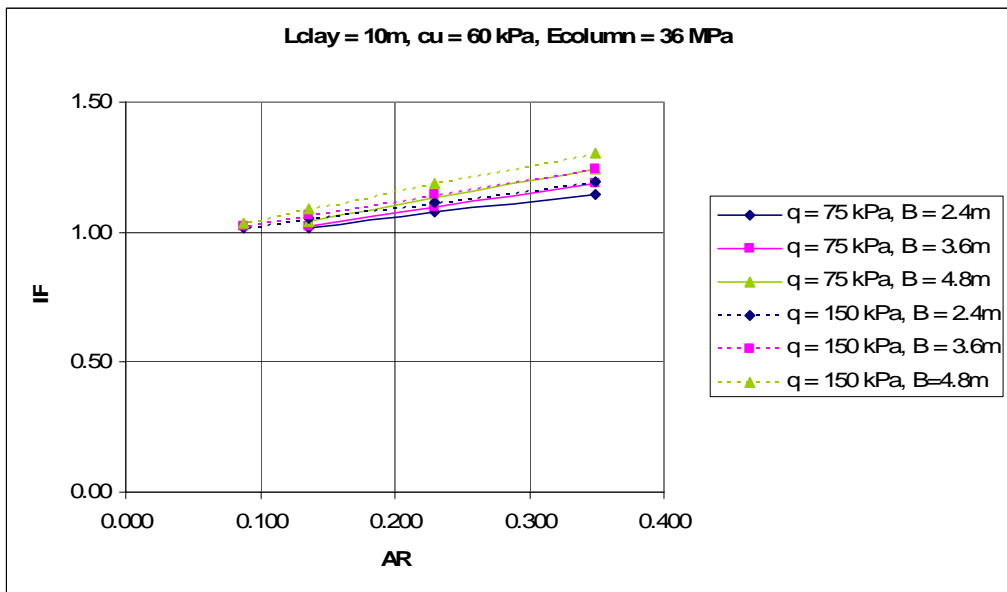
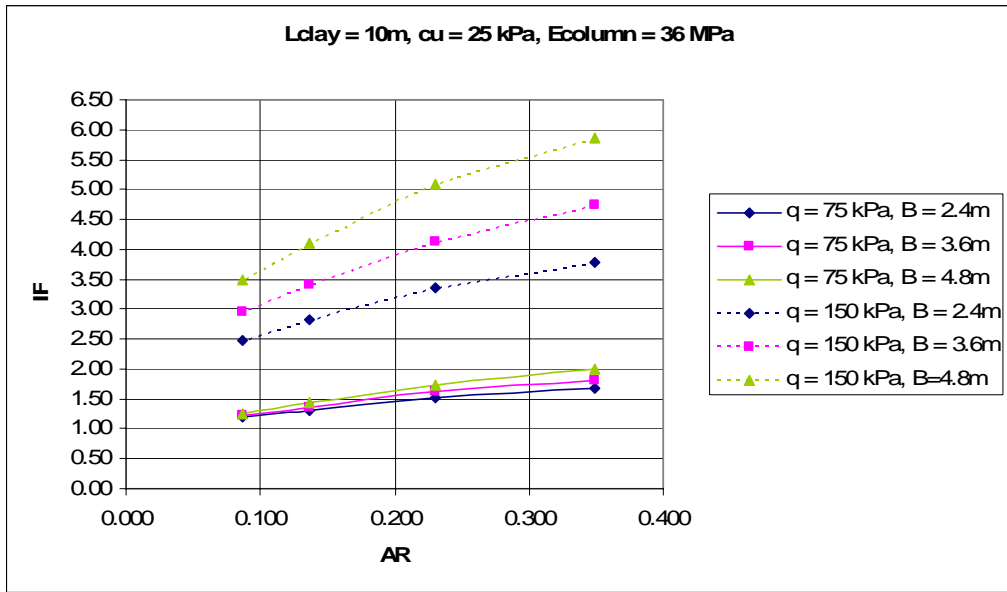


Figure 5.5 Effect of footing size (B) on settlement improvement factor (IF) for footings resting on aggregate pier groups

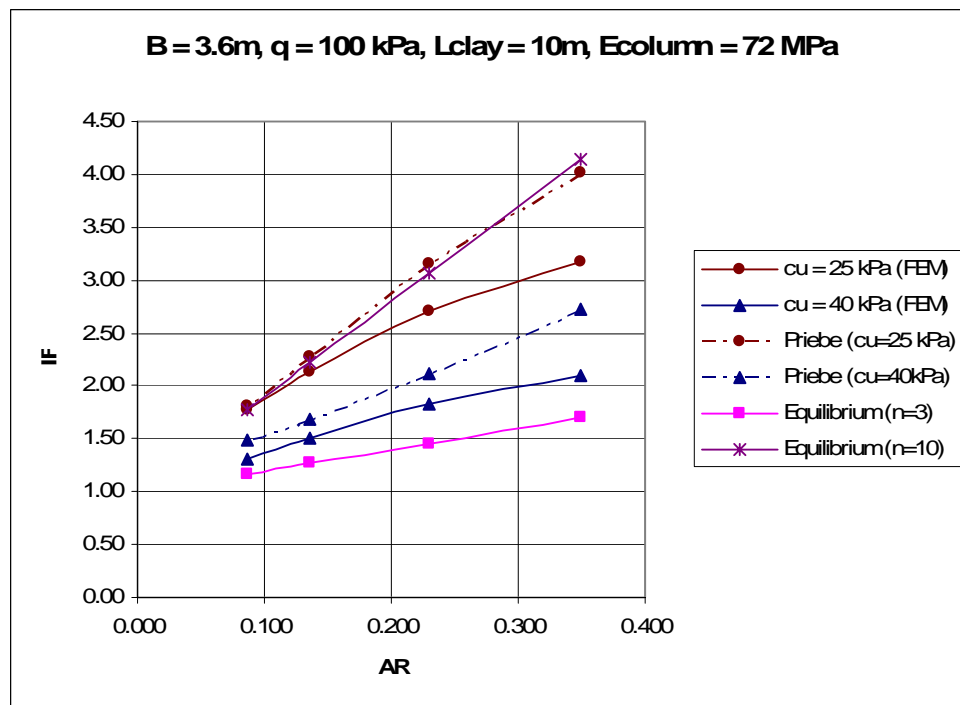
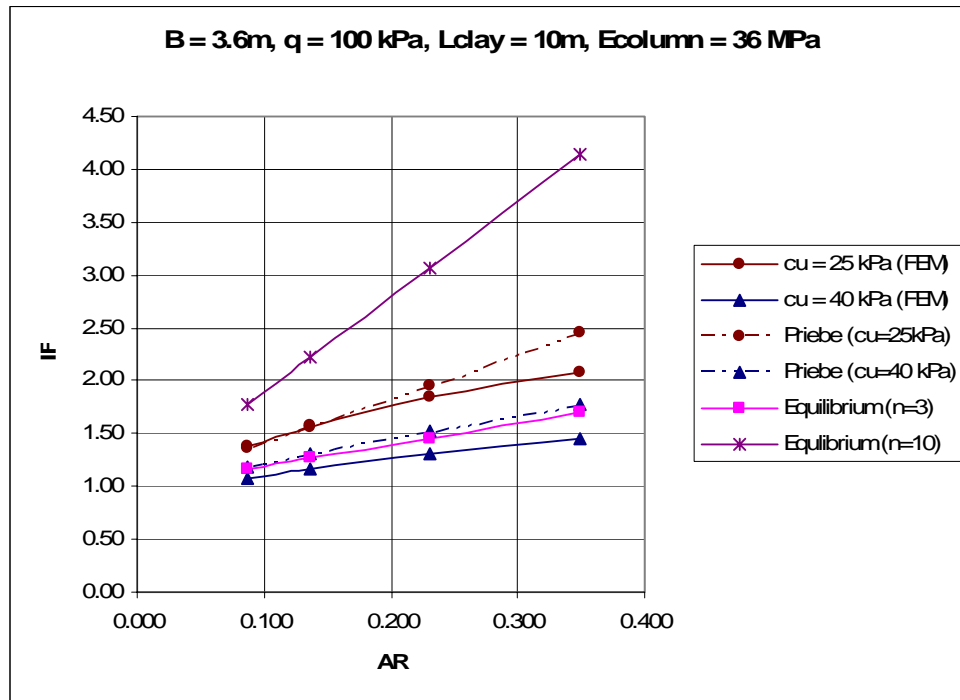
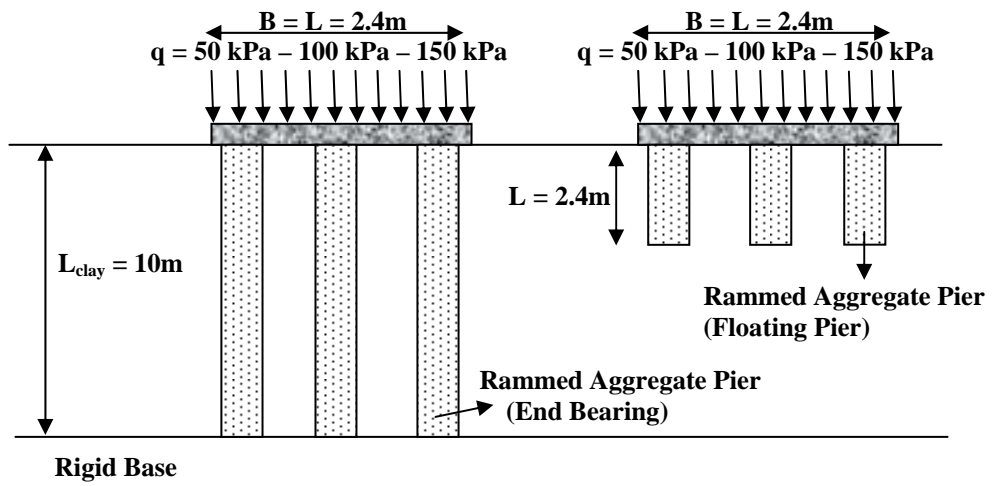
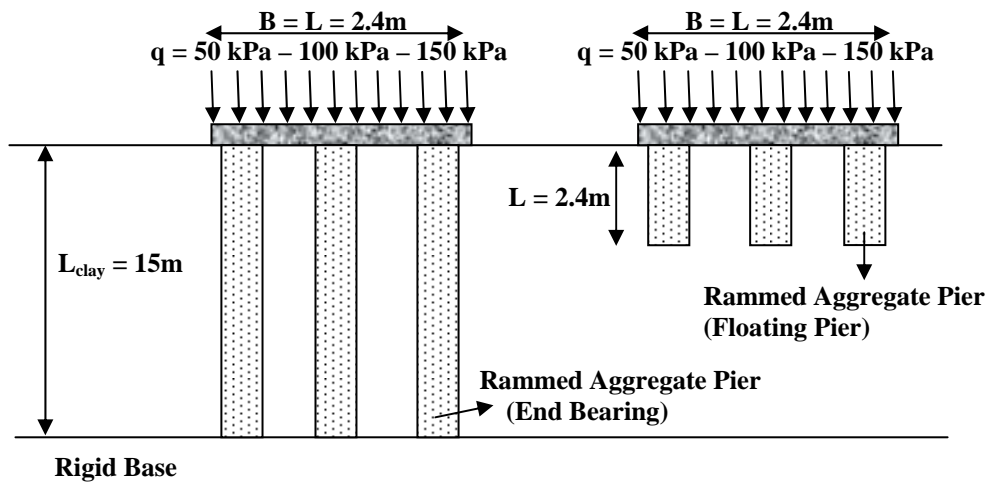


Figure 5.6 Comparison of settlement improvement factor (IF) values calculated by the Finite Element Method (FEM) with the conventional methods in the literature for footings resting on aggregate pier groups



Case I



Case II

Figure 5.7 Geometry of the cases used to investigate the effect of floating piers on the settlement improvement factor

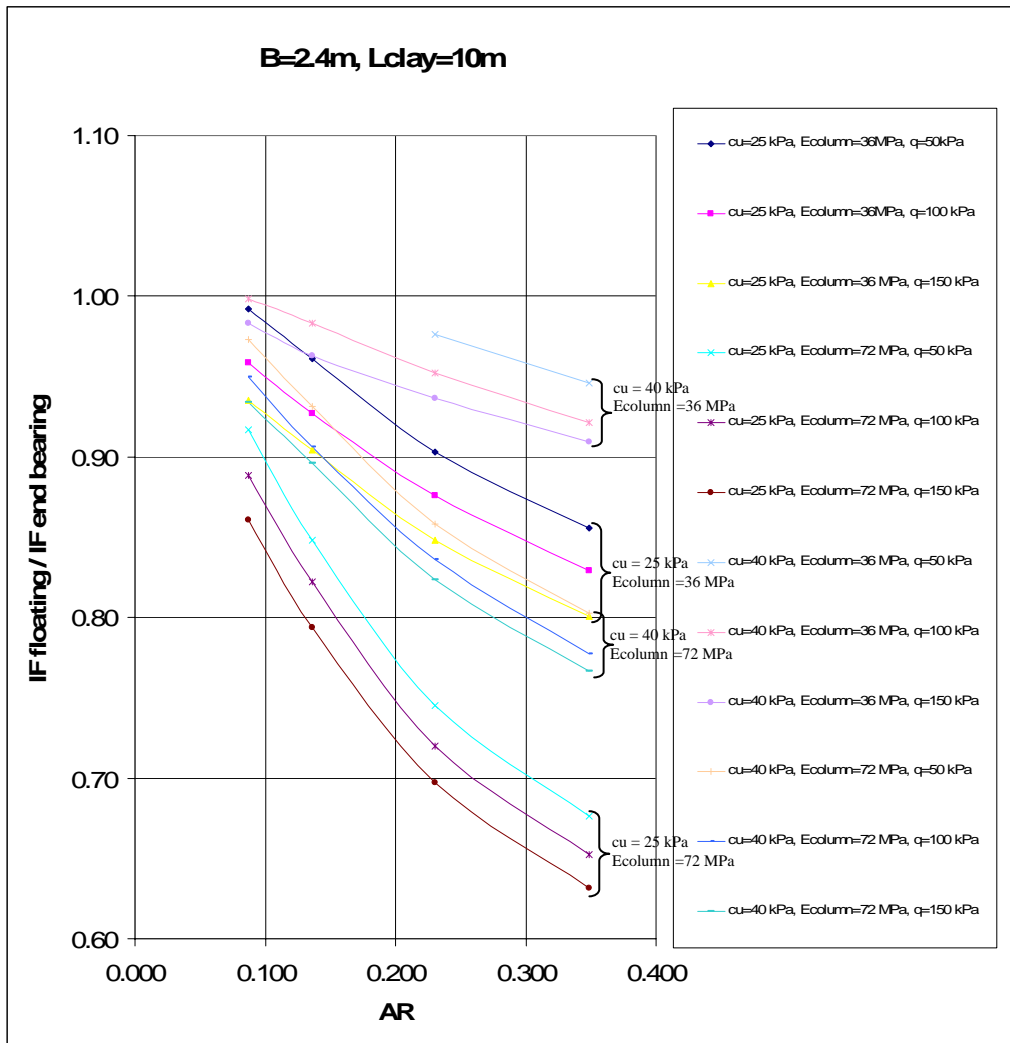


Figure 5.8 Ratio of settlement improvement factor for floating pier group over end bearing pier group vs. area ratio (for selected Case I)

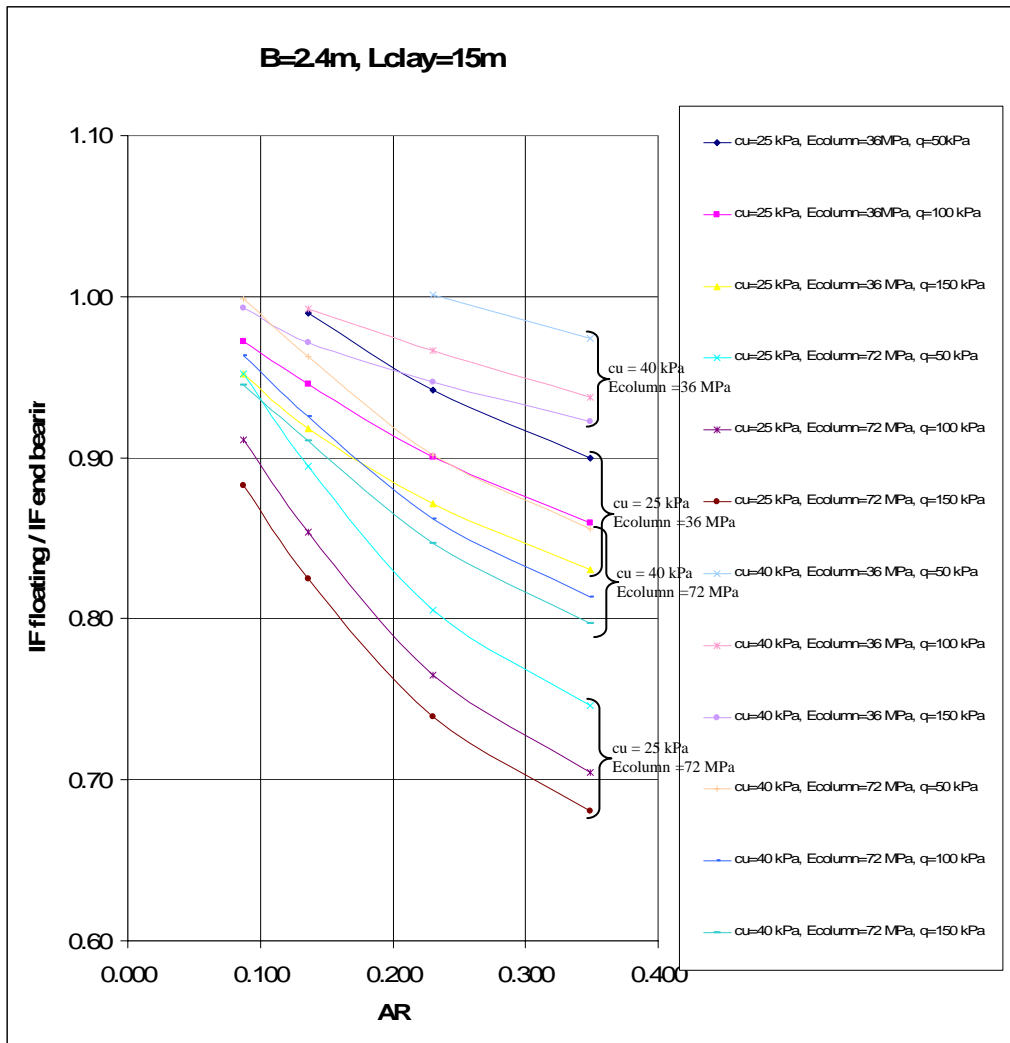


Figure 5.9 Ratio of settlement improvement factor for floating pier group over end bearing pier group vs. area ratio (for selected Case II)

## CHAPTER 6

### CONCLUSIONS AND RECOMMENDATIONS

#### 6.1 Summary

3D finite element modelling was used to model a uniformly loaded rigid footing resting on compressible clay improved by rammed aggregate piers. The results of a full-scale field load test were used to calibrate the finite element method. As a result of the calibration process, it was decided to define linear elastic improved zones around the rammed aggregate piers at the 3D finite element model. Two linear elastic improved zones with radius  $r_1=1.5r_{\text{pier}}$  and  $r_2=2r_{\text{pier}}$  are defined around the piers. The elasticity modulus value of the first improved zone is taken as  $E_1=(2/3)E_{\text{pier}}$  and that of the second improved zone is taken as  $E_2=(1/3)E_{\text{pier}}$ . It must be mentioned that these improved values are related to the ramming energy value specific to the site, which was discussed in detail at Section 3.4. Native soil was modelled by Mohr-Coulomb soil model. By this way, it was possible to model the improved stiffness properties around the piers which were caused by the increase of lateral stress in the matrix soil around the rammed aggregate piers caused by the ramming action during the installation of the piers and it was possible to match the surface settlement pattern observed at the full scale load tests.

The next step was to try to simplify this improved near-linear-elastic zone assumption (Modified Ring Model) so that it can be easily used for practical analyses. For this purpose, the area under the loading plate with the rammed aggregate piers is modeled as a linear elastic composite soil block (Composite Soil Model). The elasticity modulus of this composite soil block is calculated as the weighted average of the elasticity modulus values of the rammed aggregate piers, improved zones around the rammed aggregate piers, and

native soil, according to their respective areas. This simplified model was also satisfactory to match the surface settlement values observed at the full scale load test. In fact, the model yielded closer results to the measured values for floating pier groups.

Once the 3D finite element model (Composite Soil Model) to be used for the analysis of rigid footings resting on rammed aggregate piers was calibrated using the results of full-scale load tests, the next step was to carry out a parametric study using this finite element model to investigate the effect of both geometric parameters (area ratio of rammed aggregate piers, foundation load, width of foundation, rammed aggregate pier length) and material parameters (strength of foundation material, modulus of elasticity value of rammed aggregate piers) on the settlement improvement factor. Design charts to estimate settlement improvement factors for footings resting on compressible clay improved by end bearing rammed aggregate piers were also presented as a result of this parametric study. A design example illustrating the use of the design charts was also given.

The effect of the key parameters (i.e. area ratio of rammed aggregate pier group, undrained shear strength of compressible clay layer, elastic modulus of rammed aggregate pier, footing pressure, thickness of compressible layer and footing size) on the settlement improvement factor for footings resting on compressible clay improved by end bearing rammed aggregate piers can be summarized as below, using the results of the parametric analyses presented at Chapter 4.

## **6.2 Effect of Area Ratio on Settlement Improvement Factor**

The settlement improvement factor increases as the area ratio of the rammed aggregate pier group, AR, increases. The effect is more pronounced for smaller values of undrained shear strength of the compressible clay layer and higher values of the modulus of elasticity values of the rammed aggregate piers.

### **6.3 Effect of Undrained Shear Strength of Compressible Clay Layer on Settlement Improvement Factor**

The settlement improvement factor increases as undrained shear strength of the compressible clay layer,  $c_u$ , decreases. The effect is more pronounced for higher values of footing pressure.

### **6.4 Effect of Elasticity Modulus of Rammed Aggregate Pier on Settlement Improvement Factor**

The settlement improvement factor increases as the elasticity modulus of the rammed aggregate pier,  $E_{\text{column}}$ , increases. The effect is more pronounced for higher values of area ratio of rammed aggregate piers.

### **6.5 Effect of Footing Pressure on Settlement Improvement Factor**

The settlement improvement factor increases as the footing pressure,  $q$ , increases. The effect is more pronounced for higher pressure levels and lower undrained shear strength values of compressible clay layer.

### **6.6 Effect of Compressible Layer Thickness on Settlement Improvement Factor**

The settlement improvement factor decreases as the compressible layer thickness under the footing,  $L_{\text{clay}}$ , increases. The effect is more pronounced for higher pressure levels and lower undrained shear strength values of compressible clay layer and is not very significant for low footing pressures and comparatively high undrained shear strength values of compressible clay layer.

## **6.7 Effect of Footing Size on Settlement Improvement Factor**

The settlement improvement factor increases as the footing size,  $B$ , increases. The effect is more pronounced for higher pressure levels and lower undrained shear strength values of compressible clay layer and is not very significant for low footing pressures and comparatively high undrained shear strength values of compressible clay layer.

## **6.8 Comparison of Calculated Settlement Improvement Factors with Conventional Methods**

The settlement improvement factors calculated from the 3D finite element analyses described in Chapter 4 are compared with two of the conventional methods (i.e. Equilibrium method and Priebe method) in the literature. (Figure 5.6) Settlement improvement factors calculated from the Priebe method usually gives higher values than those obtained by the finite element method, especially for higher area ratio (AR) of rammed aggregate piers and higher elasticity modulus values of rammed aggregate piers ( $E_{\text{column}}$ ). The settlement improvement factors calculated from the Equilibrium method depends heavily on the selected value of the stress concentration factor  $n$ . Settlement improvement factor values calculated with stress concentration factor of  $n=10$  forms an upper bound to the problem and is significantly higher than the calculated values by the finite element method, especially for lower values of elasticity modulus of rammed aggregate piers. ( $E_{\text{column}}$ ). Settlement improvement factors calculated with stress concentration factor of  $n=3$ , yields closer results to the calculated values by the finite element method. It must be kept in mind that both Priebe method and Equilibrium method are derived for loading on wide areas and contains important simplifying assumptions.

## **6.9 Effect of Floating Columns on Settlement Improvement Factor**

Two cases are selected to investigate the effect of using floating rammed aggregate pier groups instead of end bearing pier groups and the length of the floating piers is selected equal to the width of the square footing for both cases. The floating pier groups are also modelled by 3D finite element model (Composite Soil Model) developed during this study. To investigate the effectiveness of using floating piers instead of end bearing piers, the ratio of settlement improvement factor for floating pier groups over settlement improvement factor for end bearing groups ( $IF_{\text{floating}} / IF_{\text{end bearing}}$ ) are plotted against area ratio of rammed aggregate pier groups (AR). These figures can be used in combination with the design charts for end-bearing piers which are presented at Appendix B to judge the feasibility of using floating pier groups for selected cases.

As a result of the study, it was concluded that, the advantage of using end bearing piers instead of floating piers for reducing settlements increases as the area ratio of piers increases, the elasticity modulus value of the piers increases, the thickness of the compressible clay layer decreases and the undrained shear strength of the compressible clay decreases.

## **6.10 Further Research**

Further research on this subject can be concentrated especially on the behaviour of footings resting on floating pier groups. Full scale field load testing concentrating on the stress distribution beneath the footing and the floating piers combined with 3D finite element modeling calibrated with the field test results will be the key to the success in that manner.

Additional research on the behaviour of rammed aggregate pier groups under large areas (rafts and embankments) equipped with 3D finite element

modelling calibrated with carefully planned full scale load tests will also be very helpful.

## REFERENCES

1. ABOSHI, H., ICHIMOTO, E., ENOKI, M., HARADA, K., 1979. "The Compozer- a Method to Improve the Characteristics of Soft Clays by Inclusion of Large Diameter Sand Columns", *Proceedings of International Conference on Soil Reinforcement: Reinforced Earth and Other Techniques*, Paris Vol.1, pp.211-216
2. AMBILY, A.P. and SHAILESH, R.D., 2007. "Behaviour of Stone Columns Based on Experimental and FEM Analysis", *Journal of Geotechnical and Geoenvironmental Engineering*, ASCE, Vol. 133, No. 4, pp.405-415
3. BACHUS, R.C. and BARKSDALE, R.D., 1989. "Design Methodology for Foundations on Stone Columns", *Vertical and Horizontal Deformations of Foundations and Embankments, Proceedings of Settlement'1994*, Texas, ASCE Geotechnical Special Publication No.40, pp.244-257
4. BALAAM, N.P. and BOOKER, J.R., 1981. "Analysis of Rigid Rafts Supported by Granular Piles", *Proceedings of Int. Journal for Numerical and Analytical Methods in Geomechanics*, Vol.5, pp.379-403
5. BALAAM, N.P. and POULOS, H.G., 1983. "The Behavior of Foundations Supported by Clay Stabilized by Stone Columns", *Proceedings of 8<sup>th</sup> ECSMFE*, Helsinki, Vol.1, pp.199-204
6. BALAAM, N.P., BROWN, P.T., and POULOS, H.G., 1977. "Settlement Analysis of soft Clays Reinforced with Granular Piles", *Proceedings of 5<sup>th</sup> Southeast Asian Conference on Soil Engineering*, Bangkok, pp.81-92
7. BARKSDALE, R.D., and BACHUS, R.C., 1983. "Design and Construction of Stone Columns", *Report No. FHWA/RD-83/026*, National Technical Information Service, Virginia, USA.

8. BARKSDALE, R.D., and GOUGHNOUR, R.R., 1984. "Settlement Performance of stone Columns in the US", *Proceedings of Int. Conference on In-Situ Soil and Rock Reinforcement*, Paris, pp.105-110
  
9. BARKSDALE, R.D., and TAKEFUMI, T., 1990. "Design, Construction and Testing of Sand Compaction Piles", *Symposium on Deep Foundation Improvements: Design, Construction and Testing*, ASTM Publications, STP 1089, Las Vegas
  
10. BAUMANN, V., and BAUER, G.E.A, 1974. " The Performance of Foundations on Various Soils Stabilized by the Vibro-Compaction Method", *Canadian Geotechnical Journal*, Vol.11, pp.509-530
  
11. BURMISTER, D.M., 1958. "Evaluation of Pavement Systems of the WASHO Road Test by Layered System Methods" *Highway Research Board Bulletin 177*, pp.26-54
  
12. CLEMENTE, J.L.M., SENAPATHY, H., DAVIE, J.R., 2005. "Performance Prediction of Stone-Column-Supported Foundations", *Proceedings of 16<sup>th</sup> International Conference on Soil Mechanics and Geotechnical Engineering*, Osaka, Japan, pp. 1327-1330
  
13. DOMINGUES, T.S., BORGES, J.L., CARDOSO, A.S., 2007. "Stone Columns in Embankments on Soft Soils. Analysis of the Effect of Deformability", *Proceedings of 14<sup>th</sup> European Conference on Soil Mechanics and Geotechnical Engineering*, Madrid, Spain, pp. 1445-1449
  
14. FOX, E.N., 1948. " The Mean Elastic Settlement of a Uniformly Loaded Area at a Depth Below the Ground Surface", *Proceedings of 2<sup>nd</sup> Intl. Conf. on Soil Mechanics and Foundation Engineering*, Vol.2, pp.236-246
  
15. GIROUD, J.P., 1970. " Stresses Under Linearly Loaded Rectangular Area", *Journal of the Soil Mechanics and Foundations Division*, ASCE, Vol.96, No.SM1, pp.263-268

16. GOUGHNOUR, R.R. and BAYUK, A.A., 1979(a). "A Field Study of Long Term Settlements of Loads Supported by Stone Columns in Soft Ground", *Proceedings of Int. Conf. on In-Situ Soil and Rock Reinforcement*, Paris
  
17. GOUGHNOUR, R.R. and BAYUK, A.A., 1979(b). "Analysis of Stone Column-Soil Matrix Interaction Under Vertical Load", *Proceedings of Int. Conf. on In-Situ Soil and Rock Reinforcement*, Paris
  
18. GREENWOOD, D.A., 1970. "Mechanical Improvement of Soils below Ground Surface", *Proceedings of the Conf. on Ground Engineering*, London, ICE.
  
19. HANDY, R.L., 2001. "Does Lateral Stress Really Influence Settlement", *Journal of Geotechnical and Geoenvironmental Engineering*, ASCE, Vol. 127, No. 7, pp.623-626
  
20. HUGHES, J.M.O., and WITHERS, N.J., 1974. "Reinforcing of Soft Cohesive Soils with Stone Columns", *Ground Engineering*, Vol.7, No.3, pp.42-49
  
21. HUGHES, J.M.O., WITHERS, N.J., GREENWOOD, D.A., 1975. "A Field Trial of the Reinforcing Effect of a Stone Column in Soil", *Geotechnique*, 25,1, pp.31-44
  
22. LAWTON, E.C., and FOX, N.S., 1994. "Settlement of Structures Supported on Marginal or Inadequate Soils Stiffened with Short Aggregate Piers", *Vertical and Horizontal Deformations of Foundations and Embankments, Proceedings of Settlement'1994*, Texas, ASCE Geotechnical Special Publication No.40, pp.244-257
  
23. LAWTON, E.C., FOX, N.S., HANDY, R.L., 1994, "Control of Settlement and Uplift of Structures Using Short Aggregate Piers" *In-Situ Deep Soil Improvement*, ASCE Geotechnical Special Publication No.45

24. LUNNE, T., ROBERTSON, P.K., POWELL, J.J.M, 1997. *Cone Penetration Testing in Geotechnical Practice*, Blackie Academic & Professional.
25. MOSOLEY, M.P., and PRIEBE, H.J., 1993. “Vibro Techniques” *Ground Improvement*, Chapman and Hall.
26. ÖZKESKİN, A., 2004. “Settlement Reduction and Stress Concentration Factors in Rammed Aggregate Piers Determined From Full Scale Load Tests ” *thesis presented to the Middle East Technical University in partial fulfillment of the requirements for the degree of Doctor of Philosophy*.
27. PRIEBE, H., 1990. “Vibro Replacement- Design Criteria and Quality Control”, *Symposium on Deep Foundation Improvements: Design, Construction and Testing*, ASTM Publications, STP 1089, Las Vegas
28. PRIEBE, H., 1993. “Design Criteria for Ground Improvement by Stone Columns”, *Proceedings of 4<sup>th</sup> National Conference on Ground Improvement*, Lahore
29. PRIEBE, H., 1995. “The design of Vibro Replacement”, *Journal of Ground Engineering*, Vol.28, No.10
30. SOVINC, I., 1969. “Displacements and Inclinations of Rigid Footings Resting on a Limited Elastic Layer of Uniform Thickness”, *Proceedings of 7<sup>th</sup> International Conference on Soil Mechanics and Foundation Engineering*, Vol.1, pp.385-389
31. TEKİN, M., 2005. “Model Study on Settlement Behaviour of Granular Columns Under Compression Loading ” *thesis presented to the Middle East Technical University in partial fulfillment of the requirements for the degree of Doctor of Philosophy*.
32. TERZAGHI, K., 1943. “Evaluation of Coefficient of Subgrade Reaction”, *Geotechnique*, Vol.5, No.4, pp.297-326

33. THORNBURN, S., 1975. "Building Structures Supported by Stabilized Ground", *Geotechnique*,(25),1, pp. 83-94
34. VAN IMPE, W.F, DE BEER, E., 1983. "Improvement of Settlement Behavior of Soft Layers by Means of Stone Columns", *Proceedings of 8<sup>th</sup> ECSMFE*, Helsinki
35. WHITE, D.J., PHAM, H.T.V., HOEVELKAMP K.K, 2007. "Support Mechanisms of Rammed Aggregate Piers. I: Experimental Results", *Journal of Geotechnical and Geoenvironmental Engineering*, ASCE, Vol. 133, No. 12, pp.1503-1511

# APPENDIX A

## SITE INVESTIGATION DATA

DERİNLİK / DEPTH (m)		KAROT / SPT / RECORD	NUMERNO / SAMPLE NO.	NUMERNE DERİNLİĞİ / SAMPLE DEPTH (from to)	ZEMİN TANIMLAMASI / SOIL DESCRIPTION	ZEMİN PROFİLİ / SOIL PROFILE	İÇ ÇAP / I.D. (mm)	AYRISMA / FRACTION	KIRIK 30 cm / FRACTURE 30 cm	KIRIK AÇISI / FRACTURE ANGLE	SU KAYBI / WATER LOSS %	STANDART PENETRASYON DENEYİ / STANDARD PENETRATION TEST								
												Darbe Sayısı / No. Of Blows		GRAFIK / GRAPH						
												0-15	15-30	30-45	N <sub>60</sub>	10	20	30	40	50
					0.15m Top Soil															
1		UD1	1.50-2.10		Grevev Silty Clay Soft															
		SPT1	1.50-1.95																3	1
2																				
		UD2	2.60-3.10																	
3																				
		SPT2	3.60-4.05																4	3
4					Sandv. gravelly clay															
		SPT3	5.90-6.55	6.00m															6	3
5					Clayey sandv gravel															
		SPT4	7.10-7.55	7.80m															7	6
6					Silty gravelly clay Stiff															
		UD3	7.55-8.05																8	11
7																				
		SPT5	8.05-8.50																	
8																				
		UD2	9.0-9.60																6	7
9					End of borehole															
		SPT6	9.60-10.05	10.05m																
10																				
11																				
12																				

KIVAM DURUMU / STIFFNESS			SİKLİK / DENSITY			ORANLAR / PROPORTIONS			KIRIKLAR / FRACTIONS 30cm		
N = 0-2	Çok yumuşak	V.soft	N = 0-4	Çok gevşek	V.loose	0-10%	Pek az (Scarcely)	Trace	=1	Scarcely	Weak (W)
N = 3-4	Yumuşak	Soft	N = 5-10	Gevşek	Loose	10-20%	Az	Little	1-2	Orta	Moderate (M)
N = 5-8	Orta katı	Med.stiff	N = 11-30	Orta sıkı	M.dense	20-35%	Sığık	Adjective (Or some)	2-10	Sık	Close (C)
N = 9-15	Katı	Stiff	N = 31-50	Sıkı	Dense	35-50%	Ve	And	10-20	Çok sık	Intense (I)
N = 16-30	Çok katı	V.stiff	N = 50	Çok sıkı	V.dense				>20	Parçalanmış	Crushed (CO)
N > 30	Sert	Hard									

DAYANIMLILIK / STRENGTH		AYRISMA / WEATHERING		KAYI KALITESİ / TANI MI / RQD		UD-Örneklemesi / Numene / Undisturbed Sample			
I	Çok zayıf	Very weak	I	Tamamen ayrışmış	Comp. weathered	0-25%	Çok zayıf	Very poor	D-Örneklemesi / Numene / Disturbed Sample
II	Zayıf	Weak	II	Çok ayrışmış	Highly weathered	25-50%	Zayıf	Poor	SPT-Standard Pen Dene yi / Standard Pen Test
III	Orta zayıf	M.weak	III	Orta ayrışmış	Mod. weathered	50-75%	Orta	Fair	VST-Vane Dene yi / Vane Shear Test
IV	Orta Dayanıklı	M.strong	IV	Az ayrışmış	Slightly weathered	75-90%	İyi	Good	P-Pressiometre Dene yi / Pressuremeter Test
V	Dayanıklı	Strong	V	Taze	Fresh	90-100%	Çok iyi	Excellent	K-Karot Numunesi / Core Sample

Figure A.1 Borehole log of SKT-1







DERİNLİK / DEPTH (m)		KAROT NO / SİSİ / CORE NO / RECORD NO	RQD %	SUMRNE DERİNLİĞİ / SAMPLE DEPTH from to	ZEMİN TANIMLAMASI / SOIL DESCRIPTION	ZEMİN PROFİLİ / SOIL PROFILE	PVC BORU / PVC PIPE	AKRİLİK / ACRYLIC	KIRIK 20 cm / FRACTURE 20 cm	KIRIK AÇISI / FRACTURE ANGLE	SULANMA / PLATE LOSS %	STANDART PENETRASYON DENEYİ / STANDARD PENETRATION TEST									
												Darbe Sayısı / No. Of Blows		GRAFIK / GRAPH							
												6-15	15-30	30-45	N <sub>60</sub>	10	20	30	40	50	
				SPT1 0.50-0.95	0.5m Top Soil							2	4	5	9						
				UD1 1.50-2.00																	
				SPT2 2.0-2.45								4	5	6	11						
				SPT3 3.50-3.95								6	6	9	15						
				SPT4 5.0-5.45								6	7	10	17						
				SPT5 6.0-6.45								8	7	4	11						
				SPT6 7.50-7.95								8	10	16	26						
				SPT7 8.50-8.95								6	9	13	22						
				SPT8 9.50-9.95								7	8	11	19						
				SPT9 10.50-10.95								9	10	16	26						
				SPT10 12.0-12.45								10	12	26	38						
				SPT11 12.80-13.25								12	14	28	42						
KIVAM DURUMU / STIFFNESS				SIKILIK / DENSITY				ORANLAR / PROPORTIONS				KIRIKLAR 30cm-FRACTIONS 30cm									
N = 0-2	Cok yumusak	Very soft		N = 0-4	Cok gevsek	Very loose	0-10%	Pek az (Scarcely)	Trace			-1	Seyrek	Wide	(W)						
N = 2-4	Yumusak	Soft		N = 5-10	Gevsek	Loose	10-20%	Az	Little			1-2	Orta	Moderate	(M)						
N = 5-8	Orta kati	Medium stiff		N = 11-30	Orta sik	Medium dense	20-35%	Sifati	Adjective (Or some)			2-10	Sik	Close	(C)						
N = 9-15	Kati	Stiff		N = 31-50	Siki	Dense	35-50%	Ve	And			10-20	Cok sik	Intense	(I)						
N = 16-30	Cok kati	Very stiff		N = 50	Cok sik	Very dense						>20	Parçali	Crushed	(CR)						
N = 30	Sert	Hard																			
DAYANIMLILIK / STRENGTH				AYRISMA / WEATHERING				KAYAKALİTESİ TANIMI / RQD				UD:Özelenmemiş Numune / Undisturbed Sample									
I	Cok zayıf	Very weak		I	Tamamen ayrılmış	Completely weathered	0-25%	Cok zayıf	Very poor			D:Özelenmiş Numune / Disturbed Sample									
II	Zayıf	Weak		II	Cok ayrılmış	Highly weathered	25-50%	Zayıf	Poor			SPT:Standard Pen Deneysi / Standard Pen Test									
III	Orta zayıf	Medium weak		III	Orta ayrılmış	Mod. weathered	50-75%	Orta	Fair			VST:Vane Deneysi / Vane Shear Test									
IV	Orta dayanımlı	Medium strong		IV	Az ayrılmış	Slightly weathered	75-90%	İyi	Good			P: Presiometre Deneysi / Pressuremeter Test									
V	Dayanımlı	Strong		V	Taze	Fresh	90-100%	Cok iyi	Excellent			K:Karet Numunesi / Core Sample									

Figure A.5 Borehole log of SK-4



DERİNLİK / DEPTH (m)		KAROT VE/VEYA ÇİZİM / CORE / RECORD	RAÇD %	NUMERİK NOT / REMARK	NÜMUNE DERİNLİĞİ / SAMPLE DEPTH from to	ZEMİN TANIMLAMASI / SOIL DESCRIPTION	ZEMİN PROFİLİ / SOIL PROFILE	PVC BORU / PVC PIPE	AYRISMA / WEATHERING	KIRILMA / FRACTURE	KIRILMA / FRACTURE	SU KAYBI / WATER LOSS %	STANDART PENETRASYON DENEYİ / STANDARD PENETRATION TEST							
												Darbe Sayısı / No. Of Blows		N <sub>60</sub>	GRAFİK / GRAPH					
												0-15	15-30		30-45	10	20	30	40	50
0.5m						Top Soil														
1																				
2					SPT1	1.50-1.95							10							
3					UD1	2.50-3.0														
4					SPT2	3.0-3.45							7							
5					UD2	4.0-4.50														
6					SPT3	4.50-4.95							5							
7																				
8					SPT4	6.0-6.45							9							
9																				
10																				
11																				
12					SPT5	7.50-7.95							11							
KIVAM DURUMU / STIFFNESS				SIKLIK / DENSITY				ORANLAR / PROPORTIONS				KIRILMA / FRACTURES: 30cm								
N=0-2	Çok yumuşak	V.soft		N=0-4	Çok gevsek	V.loose	0-10%	Fak az (Scarcely)	Fine			1	Seyrek	Wide	(W)					
N=3-4	Yumuşak	Soft		N=5-10	Gevsek	Loose	10-20%	Az	Little			1-2	Orta	Moderate	(M)					
N=5-8	Orta katı	M.stiff		N=11-20	Orta sıkı	M.dense	20-25%	Sıfır	Adjective(Or some)			2-10	Sık	Close	(C)					
N=9-15	Katı	Stiff		N=21-50	Sıkı	Dense	35-50%	Vc	And			10-20	Çok sık	Intense	(I)					
N=16-30	Çok katı	V.stiff		N>=50	Çok sıkı	V.dense						>20	Parçalı	Crushed	(Cr)					
N>30	Sert	Hard																		
DAYANIMLILIK / STRENGTH				AYRISMA / WEATHERING				KAYA KALİTESİ TANIMI / RQD				UD:Örselemedenmiş Numune / Undisturbed Sample								
I	Çok zayıf	Very weak		I	Tamamen ayrılmış	Comp. weathered	0-25%	Çok zayıf	Very poor				D:Örselemedenmiş Numune / Disturbed Sample							
II	Zayıf	Weak		II	Çok ayrılmış	Highly weathered	25-50%	Zayıf	Poor				SPT:Standard Pen Dencisi / Standard Pen Test							
III	Orta zayıf	M.weak		III	Orta ayrılmış	Mod. weathered	50-75%	Orta	Fair				VST:Vane Dencisi / Vane Shear Test							
IV	Orta Dayanımlı	M.strong		IV	Az ayrılmış	Slightly weathered	75-90%	İyi	Good				P: Pressiometre Dencisi / Pressuremeter Test							
V	Dayanıklı	Strong		V	Taze	Fresh	90-100%	Çok iyi	Excellent				K:Karot Numunesi / Core Sample							

Figure A.7 Borehole log of SA8







# ZEMAR Ltd.

Operator: Tunay Cetin  
 Sounding: CPT023  
 Cone Used: 822TC

CPT Date/Time: 10-18-03 13:13  
 Location: ODTU EYMIRGOLU  
 Job Number: CPT1

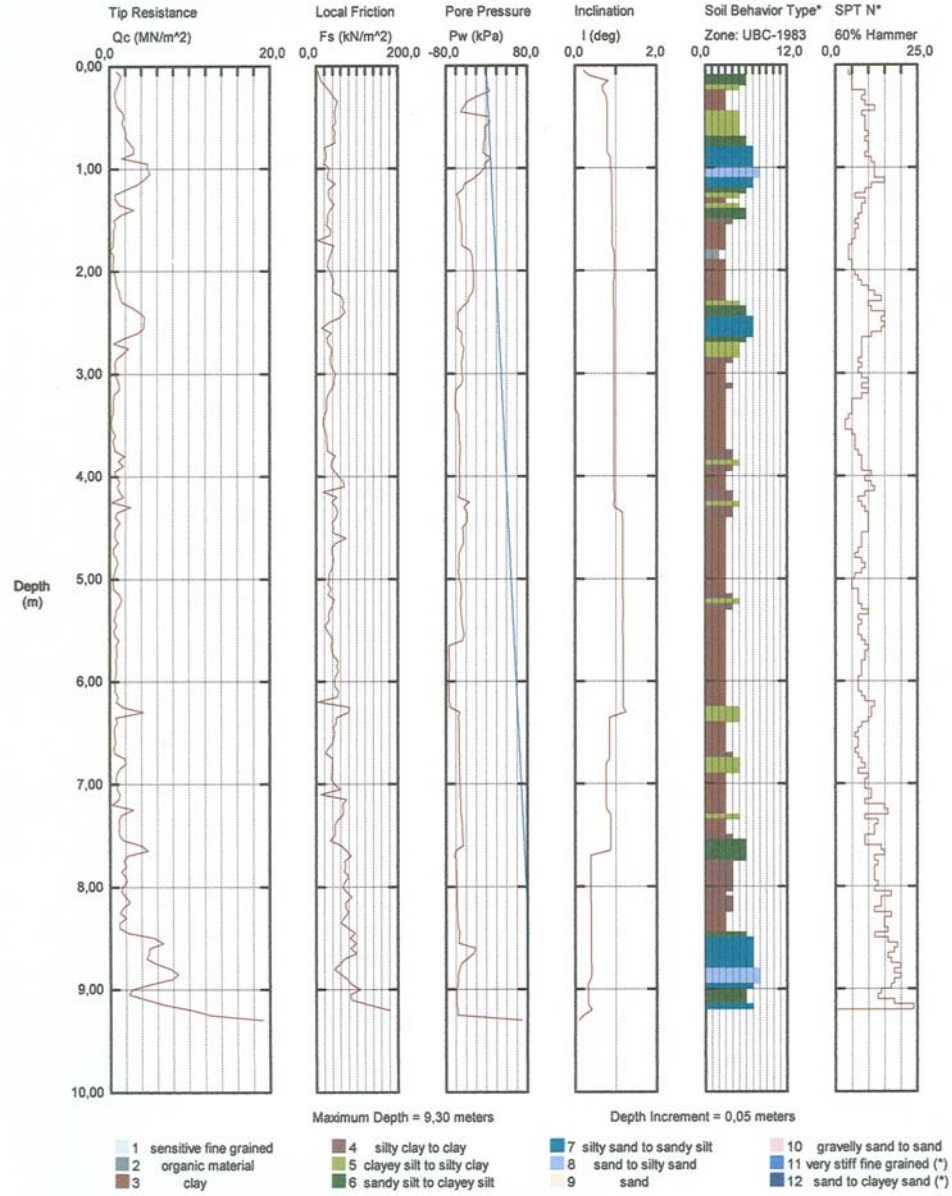


Figure A.11 Log of CPT-1

# ZEMAR Ltd.

Operator: Tunay Cetin  
 Sounding: CPT024  
 Cone Used: 822TC

CPT Date/Time: 10-18-03 14:25  
 Location: ODTU EYMIRGOLU  
 Job Number: CPT2

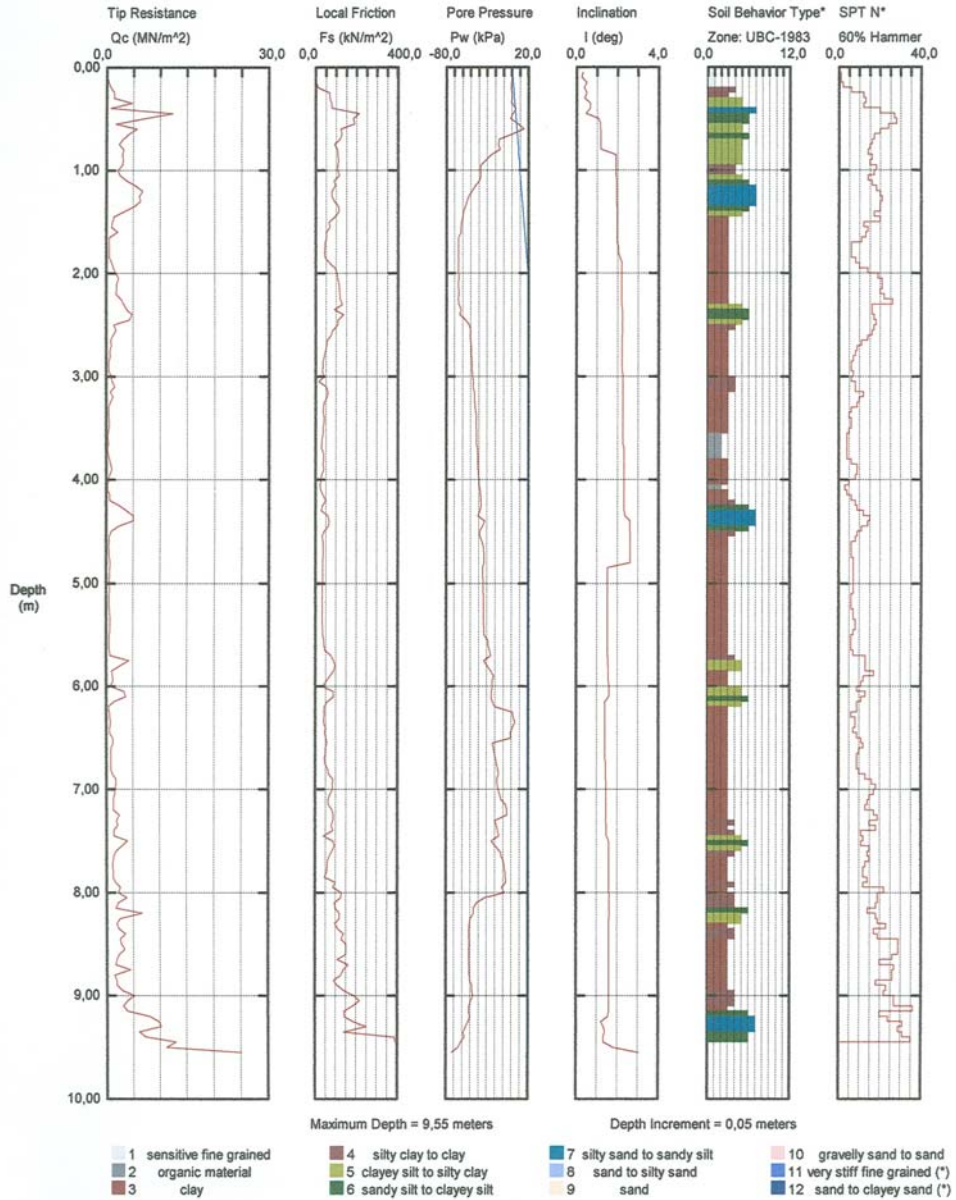


Figure A.12 Log of CPT-2

# ZEMAR Ltd.

Operator: Tunay Cetin  
Sounding: CPT025  
Cone Used: 822TC

CPT Date/Time: 10-18-03 15:47  
Location: ODTU EYMIRGOLU  
Job Number: CPT3

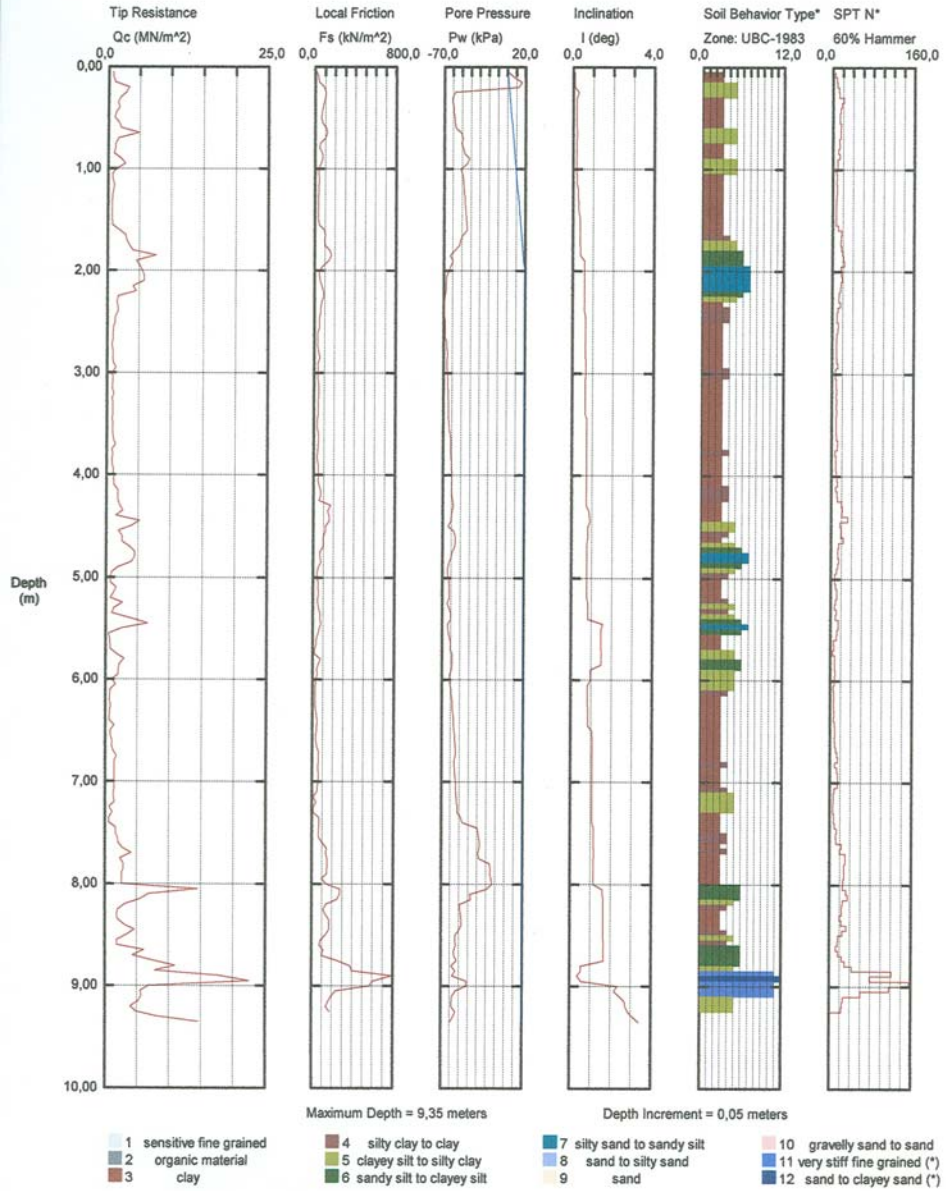


Figure A.13 Log of CPT-3

# ZEMAR Ltd.

Operator: Tunay Cetin  
Sounding: CPT023  
Cone Used: 822TC

CPT Date/Time: 10-18-03 13:13  
Location: ODTU EYMIRGOLU  
Job Number: CPT1

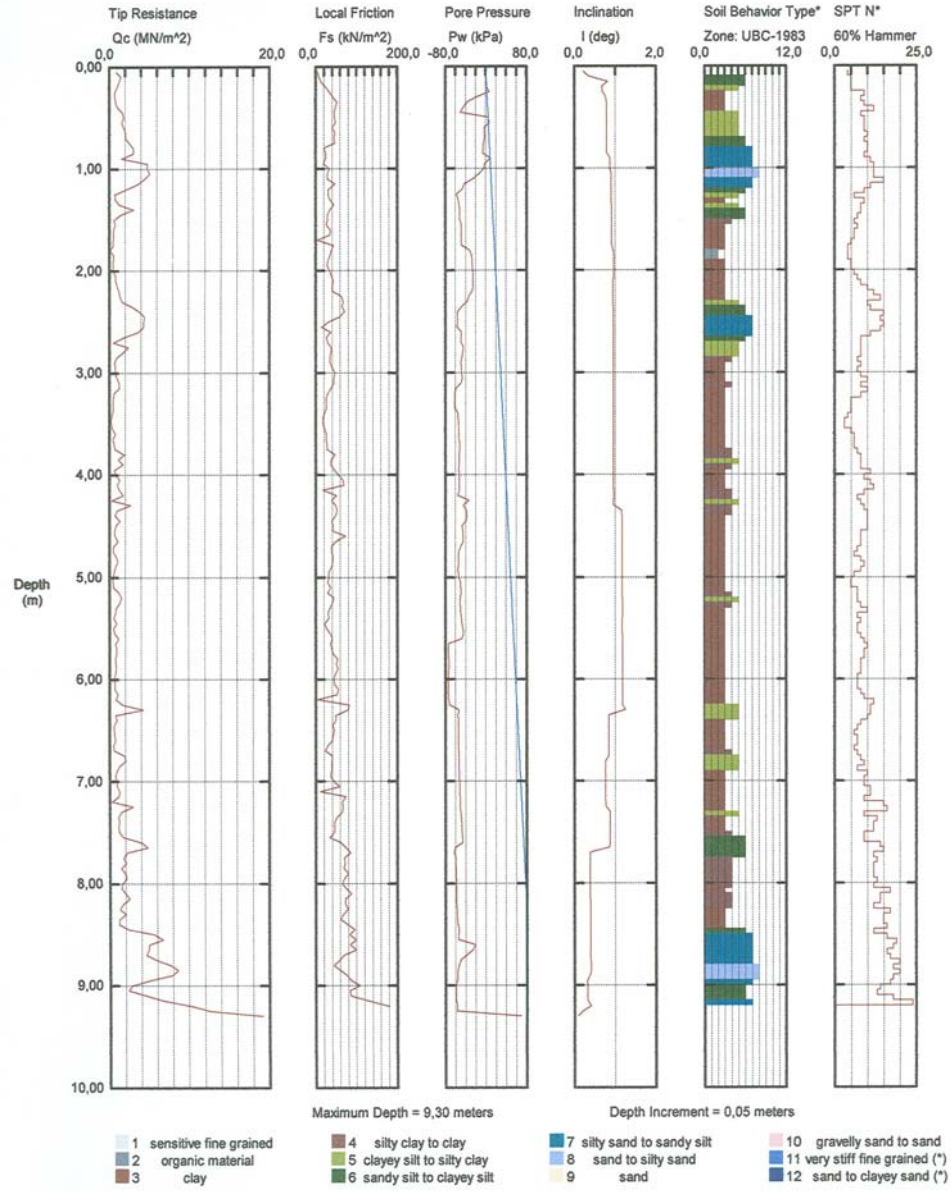


Figure A.14 Log of CPT-4

Table A.1 Laboratory Test Results of SKT-1


**M.E.T.U. SOIL MECHANICS LABORATORY**  
**O.D.T.Ü ZEMİN MEKANİĞİ LABORATUVARI**

PROJECT/PROJE: **EYMIŞ LAKE**

Sondaj Boring No	Numune Sample No	Derinlik Depth (m.)	SPT N	w <sub>p</sub> (%)	e <sub>n</sub>	γ <sub>n</sub> kN/m <sup>3</sup>	G <sub>s</sub>	Elek analizleri Sieve analysis		Atterberg limitleri Atterberg Limits			Uniformluk katsayıları Uniformity numbers		USCS	Direk Kesme Deneyi Direct Shear Test(CD)			Üç Eksenli Bas Den Triaxial Test(UU)			Kil Yüzdesi Clay Cont. (%)	
								-No.4 (%)	-No.200 (%)	LL (%)	PL (%)	PI (%)	C <sub>u</sub>	C <sub>c</sub>		c (kPa)	f (°)	c (kPa)	f (°)	f (°)			
SKT-1	SPT-1	1.50-1.95	3				2,672	99,7	95,4	40	19	21,0			CL							25	
	UD-1	1.50-2.10		24,6		19,70											55	0					
	UD-2	2.60-3.10																					
	TOR-1	3.00-3.50					2,513	88,3	40,8	32,4	16,2	16,2			SC							11	
	SPT-2	3.60-4.05	7					73,3	5,2						SW-SC								
	TOR-2	4.50					2,648	80,9	27,8	27,8	15,9	11,9			SC							6	
	TOR-3	5.00					2,642	90,7	34,5	27,3	15,5	11,8			SC							9	
	TOR-4	5.50-6.00					2,671	77,4	27,1	30,4	14,3	16,1			SC							6	
	SPT-3	5.90-6.35	8					78,4	32,4						SC								
	TOR-5	6.50-7.00					2,574	87,3	28,5	28,5	15,7	12,8			SC								7
	TOR-6	6.80-7.10					2,536	68,5	16,6						SC								5
	SPT-4	7.10-7.55	23				2,673	65,8	20,5	23,7	14,4	9,3			SC								5
	UD-3	7.55-8.05																					
	TOR-7	7.50-8.00					2,685	84,0	42,0	36,2	18,0	18,2			SC								19
	SPT-5	8.00-8.50	16				2,512	83,5	52,2	39,5	18,2	21,3			CL								24
	UD-4	9.00-9.60																					
SPT-6	9.60-10.05					2,56	89,7	52,0	33,4	17,9	15,5			CL								16	

Table A.2 Laboratory Test Results of SK-1 and SK-2



M.E.T.U. SOIL MECHANICS  
O.D.T.Ü ZEMİN MEKANİĞİ

LABORATORY  
LABORATUVARI

PROJECT/PROJE:

EYMIİR LAKE

1956

Sondaj Boring No	Numune Sample No	Derinlik Depth (m.)	SPT N	w <sub>p</sub> (%)	e <sub>n</sub>	γ <sub>n</sub> kN/m <sup>3</sup>	G <sub>s</sub>	Elk. analiziz Sieve analysis		Aterberg limitleri Aterberg Limits			Uniformluk katsayıları Uniformity numbers		Direk Kesme Denevi Direct Shear Test(CD)		Üç Ekseni Bas. Den Triaxial Test (UU)		Kil Yüzdesi Clay Cont. (%)
								<No.4 (%)	<No.200 (%)	LL (%)	PL (%)	PI (%)	C <sub>u</sub>	C <sub>c</sub>	c (kPa)	f (°)	c (kPa)	f (°)	
SK-1	SPT-1	1,00-1,45	13	14,5				71,8	19,1										
	SPT-2	2,00-2,45	10	20,3				86,8	34,4	33	16	17							
	SPT-3	3,00-3,45	2	24,8				83,2	26,7										
	SPT-4	4,00-4,45	5	17,4				78,4	30,0	31	16	15							
	SPT-5	5,00-5,45	8	15,9				59,9	13,5										
	SPT-6	6,00-6,45	12	16,2				78,6	17,1										
	SPT-7	7,00-7,45	37	7,3				50,3	15,1										
SK-2	karot	7,50-8,00		9				71,5	30,8										
	SPT-8	8,00-8,45	42	8,4				62,5	20,7										
	SPT-1	0,60-1,05	10	14,2				84,9	26,4										
	SPT-2	1,50-1,95	3	32,6				86,6	70,6	52	23	29							
	UD-1	2,00-2,50																	
	SPT-3	3,50-3,95	5	18,6				85,8	41,1	32	15	17							
	SPT-4	4,50-4,95	7	13,9				73,8	27,1										
SPT-5	6,50-7,00																		
SPT-6	7,00-7,45	21	13,9				81,5	26,9											
SPT-6	8,00-8,45	22	16,1				91,9	38,5	33	17	16								
SPT-7	9,50-9,95	33	8,5				61,9	20,1											

Table A.3 Laboratory Test Results of SK-3 and SK-4



M.E.T.U. SOIL MECHANICS  
LABORATORY  
O.D.T.Ü. ZEMİN MEKANİĞİ

LABORATUVARI  
PROJECT/PROJE:

EYMIŞ LAKE

Sondaj Boring No	Numune Sample No	Derinlik Depth (m)	SPT N	w <sub>n</sub> (%)	e <sub>n</sub>	γ <sub>n</sub> kN/m <sup>3</sup>	G <sub>s</sub>	Elek analizzi Sieve analysis			Atterberg limitleri Atterberg Limits			Uniformluk katsayıları Uniformity numbers			USCS	Direk Kesme Deneği Direct Shear Test(CD)		Uç Ekseni Bas. Den. Triaxial Test(UU)		Kil Yüzdəsi Clay Cont. (%)
								-No.4 (%)	-No.200 (%)	-No.4 > -No.200 (%)	LL (%)	PL (%)	PI (%)	C <sub>u</sub>	C <sub>c</sub>	c (kPa)		f (°)	c (kPa)	f (°)		
SK-3	SPT-1	1,00-1,45	23	12,3				69,3	15,6													
	SPT-2	2,00-2,45	14	38,7				87,6	77,4	56	24	32										
	UD-1	2,50-3,00																				
	SPT-3	3,00-3,45	14	16,1				66,8	27,2													
	SPT-4	4,50-4,95	23	13,4				78,1	25,6	29	16	13										
	UD-2	7,50-8,00																				
	SPT-5	8,00-8,45	8	18,2				81,8	41,6	33	16	17										
	SPT-6	8,50-8,95	5	16,2				66,5	37,1													
	SPT-7	9,50-9,95	11	15,9				82,5	46,3													
	SPT-8	10,50-10,95	29	16,5				65,5	35,3	35	21	14										
	SPT-1	0,50-0,95	9	31,3				87,4	54,0													
SK-4	UD-1	1,50-2,00																				
	SPT-2	2,00-2,45	11	14,5				70,5	19,7													
	SPT-3	3,50-3,95	15	12,7				78,0	20,5													
	SPT-4	5,00-5,45	17	11,7				76,9	18,8													
	SPT-5	6,00-6,45	11	12,4				63,6	21,5													
	SPT-6	7,50-7,95	26	20,5				94,6	56,6	44	21	23										
	SPT-7	8,50-8,95	22	17,8				88,7	49,5													
	SPT-8	9,50-9,95	19	17,7				87,0	51,9													
	SPT-9	10,50-10,95	26	13,2				60,0	25,4	33	17	16										
	SPT-10	12,00-12,45	38	11				70,5	28,6													
	SPT-11	12,80-13,25	42	12,6				75,3	35,0													

Table A.4 Laboratory Test Results of SU8, SA8 and SB8

1956		M.E.T.U SOIL MECHANICS LABORATORY		O.D.T.Ü ZEMİN MEKANİĞİ LABORATUVARI		PROJECT/PROJE:		EYMİR LAKE											
Sondaj Boring No	Numune Sample No	Derinlik Depth (m)	SPT N	w <sub>p</sub> (%)	e <sub>s</sub>	Y n	G <sub>s</sub>	Atterberg Limitleri			USCS			Direct Shear Test(CD)		Uy Ekseni Has.Den. Triaxial Test (UU)		Kil Yüzdeleri Clay Cont. (%)	
								LL (%)	PL (%)	PI (%)	C <sub>c</sub>	C <sub>u</sub>	e	f	c	f	e		f
SU8	SPT-1	1,50-1,95	7	22,3				94,0	69,8	30	15	15							
	UD-1	1,50-2,00		26			2,7	87,9	43,2	33	15	18							10
	SPT-2	3,00-3,45	8	14,9				79,4	34,1	27	15	12							
	SPT-3	4,50-4,95	7	15				72,8	37,3										
	UD-2	4,50-5,00		15			2,7	75,1	41,1	29	15	14					31	0	12
	SPT-4	6,00-6,45	9	18,5				88,7	35,1	34	15	19							
	SPT-5	7,50-7,95	6	19,8				94,5	53,0	35	15	20							
	UD-3	7,50-8,00		17			2,7	78,3	37,1	33	17	16					20	9	10
	UD-4	9,00-9,50																	
	SPT-1	1,50-1,95		10				66,3	25,3										
SA8	UD-1	2,50-3,00																	
	SPT-2	3,00-3,45	7					88,6	26,9	28	14	14							
	UD-2	4,00-4,50																	
	SPT-3	4,50-4,95	5					73,3	26,3	28	13	15							
	SPT-4	6,00-6,45	9					75,5	33,7										
	SPT-5	7,50-7,95	11					96,9	51,1	33	15	18							
	SPT-1	1,50-1,95	8							36	18	18							
	UD-1	2,50-3,00																	
	SPT-2	3,00-3,45	4																
	SB8	UD-2	4,00-4,50																
SPT-3		4,50-4,95	12							36	18	18							
SPT-4		6,00-6,45	5							34	14	20							
SPT-5		7,50-7,95	11							26	14	12							
SPT-5		7,50-7,95	11																

Table A.5 Laboratory Test Results of SC8 and SC10

 M.E.T.U. SOIL MECHANICS LABORATORY O.D.T.Ü. ZEMİN MEKANİĞİ LABORATUVARI		LABORATORY LABORATUVARI		PROJECT/PROJE: EYMİR LAKE																	
Sondaj Borung No	Numune Sample No	Derinlik Depth (m)	SPT N	w <sub>n</sub> (%)	e <sub>n</sub>	γ <sub>n</sub> KN/m <sup>3</sup>	G <sub>s</sub>	Elek. analiz Sieve analysis			Aterberg limitleri Atterberg Limits			Uniformluk katsayıları Uniformity numbers		USCS	Direk Kesme Deneyi Direct Shear Test(CD)		Üç Ekseni Bas. Den. Triaxial Test(UU)		Kil Yüzdesi Clay Cont. (%)
								-No.4 (%)	-No.200 (%)	LL (%)	PL (%)	PI (%)	C <sub>u</sub>	C <sub>c</sub>	c (kPa)		τ (°)	c (kPa)	τ (°)		
SC8	SPT-1	1,50-1,95	7					80,3	43,1	43	22	21									
	SPT-2	3,00-3,45	8					60,6	32,5	31	15	16									
	SPT-3	4,50-4,95	16					83,1	19,4												
	SPT-4	6,00-6,45	9					89,7	35,2												
	SPT-5	7,50-7,95	7					71,2	30,6	33	18	15									
SC10	UD-1	1,00-1,50																			
	SPT-1	1,50-1,95	6					78,2	39,9	42	22	20									
	SPT-2	3,00-3,45	11					76,5	29,5												
	UD-2	4,00-4,50																			
	SPT-3	4,50-4,95	15					66,0	15,1												
	SPT-4	6,00-6,09	50/9					72,3	23,1												
	UD-3	7,00-7,50																			
	SPT-5	7,50-7,95	9					88,4	45,5	38	18	20									
	SPT-6	9,00-9,45	7					86,9	51,6	38	17	21									

## APPENDIX B

### DESIGN CHARTS

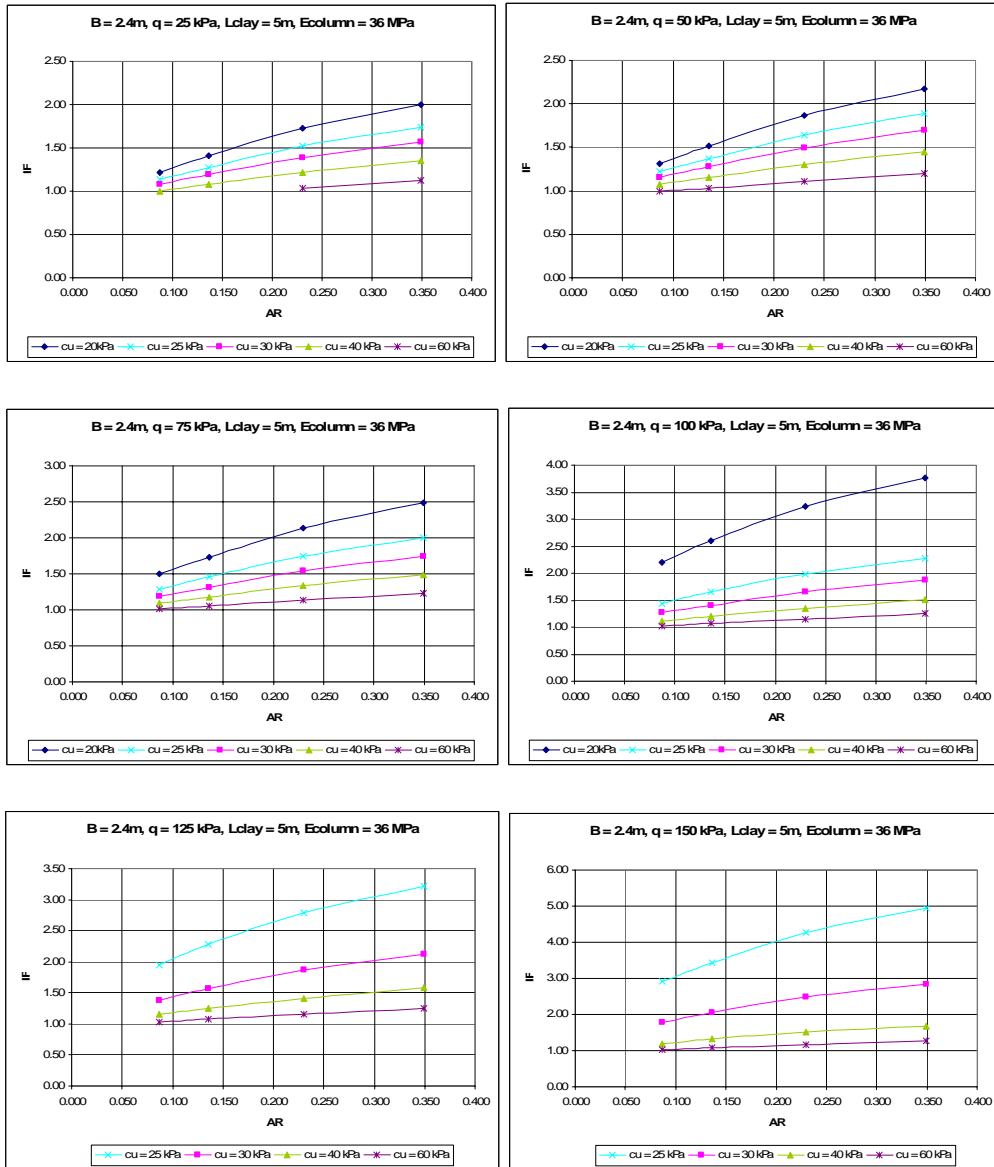


Figure B.1 Settlement improvement factor (IF) vs. area ratio (AR) charts for a rigid square footing (B=2.4m) resting on end bearing rammed aggregate piers (L=5m, E=36 MPa)



Figure B.2 Settlement improvement factor (IF) vs. area ratio (AR) charts for a rigid square footing ( $B=2.4\text{m}$ ) resting on end bearing rammed aggregate piers ( $L=5\text{m}$ ,  $E=72\text{ MPa}$ )

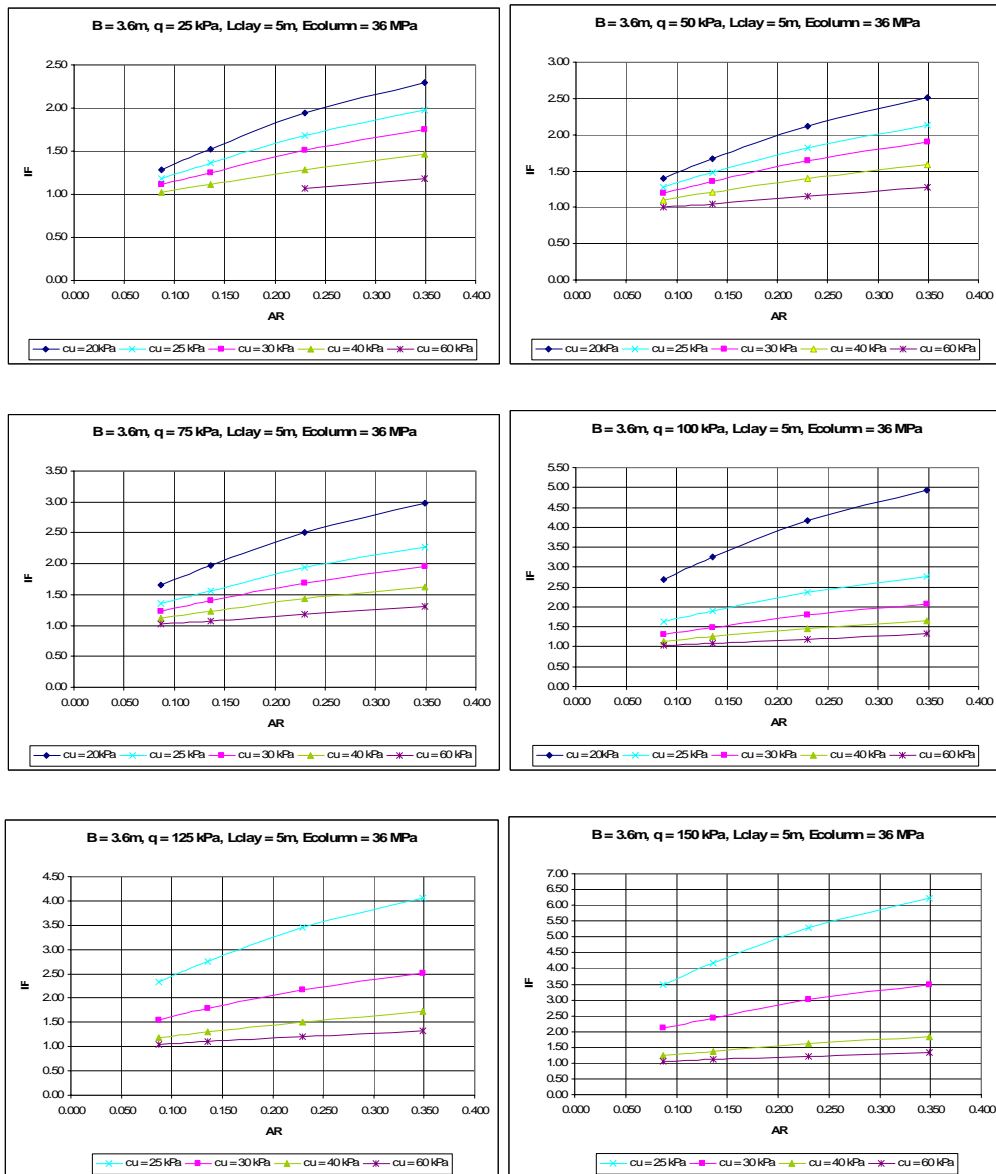


Figure B.3 Settlement improvement factor (IF) vs. area ratio (AR) charts for a rigid square footing (B=3.6m) resting on end bearing rammed aggregate piers (L=5m, E=36 MPa)

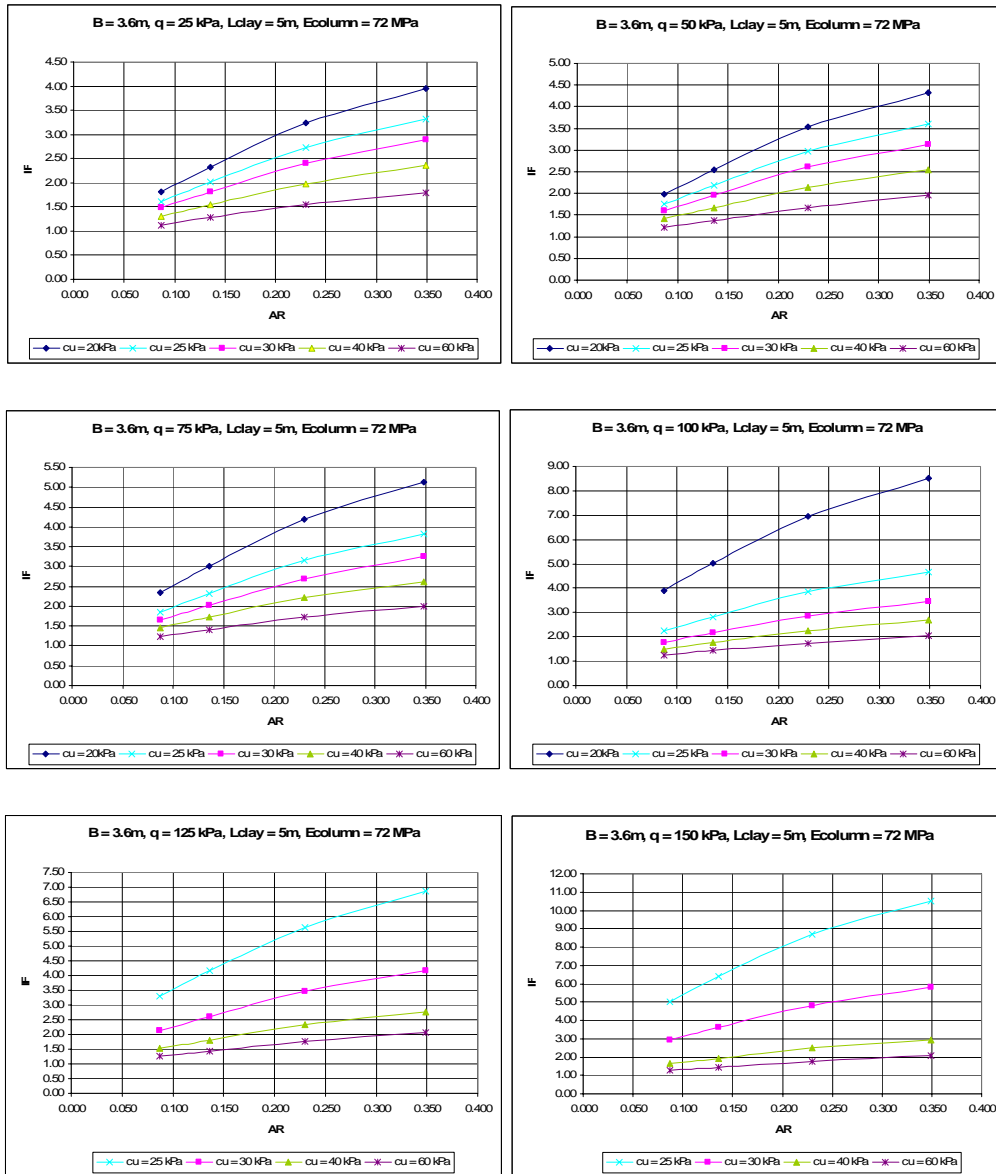


Figure B.4 Settlement improvement factor (IF) vs. area ratio (AR) charts for a rigid square footing (B=3.6m) resting on end bearing rammed aggregate piers (L=5m, E=72 MPa)

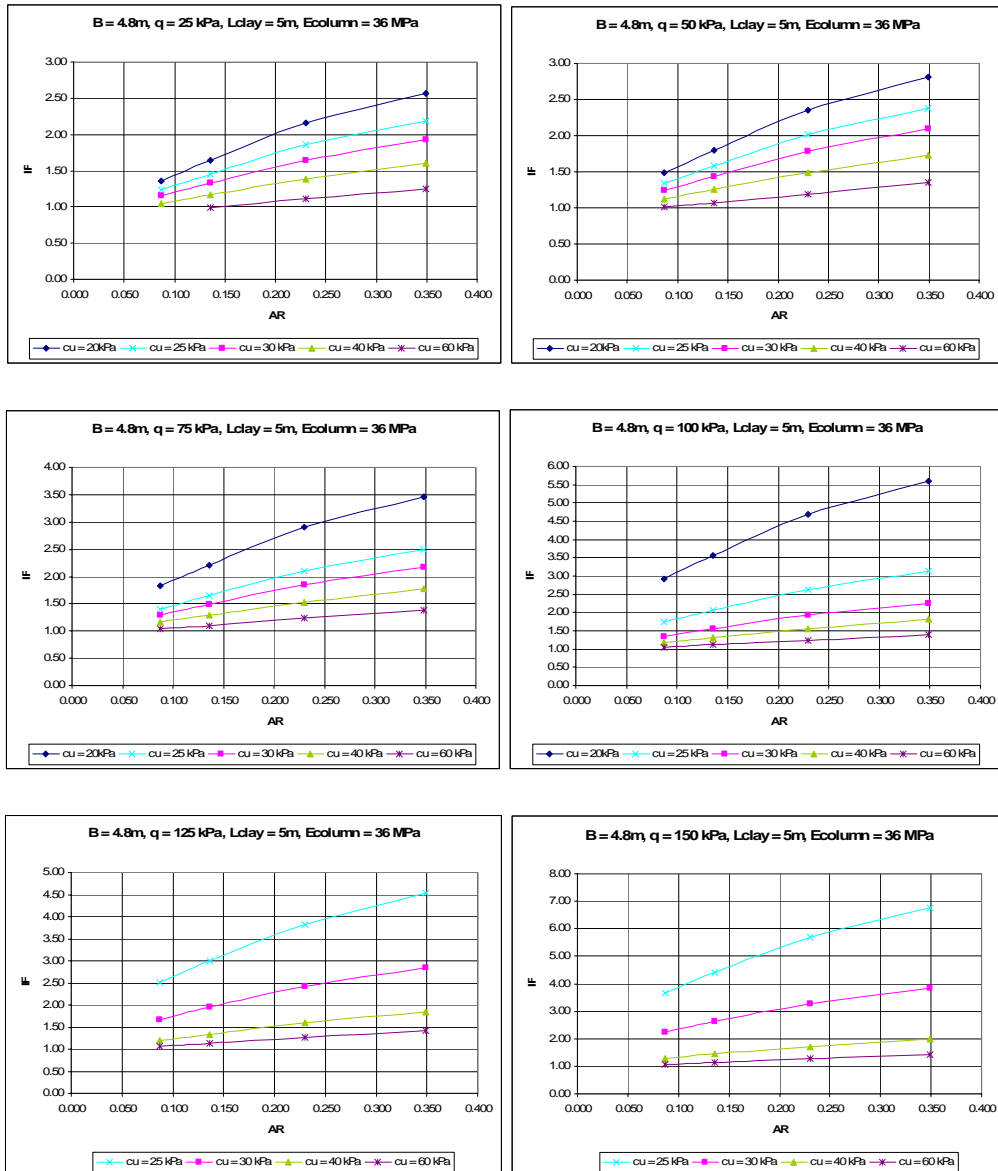


Figure B.5 Settlement improvement factor (IF) vs. area ratio (AR) charts for a rigid square footing (B=4.8m) resting on end bearing rammed aggregate piers (L=5m, E=36 MPa)



Figure B.6 Settlement improvement factor (IF) vs. area ratio (AR) charts for a rigid square footing ( $B=4.8\text{m}$ ) resting on end bearing rammed aggregate piers ( $L=5\text{m}$ ,  $E=72\text{ MPa}$ )

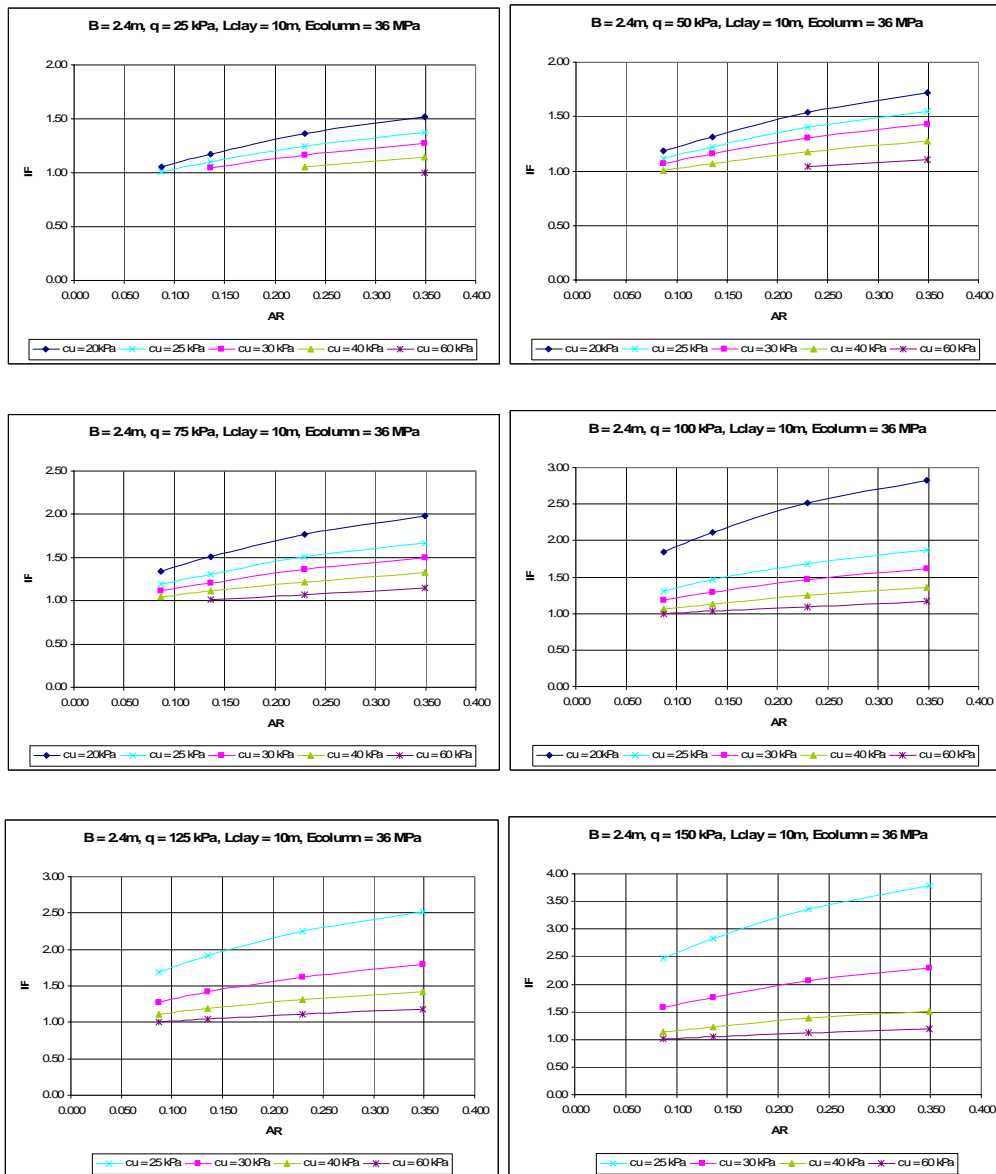


Figure B.7 Settlement improvement factor (IF) vs. area ratio (AR) charts for a rigid square footing (B=2.4m) resting on end bearing rammed aggregate piers (L=10m, E=36 MPa)

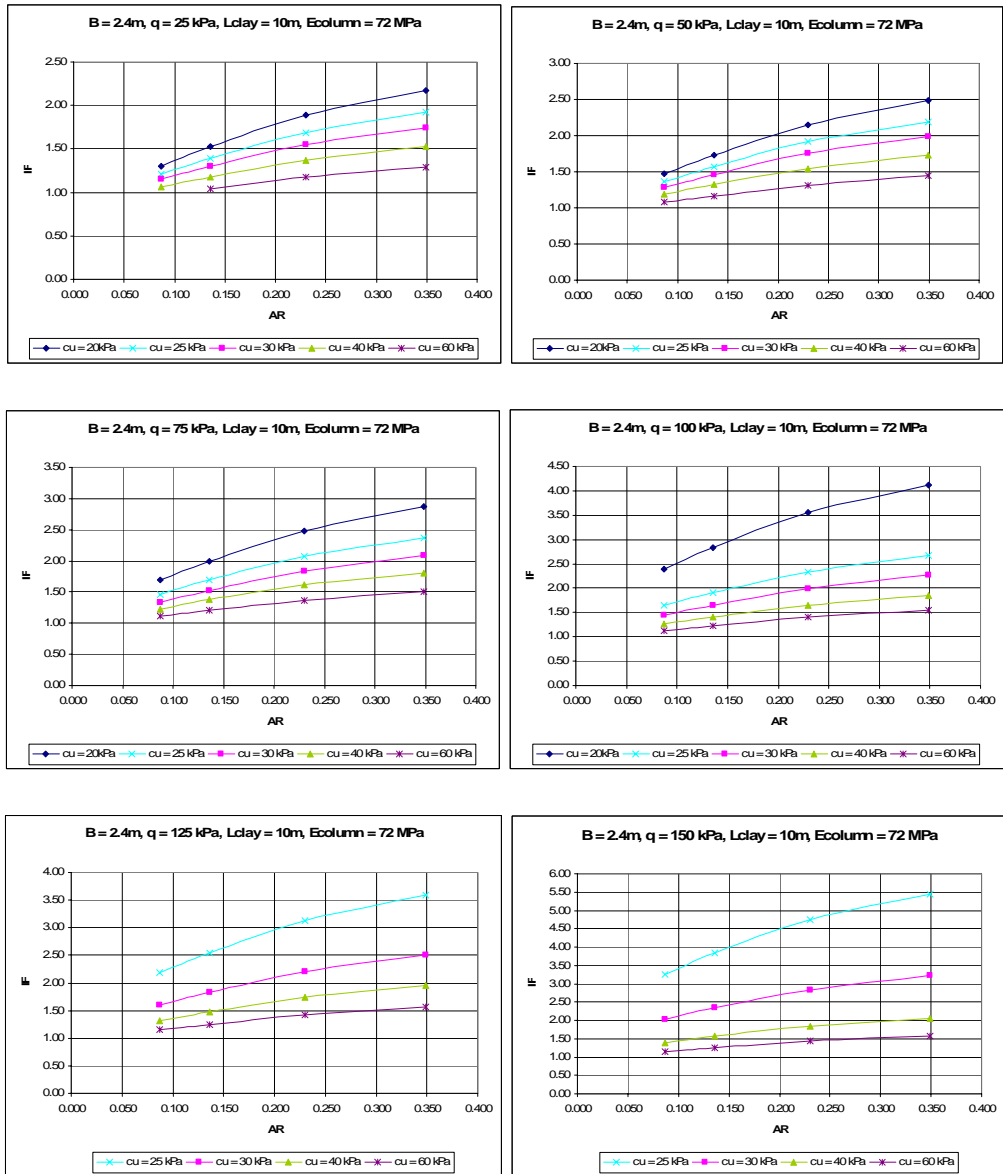


Figure B.8 Settlement improvement factor (IF) vs. area ratio (AR) charts for a rigid square footing ( $B=2.4\text{m}$ ) resting on end bearing rammed aggregate piers ( $L=10\text{m}$ ,  $E=72\text{ MPa}$ )

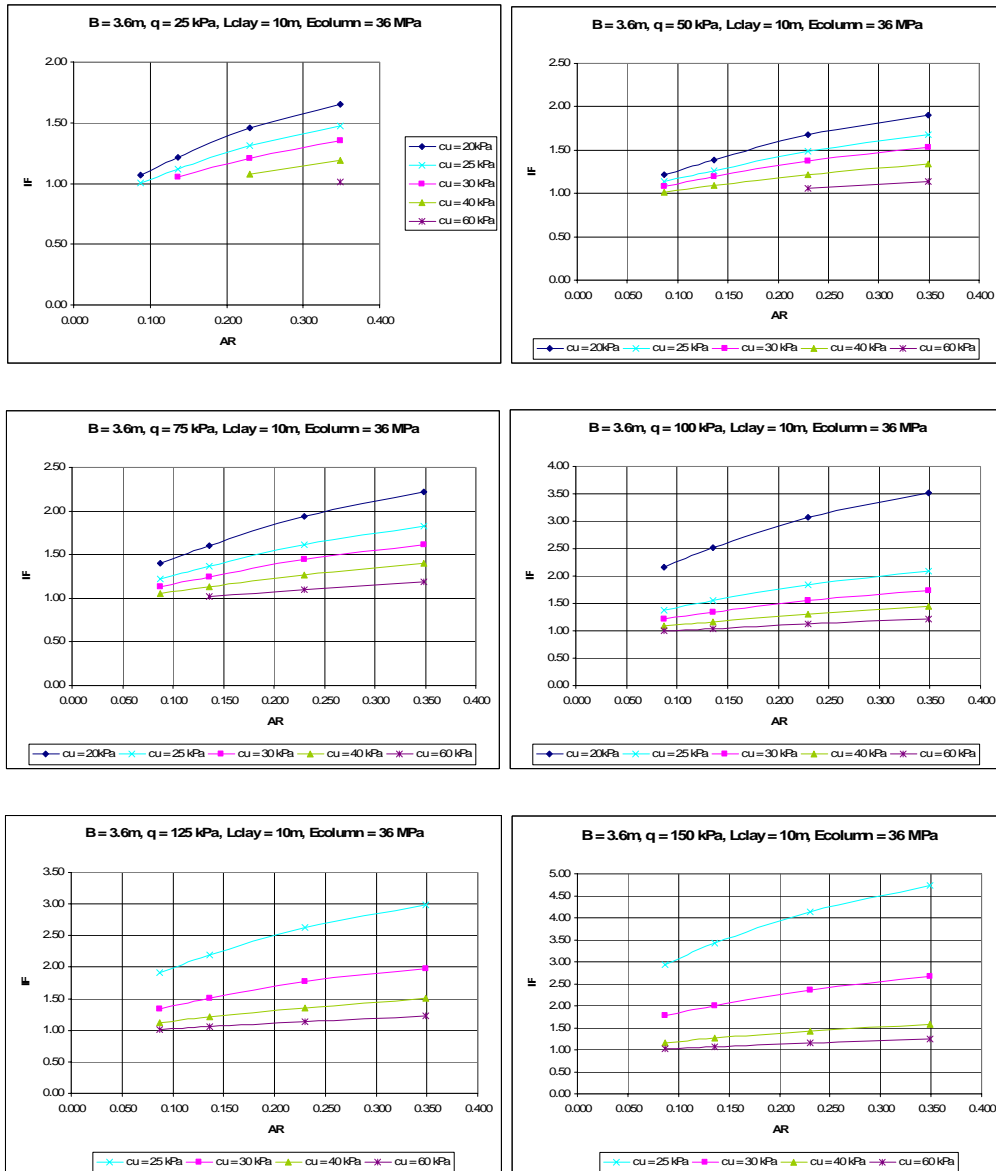


Figure B.9 Settlement improvement factor (IF) vs. area ratio (AR) charts for a rigid square footing (B=3.6m) resting on end bearing rammed aggregate piers (L=10m, E=36 MPa)

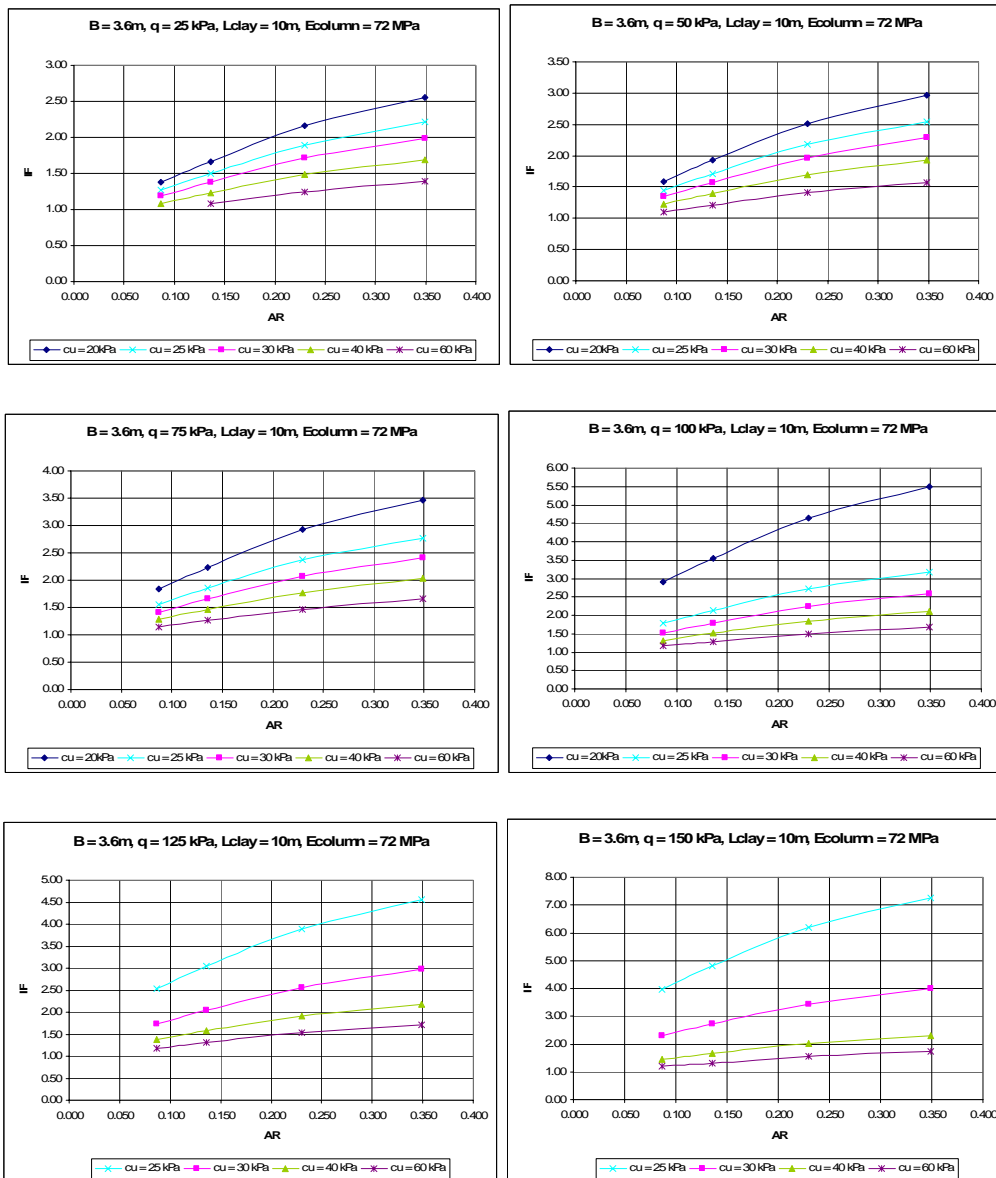


Figure B.10 Settlement improvement factor (IF) vs. area ratio (AR) charts for a rigid square footing ( $B=3.6\text{m}$ ) resting on end bearing rammed aggregate piers ( $L=10\text{m}$ ,  $E=72\text{ MPa}$ )

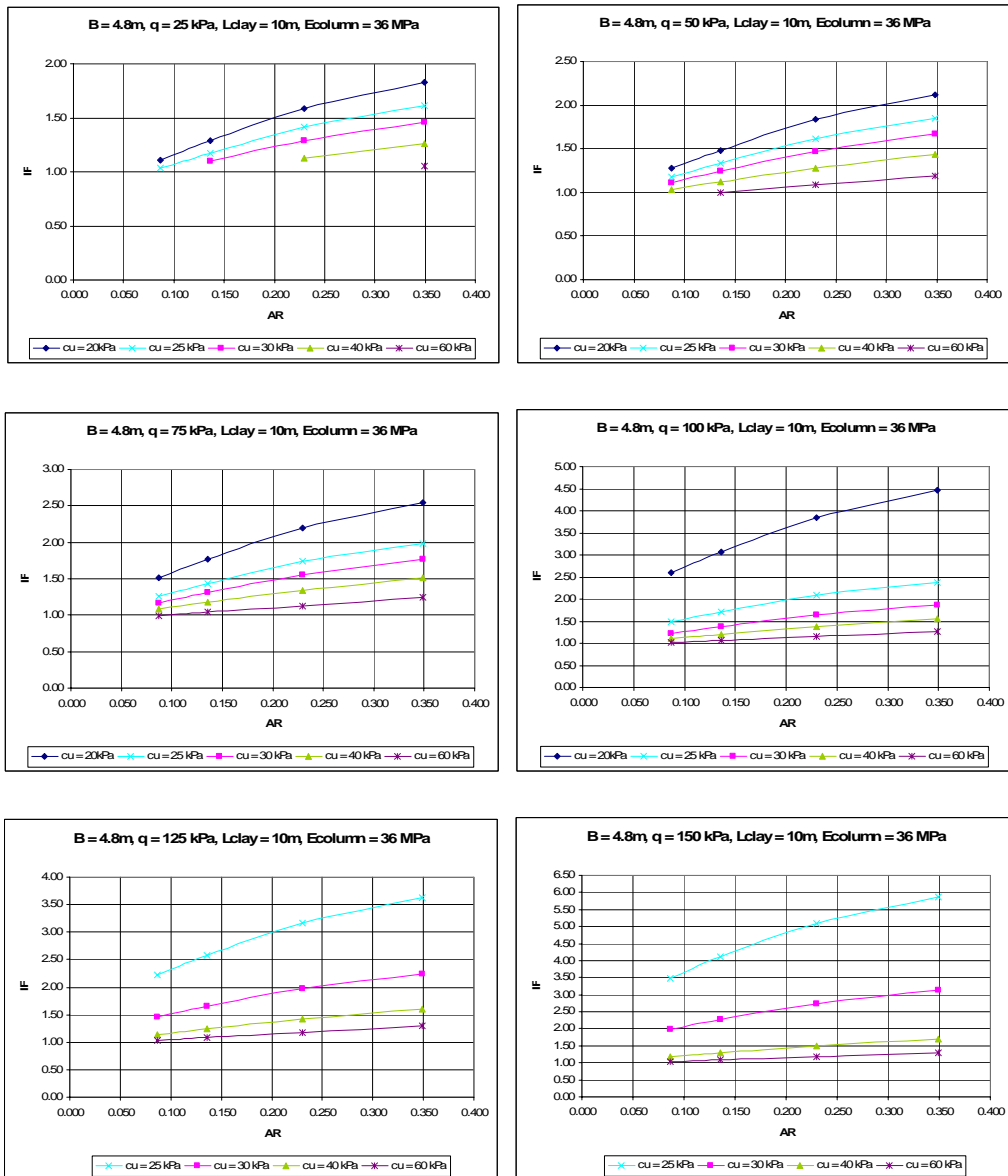


Figure B.11 Settlement improvement factor (IF) vs. area ratio (AR) charts for a rigid square footing ( $B=4.8\text{m}$ ) resting on end bearing rammed aggregate piers ( $L=10\text{m}$ ,  $E=36\text{ MPa}$ )

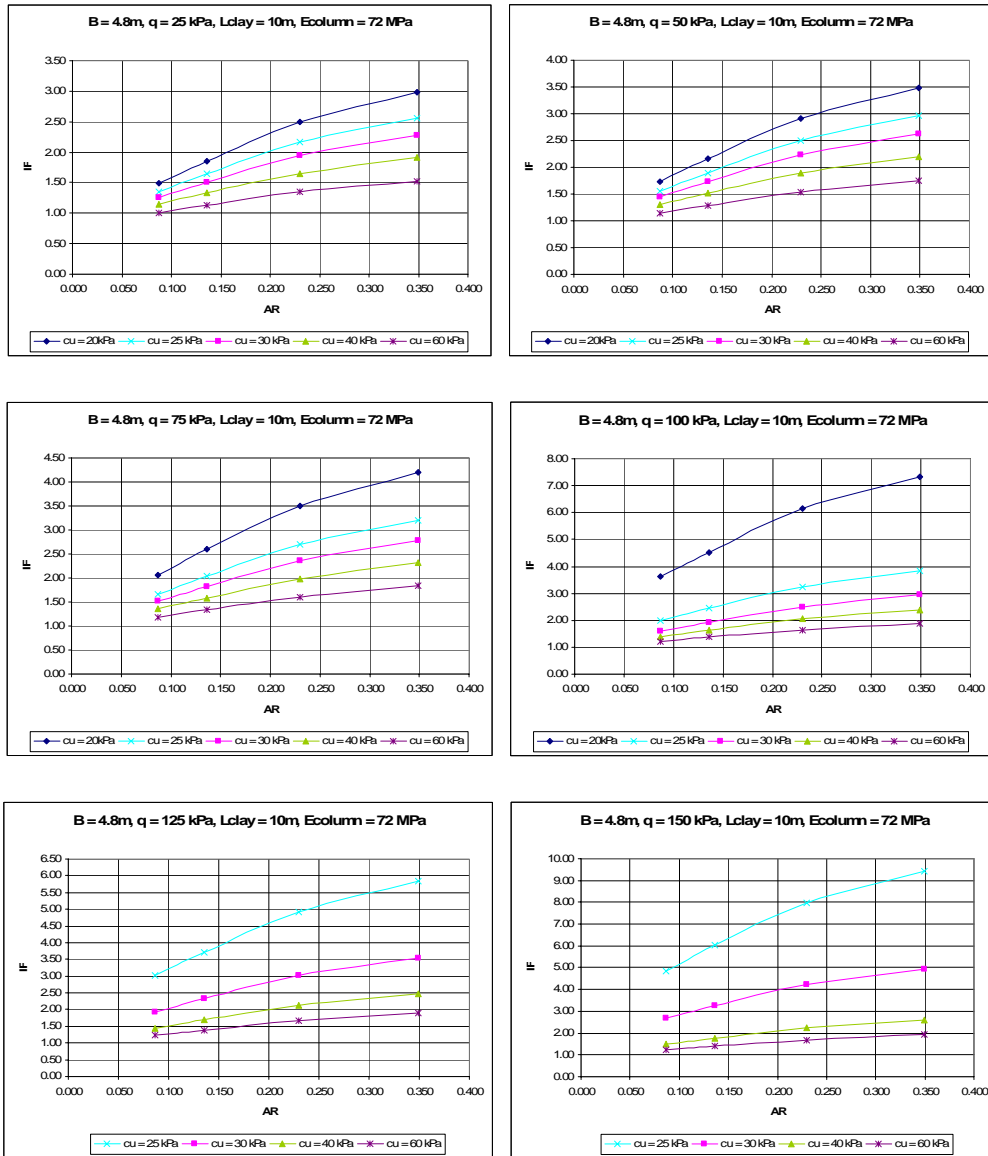


Figure B.12 Settlement improvement factor (IF) vs. area ratio (AR) charts for a rigid square footing ( $B=4.8\text{m}$ ) resting on end bearing rammed aggregate piers ( $L=10\text{m}$ ,  $E=72\text{MPa}$ )

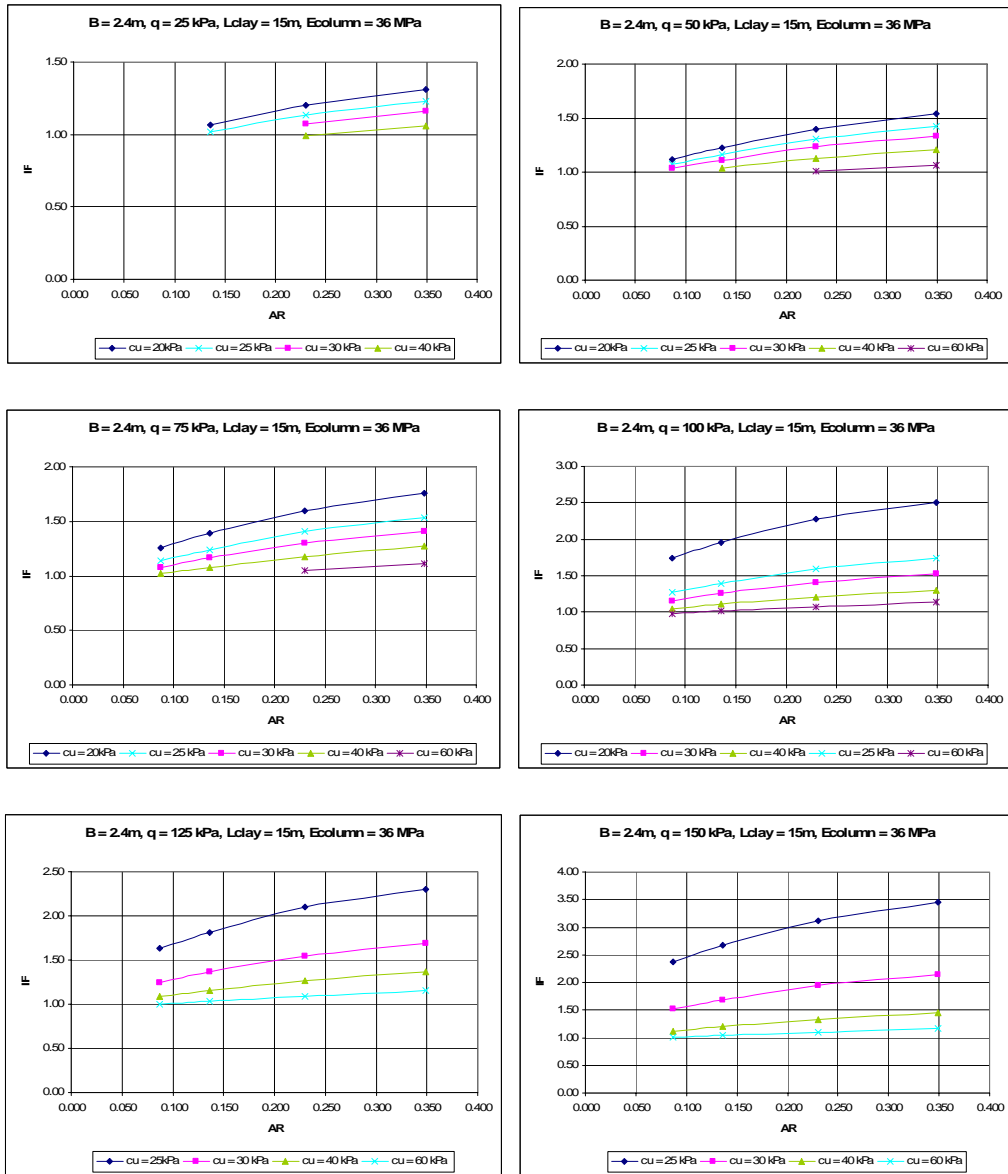


Figure B.13 Settlement improvement factor (IF) vs. area ratio (AR) charts for a rigid square footing ( $B=2.4\text{ m}$ ) resting on end bearing rammed aggregate piers ( $L=15\text{ m}$ ,  $E=36\text{ MPa}$ )

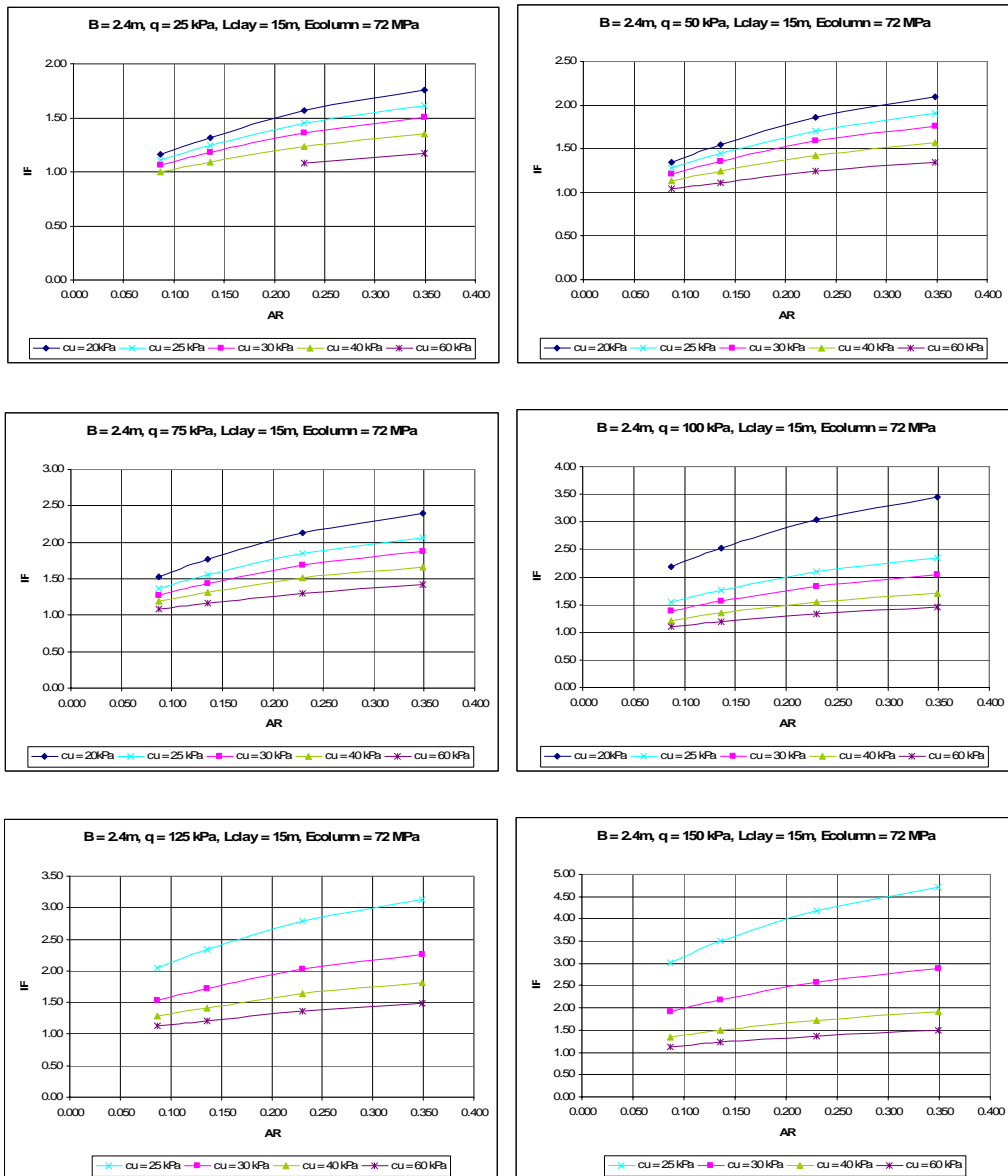


Figure B.14 Settlement improvement factor (IF) vs. area ratio (AR) charts for a rigid square footing (B=2.4m) resting on end bearing rammed aggregate piers (L=15m, E=72 MPa)

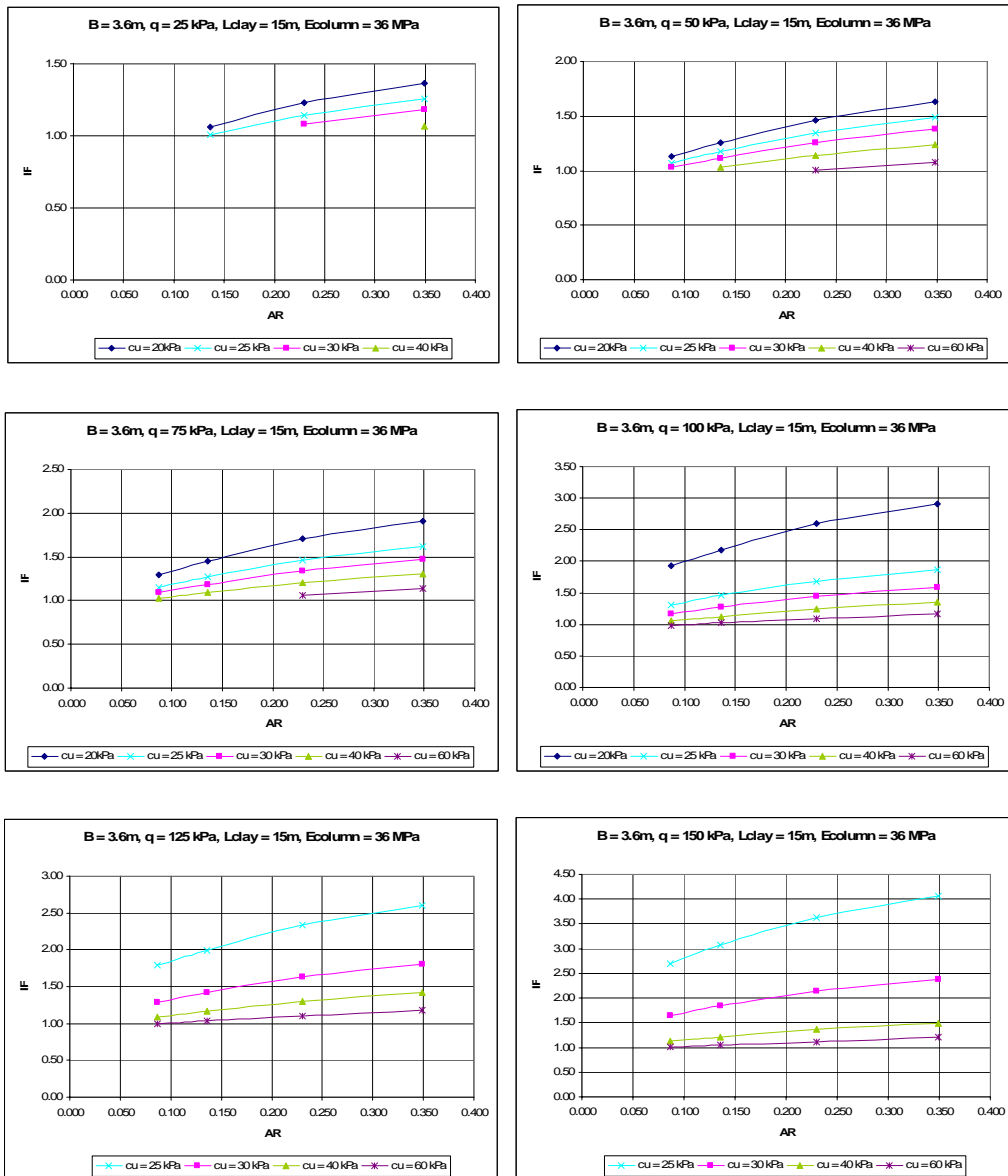


Figure B.15 Settlement improvement factor (IF) vs. area ratio (AR) charts for a rigid square footing ( $B=3.6\text{m}$ ) resting on end bearing rammed aggregate piers ( $L=15\text{m}, E=36\text{ MPa}$ )

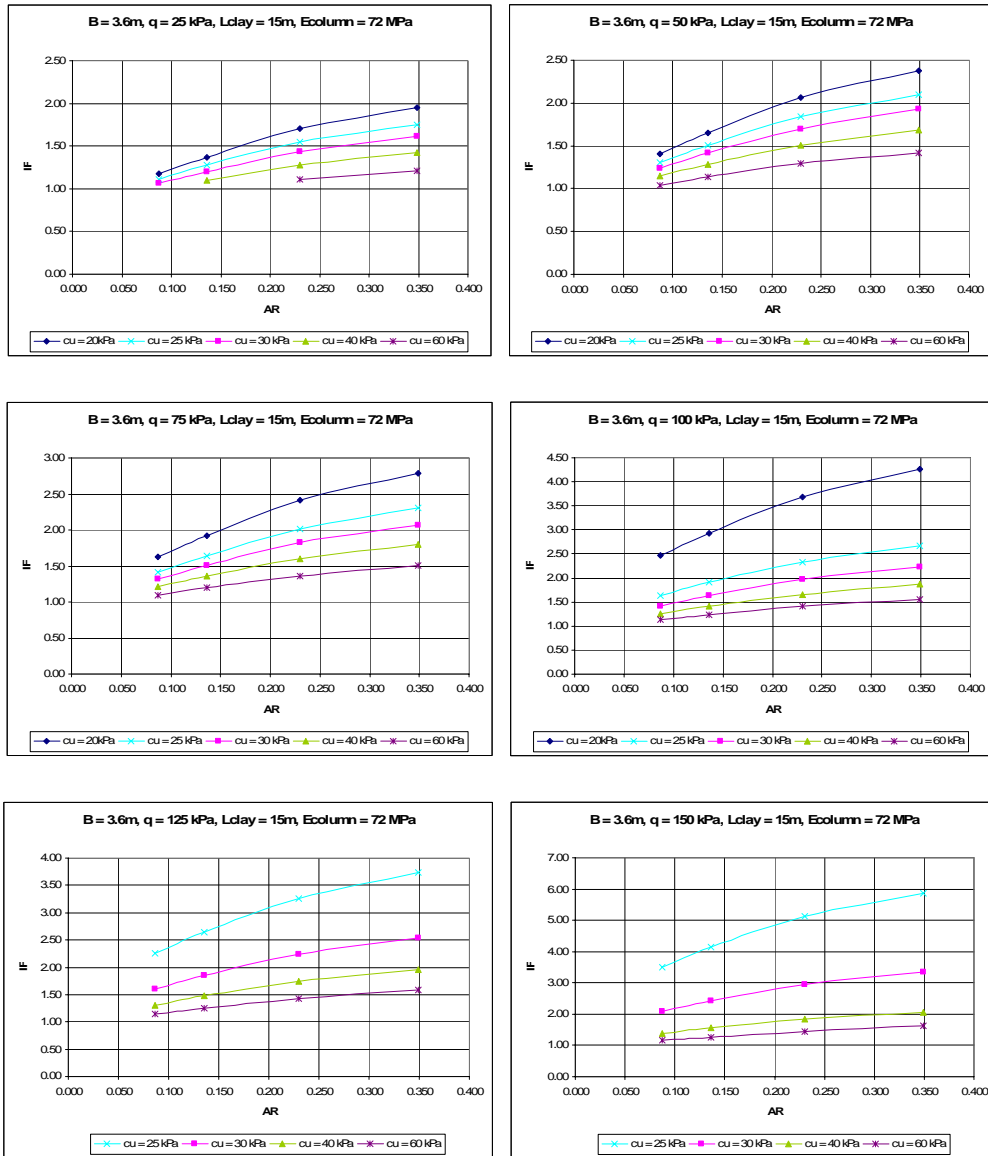


Figure B.16 Settlement improvement factor (IF) vs. area ratio (AR) charts for a rigid square footing ( $B=3.6\text{m}$ ) resting on end bearing rammed aggregate piers ( $L=15\text{m}$ ,  $E=72\text{MPa}$ )

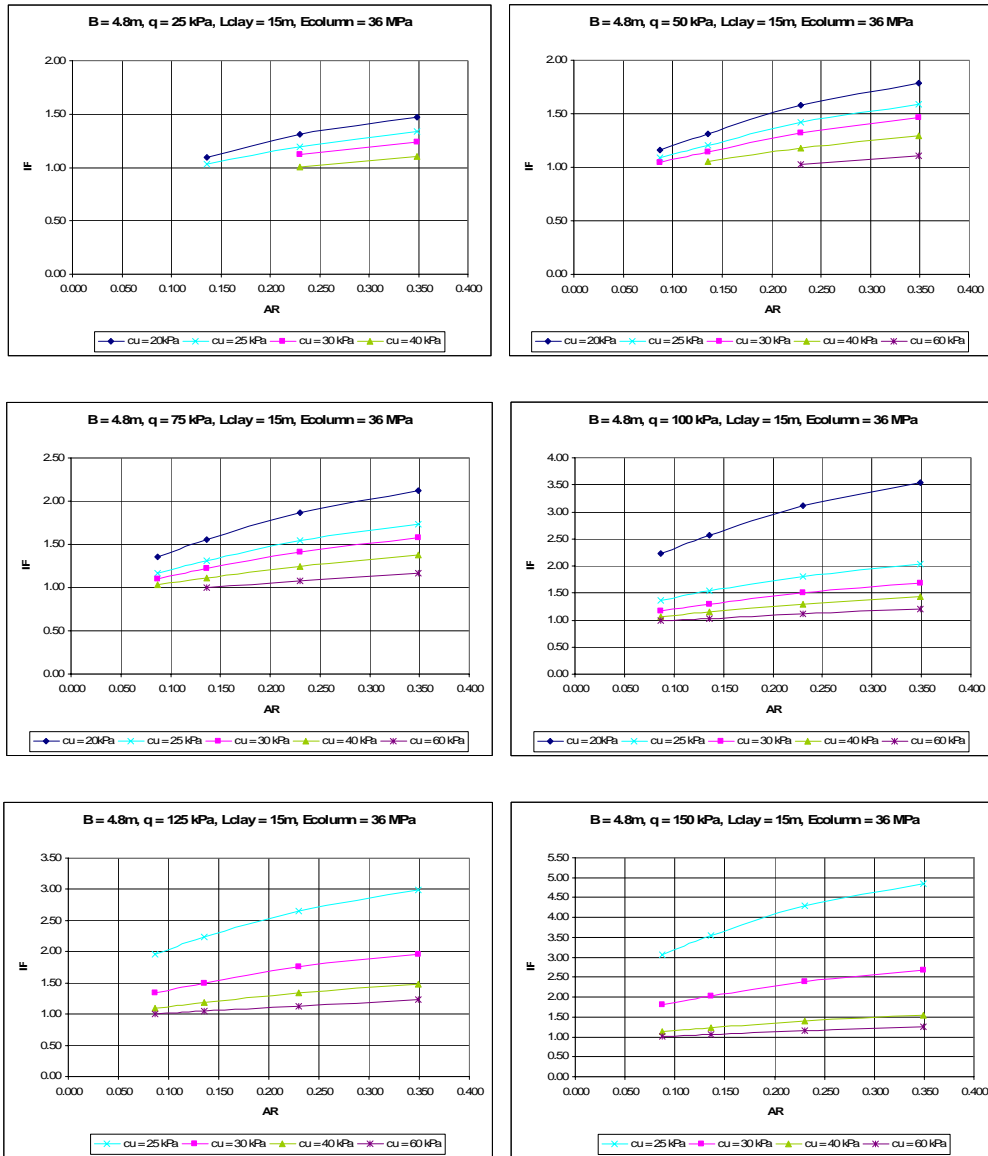


Figure B.17 Settlement improvement factor (IF) vs. area ratio (AR) charts for a rigid square footing (B=4.8m) resting on end bearing rammed aggregate piers (L=15m, E=36 MPa)

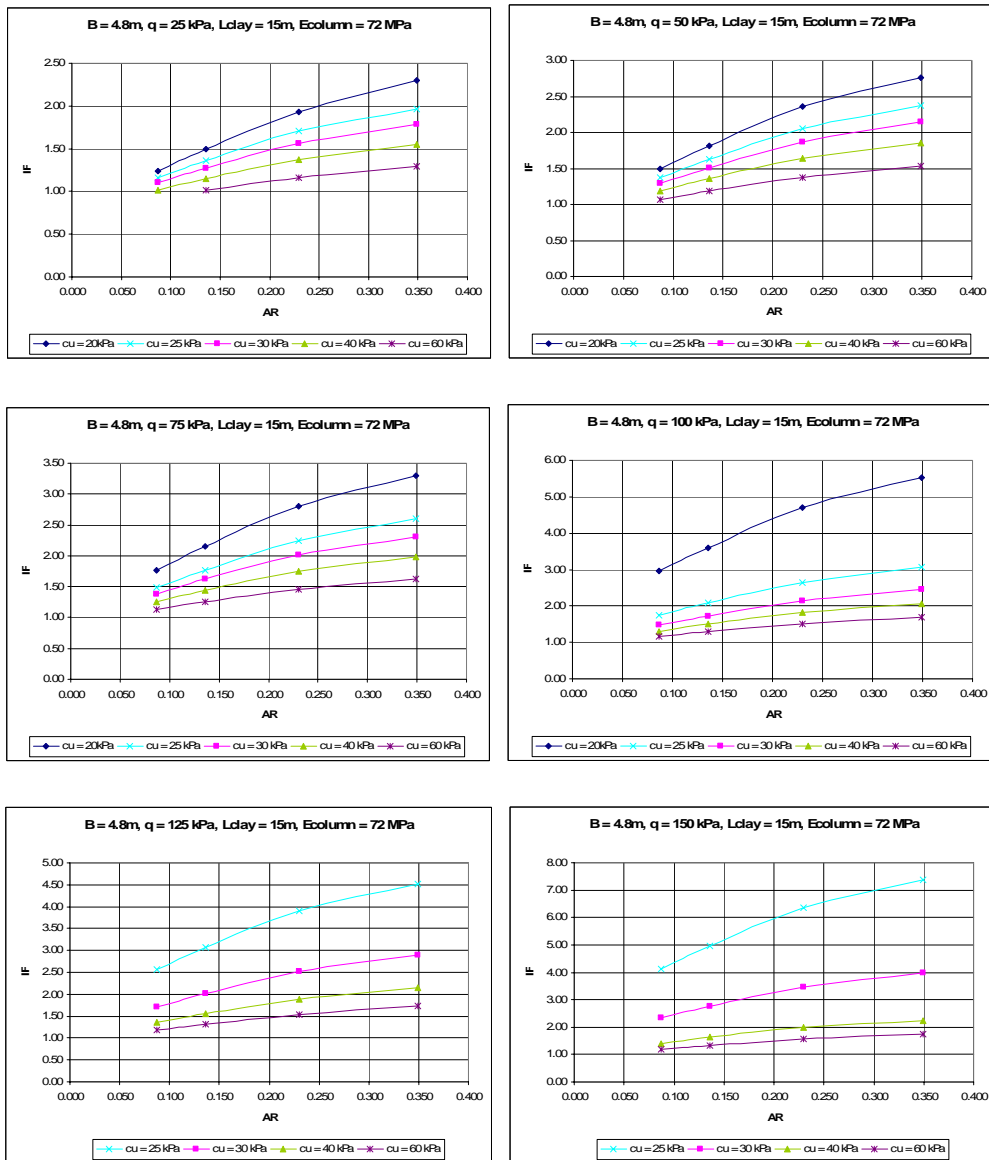


Figure B.18 Settlement improvement factor (IF) vs. area ratio (AR) charts for a rigid square footing ( $B=4.8\text{m}$ ) resting on end bearing rammed aggregate piers ( $L=15\text{m}$ ,  $E=72\text{ MPa}$ )

## CURRICULUM VITAE

### PERSONAL INFORMATION

Surname, Name : Kuruoğlu, Özgür  
Nationality : Turkish  
Date and Place of Birth : 13 April 1974, Ankara  
Marital Status : Married  
Phone : + 90 312 495 70 00  
Fax : + 90 312 495 70 24  
email : ozgurk@yukseproje.com.tr

### EDUCATION

Degree	Institution	Year of Graduation
MS	METU Civil Engineering	1998
BS	METU Civil Engineering	1995
High School	Atatürk Anadolu High School, Ankara	1991

### WORK EXPERIENCE

Year	Place	Enrollment
2000-present	Yüksel Proje	Foundation Eng. Group Manager
1995-2000	Yüksel Proje	Geotechnical Engineer

### FOREIGN LANGUAGES

Advanced English

### PUBLICATIONS

1. KURUOĞLU, Ö., HOROZ, A. and EROL, O., 1998. "İçten Destekli Rijit İksa Yapılarında Yatay Zemin İtkileri ve Deplasmanlar", *Zemin Mekaniği ve Temel Mühendisliği Yedinci Ulusal Kongresi*, İstanbul, Cilt 2, pp.373-381